The Thesis Committee for Krystian Amadeusz Zimowski
Certifies that this is the approved version of the following thesis:

Next Generation Wind Energy Harvester to Power Bridge Health Monitoring Systems

APPROVED BY
SUPERVISING COMMITTEE:

Supervisor: _____
Richard H. Crawford

Co-supervisor: _____
Kristin L. Wood

Next Generation Wind Energy Harvesting to Power Bridge Health Monitoring Systems

by

Krystian Amadeusz Zimowski, B.S.M.E.

Thesis

Presented to the Faculty of the Graduate School of

The University of Texas at Austin

in Partial Fulfillment

of the Requirements

for the Degree of

Master of Science in Engineering

The University of Texas at Austin

May 2012

Dedication

This thesis is first of all dedicated to my parents, who sacrificed everything for me and for my education.

Acknowledgements

I would like to acknowledge Dr. Kristin Wood, Dr. Richard Crawford, and Dr. Sharon Wood, for allowing me to work on such a fantastic research project and for mentoring me throughout my graduate studies at The University of Texas at Austin. I am grateful that the National Science Foundation and the National Institute for Standards and Technology (NIST) Technology Innovation Program (TIP) provided funds to address the critical issue of bridge health monitoring systems. I would like also extend a personal thank you to Dr. Dan Jensen at the United States Air Force Academy for granting me the funding to work on this project through a National Science Foundation (NSF) grant for improving student learning using finite element learning modules. Finally, I would like to extend a personal thanks to my fellow mechanical engineers with whom I worked on this project: Sumedh Inamdar, Eric Dierks, and Travis McEvoy.

May 4, 2012

Abstract

Next Generation Wind Energy Harvester to Power Bridge Health Monitoring Systems

Krystian Amadeusz Zimowski, M.S.E.

The University of Texas at Austin, 2012

Supervisor: Richard H. Crawford

The research reported in this thesis is part of a project to develop a remote wireless sensing network for monitoring the health of highway bridges. Remote health monitoring that does not require direct human observation has many advantages in terms of cost and increased productivity. However, bridges that cannot be easily connected to the power grid require alternative means of acquiring power. This thesis describes the design of a wind energy harvester to power a particular component in the sensor network, the wireless router. The work discussed in this thesis provides a review of relevant literature and development of a detailed analytical modeling of wind turbine behavior. The analytical model provides key information on sizing generators and choosing appropriate wind turbine dimensions to provide the required amount of power. The analytical model also distinguishes the performance of vertical and horizontal axis wind turbines. The model is verified through design and testing of a first generation prototype

and benchmarking of a commercially available turbine. Based on these results, the design of the next generation wind harvesting system is described. A new methodology to design non-destructive attachment systems is also discussed.

Table of Contents

List of Tables

List of Figures

Chapter 1: Introduction

1.1 PROJECT DECRIPTION AND PAIN

Bridge 9340 was an eight-lane, steel truss arch bridge that transported over 140,000 cars daily over the Mississippi river on Interstate 35W in Minneapolis (U.S. Department of Transportation, 2006). On August 1, 2007 the I-35W bridge suddenly and unexpectedly collapsed, killing 13 people and injuring 145 (see Figure 1.1). The engineering firm responsible for the inspection of Bridge 9340 examined the bridge a mere year before the tragic collapse, but will now have to pay $52.4 million as settlements (Dierks, 2011 & CNN Wire Staff, 2010).

Figure 1.1: I-35W bridge collapse in Minneapolis in 2007 (CNN Wire Staff, 2010).

This is only one, grave example of what can happen if our national highway system is not monitored more closely and more often. Just in Texas alone, there are currently over 9,300 bridges that are considered structurally deficient or functionally obsolete out of the 51,000 that span across the state (CNN Write Staff, 2010).

Nationwide, 24% of all highway bridges exhibit the same structural deficiencies by definition, as can be seen in Figure 1.2 (Dierks, 2011). This shocking statistic calls for a more efficient and reliable method to monitor the health of these highway bridges.

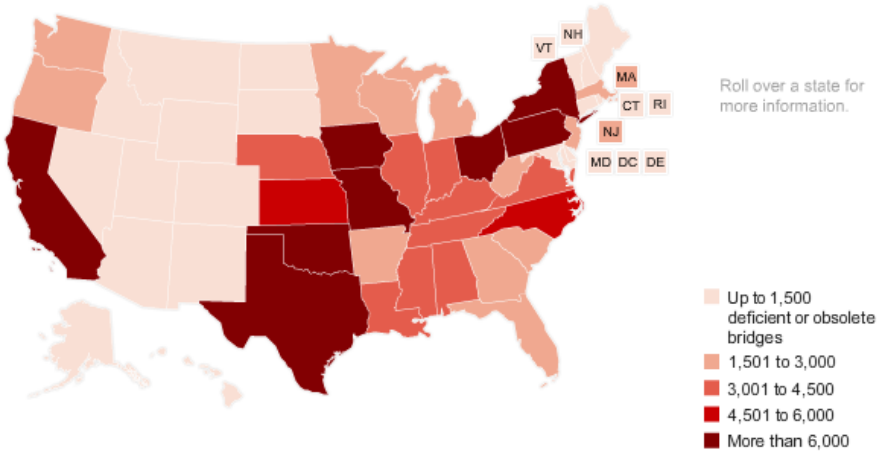

Figure 1.2: Structurally deficient and functionally obsolete bridges across the U.S. (CNN Wire Staff, 2010).

The current method for inspection of highway bridges requires long and intensive human labor. Large pieces of machinery, such as Snooper trucks (see Figure 1.3), are hauled out onto the bridges themselves and their long, multi-jointed arms are then contorted and extended to inspect certain areas underneath the bridge.

Figure 1.3: Snooper truck to manually inspect the health of bridges (LG Barcus & Sons, 2012).

This process not only requires an extensive amount of time, but it can also be subjective because of the variability of human perception. Proper sensing equipment should be required to adequately measure strain or corrosion that can be implicative of failure. Disasters such as the Minnesota bridge collapse could be avoided if state-of-the-art structural health monitoring systems are remotely employed on bridges to continuously monitor their well-being.

1.1.1 Project Description

The Technology Innovation Program (TIP), a research program administered by the National Institute for Standards and Technology (NIST), has funded a five-year research project to address the issue of wireless and remote structural health monitoring of highway bridges. NIST has stressed the importance of this project and the impact it can have nationwide in order to avoid disasters such as the Minnesota bridge collapse. The group associated with this project consists of professors and graduate students at The University of Texas at Austin (UT Austin), mechanical and computer science engineers at National Instruments (NI), as well as structural engineering consultants at Wiss, Janney, Elstner Associates (WJE). The team at UT Austin is composed of an interdisciplinary team of engineers. The electrical engineers are building passive corrosion sensors powered by passing traffic; the civil engineers are working on the structural health monitoring equipment directly with NI; the mechanical engineers are developing innovative energy harvesting solutions to power the sensing equipment.

Remote Health Monitoring System

The structural health monitoring system will be enabled by a wireless sensor system designed and constructed by NI. The hierarchy of components will consist of Wireless Sensor Nodes (WSNs) that monitor signals from strain gauges scattered across critical points on a bridge. These "end nodes" will communicate with a central WSN that will be in continuous router mode. The difference between the WSN "end node" and the WSN "router" is its basic function, which is relevant to its inherent power consumption. The end node monitors the gauges at a given frequency, and transmits that information at another frequency. For example, the end node can monitor the voltage of the strain gauges at 30 Hz, and then transmit this information stored in its memory once per hour. The router is constantly on and transmits information wirelessly from the end nodes to a "gateway", which is directly connected the host program or computer. The entire system can be seen in Figure 1.4.

Figure 1.4: NI wireless monitoring system (Dierks, 2011).

The idea of this network is to remotely monitor the health of structures in order to replace the more cumbersome and time intensive manual inspections.

Need for Energy Harvesting

The remote health monitoring system described in the previous section should ideally be a "set-it" and "forget-it" type of system, meaning that the once installed, there should be no physical interaction with the system unless there is some unforeseen failure. Engineers would be able to remotely access information about the bridge health at any point in time without having to travel and manually download data. However, there is one need essential to complete the intended functionality of the system, and that is the need for energy harvesting.

Energy sources such as grid electricity can be excluded in order to avoid unnecessary wiring across the bridge. The most desirable form to power the health monitoring system is one that exhibits similar traits: wireless and remote. Batteries are therefore currently used to power certain parts of the system, such as the WSNs. On the other hand, batteries have a limited lifespan, and would have to be manually replaced every so often by engineers physically going out in the field. Manual replacement of these batteries in each piece of sensing equipment scattered across numerous bridges would be extremely costly (Dierks, 2011). In order to avoid reverting back to a cumbersome manual process, energy harvesters can deployed to directly provide power for the system or to recharge an energy storage device. The energy harvesters can easily be installed in conjunction with the health monitoring system and truly left alone to function remotely for a much longer time period as originally intended.

Power Requirements

Each subsystem of the health monitoring system has a different power requirement. The gateway, which relays information back to the home network,

consumes around 10W of power. The router, which communicates between the end nodes and the gateway, consumes around 200 mW of power. The end nodes have a variable power consumption depending of their configuration. A strain gauge sampling rate of once per hour consumes around 300 μW, while a sampling rate of once per day consumes around 9 μW. Table 1.1 outlines the different power configurations.

Table 1.1: Power and energy consumption for test scenarios (Weaver et al., 2010)

Scenario	**Average Power**	**Yearly Energy**	
Router mode (radio always on)	207 mW	6.53 MJ	1.81 kWh
30 Hz (10 weeks)/ hourly rest of year	60.7 mW (30Hz) 300 μW (hourly)	375 kJ	104 Wh
One sample/day (with deep sleep)	9 μW	284 J	78.8 mWh

Based on an analysis of available energy sources, the current system design assumes that solar energy powers the gateway, wind energy powers the router, and vibration energy powers the end nodes.

Functional Requirements and Constraints

The main functional requirements and constraints of the energy harvester were organized into Table 1.2. The power requirements addressed in the previous section are also included in the table. The key item to address is that the WSN router requires a 6V DC voltage in order to operate properly. The energy harvester also has to have a service life of 10-15 years, and must be weatherproof to protect the electronics and sensing equipment. The constraints are also crucial to the design of the harvester itself: no portion

can extend below any portion of the bridge, and no permanent alterations, such as welds or holes, can be made to the bridge.

Table 1.2: Functional requirements for the energy harvester (Dierks, 2011).

Functional Requirements	
Generate long-term energy level	> 104 Wh/year
Provide power level continuously for 2 weeks	> 61 mW
Provide continuous power for router	> 207 mW (1.8 kWh/year)
Provide continuous power for gateway	> 10 W (88 kWh/year)
Store enough energy to go two weeks with no harvesting input	> 20 Wh
Provide DC voltage	6 V DC, constant
Service Life	10-15 years
Weatherproof	Rain, ice, dust, etc.
Maintenance interval	5 years
Constraints	
Number of inches that the harvester can extend below the lowest part of the bridge	0
Number of permanent alterations to metal parts of bridge, such as welds or holes	0

1.2 CHALLENGES AND OPPORTUNITIES

The proposed work for this thesis focuses on creating a wind energy harvesting system to power a router. If we briefly consider the micro-Watt power requirement for said router, it is orders of magnitude smaller than the energy production achieved from large wind farms (Mega-Watts) or even home wind-systems (kilo-Watts). There are numerous challenges and opportunities for small scale wind energy harvesting for the purpose of bridge health monitoring, but the overarching issue ultimately boils down a

coupled design problem: to properly size the turbine and to choose the specifications of the generator for a given a power load requirement.

The predominant requirement of this project is to build a wind harvester to power a NI router. However, at this time, the given constraints from previous work suggest to mount the wind harvester underneath the bridge so that no permanent alterations are made to the bridge. Consequently, the wind harvester cannot interfere with bridge traffic below, which places a further constraint on the dimensions of the wind turbine blades. One of the challenges of this project is to verify whether or not there will be enough power given an area that satisfies the limitations of said constraint. The other challenge is to prove whether or not the turbine can achieve rotational speeds high enough to induce enough voltage in the generator and produce enough energy to power the load, given typical wind profiles under the bridge.

Previous work also suggested using a vertical axis wind turbine (VAWT), specifically one of the Savonius type. One of the main reasons behind this decision was the initial choice of the location of the prototype. Mounting the wind turbine underneath the bridge would result in the prototype being exposed to turbulent flow, varying wind speeds and directions. The Savonius style turbine was chosen because it handles those characteristics of wind profiles better than other turbines, and has a high start-up torque, meaning it can start turning at low wind speeds. However, Savonius turbines have performance limitations in that they can never rotate faster than the oncoming wind. Therefore, both horizontal axis wind turbines (HAWTs) and vertical axis wind turbines (VAWTs) should be explored and properly modeled to verify which type better satisfies

the predominant load requirement without any given constraints. In order to properly attack the coupled design problem, a hypothesis and a series of research objectives are outlined in the next section.

1.3 HYPOTHESIS AND RESEARCH OBJECTIVES

The hypothesis of this thesis is as follows:

> *A vertical axis wind turbine is more suitable to power a NI router than a horizontal axis wind turbine.*

The objectives of the research to support or reject this hypothesis are as follows:

- *Fully explore the design space of wind turbines in order to understand their performance and function*
- *Develop a detailed analytical model of dynamic wind turbine behavior*
- *Model the difference between horizontal and vertical axis wind turbines*
- *Design, build and test a prototype to validate the results achieved from the analytical model*
- *Benchmark the performance capabilities of a commercially available turbine*
- *Propose the next generation design of a wind turbine prototype*
- *Devise and test a methodology for non-destructively integrating energy harvesting onto structures*

1.4 ORGANIZATION OF THESIS

Chapter 1: Introduction

> This chapter gives the project overview as well as the challenges and opportunities for small scale wind energy harvesting for bridge health monitoring.

Chapter 2: Review of Literature

This chapter answers key issues proposed as questions that were addressed in order to gain a better understanding and perspective of the project.

Chapter 3: Analytical Modeling of a Wind Turbine

This chapter covers modeling the key equations that govern the general dynamic behavior of a wind turbine, as well the difference between VAWTs and HAWTs.

Chapter 4: Prototype Development and Experimentation

This chapter addresses the hypothesis proposed in the previous chapter through the design, construction and testing of a Savonius style VAWT.

Chapter 5: Next Generation Wind Turbine Design

This chapter discusses the benchmarking of a commercially available turbine and the design process of the next generation system, from blade size and geometry to generator specifications.

Chapter 6: Next Generation Attachment System

This chapter describes the methodology, case studies, design experiments and concepts associated with non-destructive attachment systems.

Chapter 7: Conclusions and Future Work

This chapter gives the conclusions derived from the thesis, as well as recommendations for work that lies ahead for this project as well as for the future of wind energy harvesting from a high level design standpoint.

Chapter 2: Review of Literature

2.1 INTRODUCTION

Wind power alone has enough potential to provide four times the amount of America's current electric capacity just by itself (Fernando, 2010). With a global energy crisis imminent in the near future, steps are being taken to harness reusable sources of energy such as wind to power commercial and residential sectors in order to decrease dependency on foreign oil and reduce overall carbon footprint. There have been numerous and significant efforts to explore the vast design space of wind turbines as well as to improve on existing ones. In order to gain more knowledge and a better perspective of the current level of maturity of wind turbine technology, the following questions have been proposed and thoroughly researched in preparation for the work to be completed on this project:

- *What is the current design space of wind turbines? How does one categorize them based on aerodynamic performance and function?*
- *What is the current state-of-the-art technology for small scale wind turbines and residential applications?*
- *Is it more optimal from an electricity generation and cost standpoint to have many smaller turbines or one larger one?*
- *What efforts have been made to optimize blade design for a given wind turbine?*
- *How does one decide upon the type and size of generator for wind turbines? What are the key specifications to consider?*

2.2 What is the current design space of wind turbines? How does one categorize them based on aerodynamic performance and function?

For over two millennia, mankind has been building wind turbines to harness renewable energy to aid in everyday tasks. Today's design space of wind turbines has expanded to drive machinery, pump water, and generate electricity. More and more ideas for new turbines have been evolving in order to perfect their ability to perform their respective tasks, but they can all still be classified based on function and aerodynamic performance. Wind turbines come in many shapes and sizes, but each turbine can generally be classified as either a Vertical Axis Wind Turbine (VAWT) or a Horizontal Axis Wind Turbine (HAWT). Each type of turbine has its respective advantages and disadvantages, which will be highlighted in this section.

Horizontal Axis Wind Turbines

HAWTs have been the most pervasive type of turbines since their origin with mankind and still continue to hold a majority of the wind energy harvesting market today. The current industry has concentrated most of its efforts to perfect all aspects of the HAWT and evolved it to be the most cost-effective and efficient way to harvest wind energy.

The superiority of the HAWTs is based on a couple of significant technological advances: pitch control and optimized blade design (Hau, 2011). In wind energy harvesting, it is extremely important to control the speed of the turbine in order to protect it from being damaged. There are currently two ways of accomplishing this task: stall and pitch regulation. In pitch regulation, blades are mechanically adjusted for an optimal

angle of attack based on changing wind speeds, while in stall regulation, blades do not change their angle of attack, but are designed to literally "stall" the turbine from reaching increasingly higher speeds (Horizon Wind, 2012). Stall regulation involves a more passive way to control the speed of the turbine, both aerodynamically and electrically (Design Styles, 2012). There is a limit to how fast the turbine can spin based on the design of the blades and its connection to the grid. The turbine essentially becomes a flywheel that keeps a constant speed (Design Styles, 2012). Stall regulation can cause problems with unnecessary vibrations in the turbine once it reaches this constant speed limit. This has led to a significant increase in the amount of pitch regulation turbines by a factor of 4 in the past 10 years. (Pitch vs. Stall, 2012). Pitch regulation has also proven to be more efficient in terms of power generation, because the cost of both systems is similar while pitch regulation can harness energy at higher wind speeds (Pitch vs. Stall, 2012). Smaller or less expensive turbines usually have an electro-mechanical way to essentially halt the turbine at the instant it reaches too high of a speed.

Traditional HAWTs harvest wind by pointing directly into the wind, and therefore require a yaw system. Large mega-watt HAWTs have a feedback-controlled yaw system that detects the wind direction and electro-mechanically adjusts the turbine for the appropriate attack angle, while small scale turbines have a simple vane to passively change the angle. Due to the shape and placement of the fins against the direction of the wind, a HAWT is self-starting yet it is propelled by lift forces and it can reach a tip to speed ratio much higher than 1. The tip to speed ratio (TSR) is defined as the ratio of the speed of the blade tip to the oncoming wind speed. Once it is rotated in the proper

direction thanks to the vane, the HAWT can easily reach high enough speeds to generate a beneficial amount of power.

There have been recent developments to modify the traditional HAWTs by changing the number of blades. Although much less popular, single and two bladed systems have a more structurally sound rotor and achieve a much higher TSR. However, they experience much higher stresses due to imbalances and cyclical loading, which make them less aerodynamically efficient. Additionally, they are much less aesthetically pleasing.

A revolutionary HAWT has also been recently introduced that abandons the use of a generator and produces voltage by passing magnets on the blade tips across stators mounted on the outer ring of the system (WindTronics, 2012). Because resistance is reduced, the start-up speed and efficiency of the system is increased. Conversely, it is extremely heavy and very expensive. The full classification table of HAWTs with their respective pictures is shown in Table 2.1.

Table 2.1: Classifications for different types of HAWTs and their advantages and disadvantages.

HAWT	Notes
 Three-bladed turbine (WindDose, 2012)	• Most pervasive turbine • Low torque ripple • Large swept area proportional to blade size • Max efficiency at TSR ~7 • Gear box included in large scale turbines • Upwind variety has ability for yaw and blade pitch control • Downwind variety always keeps in line with wind, but mast wake causes turbulence • Most aesthetically pleasing
 Two-bladed turbine (Design Styles, 2012)	• Simpler and more efficient rotor structure • Max efficiency at TSR ~10 • Higher cyclic loading • Teeter hinge can be introduced to reduce high cyclic loading • Less aerodynamically efficient than three-bladed system

Table 2.1: Classifications for different types of HAWTs and their advantages and disadvantages (cont'd).

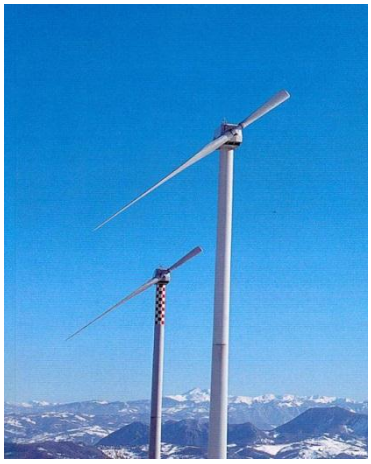 One-bladed turbine (Design Styles, 2012)	• Most structurally efficient for rotor blade • Max efficiency at TSR ~15 • High TSR violates noise emission requirements • Less efficient and has more complex dynamics to relieve loads due to counterweight
 Blade Tip Power System (WindTronics, 2012)	• Produces voltage by passing magnets across stators mounted on outer ring • Eliminates need for generator and gearbox, decreasing resistance • Extremely low start-up speed ~0.5 mph • Fairly heavy ~250 lbs.

Vertical Axis Wind Turbines

VAWTs have progressed to expand into a much wider design space than HAWTs. The first ever VAWTs were used on Persian boats in 900 AD. Significant technical advances and innovations have been made in the past century (Eriksson et al., 2008). They originally started out as drag-based turbines, but a revolutionary leap occurred when French engineer Darrieus proposed the idea of a lift-based VAWT in 1925.

Continual progress has been made ever since (Hau, 2011). VAWTs have many advantages over HAWTs in that the gearbox, generator, and all other supporting electronics can be mounted at the ground level. This not only reduces the weight and cost of the transmission shaft, but it is also much easier to access for installation and repair (Design Styles, 2012). VAWTs also do not need a yaw system because they are omni-directional and can harness wind from any direction instantaneously. Another advantage is that VAWTs can be installed more closely together in wind farms. HAWTs have a detrimental effect on the laminar flow of the surrounding air, and therefore need to be placed apart at a distance of at least ten times their width (Coyle, 2011). However, because VAWTs have only recently been introduced to the market, they still have much room for development in order to make them competitive with HAWTs based on a cost per Watt-hour produced.

VAWTs exhibit the most amount of variety within their category. Derivatives of the vertical axis types have explored different structures in order to try to account for the disadvantages associated with their predecessors. However, most VAWTs can be classified as either a Savonius or Darrieus based on their aerodynamic performance. Savonius style turbines use drag forces to commence their rotation, while Darrieus style turbines rely on lift forces. The advantages that Savonius turbines have are that they are self-starting if they have more than three blades, and are therefore extremely reliable in a turbulent wind conditions. Savonius turbines are used in most scenarios where reliability is a more important factor than efficiency, such as anemometers in remote locations (Coyle, 2011). They have a high start-up torque, meaning they generate a lot of torque

when a wind force is applied. This makes them appealing for high torque, low speed applications such as driving machinery or grinding grain. On the other hand, the drag-based turbine can never reach a TSR higher than 1, meaning that the tips of the turbine can never spin faster than the relative cut-in wind speed. This is very detrimental to electricity generation because it becomes difficult to reach speeds high enough to power a generator. Most existing Savonius turbines on the market are constructed at a large scale so that their torque can be high enough to turn a generator connected to a gearbox. Savonius turbines of the twisted variety have been developed in order to reduce the high torque ripple of their predecessors. The twisted Savonius experiences a constant torque due to the wind, as opposed to the original Savonius that experiences resistance during certain orientations of the blades. However, multiple experiments have been conducted and results have proven that there is no significant difference between the power coefficients of the two types of Savonius turbines (Kamoji et al, *Renewable Energy* 2008). Furthermore, their complicated shape makes them very expensive.

On the complete opposite side of the VAWT spectrum, Darrieus style turbines are used for high speed and low torque applications. The traditional ones exhibit an "egg-beater" shape, and have blades shaped similarly to the wings of an airplane, and are therefore powered by lift forces. This enables them to reach a TSR much greater than 1, which is more beneficial to electricity generation. The problem with traditional Darrieus turbines is that they are not self-starting and therefore need an external power source or a Savonius turbine in order to begin their rotation. Darrieus turbines also have a high-torque ripple which induces large cyclical loads onto the shaft and bending moments on

the blades, so they were originally supported with tension cables (WindDose, 2012). Giromills, or H-rotors, mirror the behavior of Darrieus turbines but bear straight blades. They also have the option of blade pitch control like HAWTs commonly do, further categorizing them as cycloturbines. Cycloturbines are more efficient in turbulent wind conditions, but are much more expensive due to the machinery and electronics required to sense wind direction and appropriately adjust the blades. Finally, Gorlov Helical turbines are the most advanced derivatives of the Darrieus variety. By essentially twisting the blades of an H-rotor turbine, Gorlov turbines solve most problems that Darrieus turbines originally had; they are self-starting, have a low-torque ripple and essentially zero head, meaning there are no friction forces against the fluid's motion (Munson et al., 1998). However, their complicated shape makes them very expensive. Hybrid Darrieus-Savonius turbines have been tested to have higher power coefficients than traditional Savonius turbines, and have the ability to self-start unlike traditional Darrieus turbines (Gupta, 2006). Additional concepts include the Venturi turbine, which claims to have a higher efficiency than Betz's limit based on the spherical shape inducing a low pressure area that attracts an additional laminar flow (Ragheb, 2011). Betz's limit will be defined in a later section. The advantages and disadvantages of various VAWTs are summarized in Table 2.2.

Table 2.2: Classifications for different types of VAWTs and their advantages and disadvantages.

VAWT	Notes
 Savonius (Green Energy, 2012)	• Low speed, high torque • Uses drag-based forces • Self-starting with more than three blades • Max efficiency at TSR < 1 • Used to drive machinery (grind grain, pump water) • High resistance head • Can deal with turbulent conditions • Used for anemometers
 Twisted Savonius (Helix Wind, 2012)	• Modified Savonius blade • Max efficiency at TSR < 1 • Torque due to wind is smoothed out over entire rotation period • More efficient than conventional Savonius • Expensive to manufacture

Table 2.2: Classifications for different types of VAWTs and their advantages and disadvantages (cont'd).

 Darrieus (WindDose, 2012)	• High speed, low torque • Uses lift-based forces • Not self-starting, needs external power source • Max efficiency at TSR ~5 • High torque ripple • Inability for blade pitch control • Expensive to manufacture
 Giromill or H-rotor (WindDose, 2012)	• Exemplifies same behavior as Darrieus, but with more simple, straight blades • Ability for blade pitch control
 Gorlov helical (WindDose, 2012)	• Darrieus turbine in a helical formation • Self-starting • Max efficiency at TSR ~5 • Low torque ripple • Zero resistance head • More efficient than conventional Darrieus turbines • Very expensive to manufacture

Table 2.2: Classifications for different types of VAWTs and their advantages and disadvantages (cont'd).

 Hybrid Darrieus-Savonius (HiVAWT, 2012)	• Combination of lift-based and drag-based forces • Self-starting • TSR limited by the Savonius blades
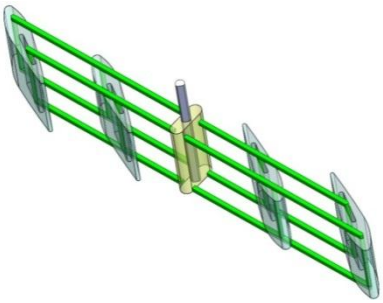 Cycloturbine	• Giromill variation with blade pitch control • Maximizes power output by pitching blades always in direction of wind • Self-starting • More efficient in turbulent conditions • Complex, heavy, and needs wind direction sensing equipment
 Venturi turbine (Venturi Wind, 2012)	• Darrieus-style turbine mounted horizontally • Claim to have higher efficiencies than Betz's limit, up to 80% • High start-up torque • Low torque ripple

Table 2.2: Classifications for different types of VAWTs and their advantages and disadvantages (cont'd).

 Aerogenerator (Grimshaw, 2012)	• Offshore wind turbine concept • Rigid sails that generate lift • Concentrates weight at base, less prone to fatigue and failure from high winds • Half the height and easier to service than traditional VAWTs • Capable of up to 10MW

Power Coefficients

The existing design space of wind turbines has been explored, and the advantages/disadvantages have been discussed. There still remains one important aspect to consider when choosing a turbine for a specific application: the power coefficient. The power coefficient is the ratio of electrical power produced over the amount of power available in the wind. Using conservation of energy and mass equations, this theoretical efficiency limit of a wind turbine can be calculated to be .593, meaning that no turbine can capture more than 59.3% of the energy available in the wind. (Khaligh & Onar, 2010). This is known as Betz's Law. The aerodynamic behavior varies according to the wind turbine type, which leads to each turbine exhibiting a different power characteristic curve. Analytically, this curve can be determined through complicated fluid dynamic models or through methods that estimate power coefficients by solving continuous-time nonlinear systems (Mok, 2005). However, what is more common is to model the curve

using empirical models by running a series of controlled experiments. The power coefficient can be calculated in one of two ways. The first method is to calculate the energy available in the wind before and after it hits the turbine, and assume the decrease of energy was transferred to the turbine. The second method is to calculate the ratio of electrical power produced to the amount of power available in the wind.

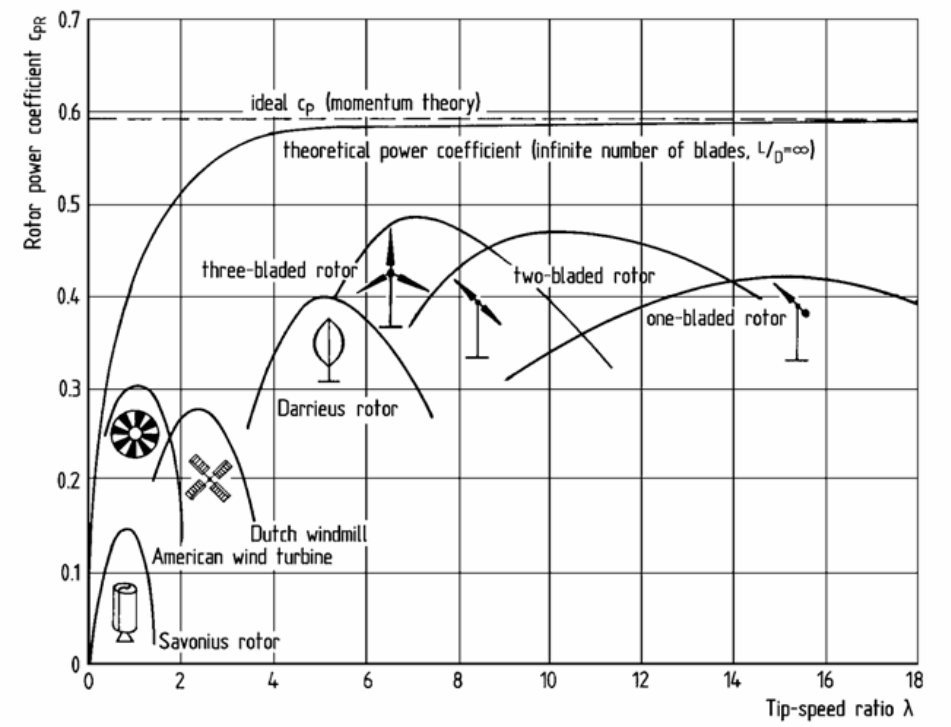

Figure 2.1: Power characteristic curves for different types of wind turbines (Hau, 2011).

As Figure 2.1 shows, the theoretical power coefficient assumes an infinite number of blades and reaches a limit just below 0.6. Different power characteristic curves for practical turbines are shown in the figure as well. It should be noted that the Savonius rotor has a maximum efficiency of 0.15 at a TSR of around 1. Once the TSR increases past 1, the Savonius rotor rapidly decreases in efficiency. All of the other turbines which

are lift based exhibit significantly higher efficiency levels and TSRs, meaning that they can harness more energy from the wind and rotate at speeds beneficial to electricity generation. The Darrieus rotor has a power coefficient of 0.4 and spins at much higher TSRs, while the HAWT has the highest power coefficient at around 0.5 and spins at even higher TSRs. These power characteristic curves will be slightly different based on the many derivations of the traditional VAWTs and HAWTs, and will even vary from turbine to turbine. However, because the aerodynamic fundamentals are maintained for each turbine, the assumption can be made that each turbine follows the basic curve shown in Figure 2.1.

2.3 What is the current state-of-the-art technology for small scale wind turbines and residential applications?

The wind harvesting technology introduced with the large-scale commercial turbines has been scaled down and optimized for residential and other small scale applications in recent decades. State-of-the-art small-scale wind turbines are now widely available on the market for personal and business use. In order to understand which turbines are most suitable for residential applications, it is important to understand how they are categorized with respect to type and scale.

As stated in the previous section, VAWTs are beneficial because they can deal with turbulent wind conditions and can therefore harness wind energy from any direction. This sounds beneficial for a resident who is unsure of the wind characteristics in his area, but there are many downsides to VAWTs, as have been discussed in the previous section. These downsides create complications for home users who want a simple “set it and forget it” type of wind turbine, and do not want to spend an excessive amount of money.

The HAWT is the cheapest, most feasible wind turbine for residential applications based on its pervasiveness in the market and its ability to reach speeds high enough for electricity generation.

The idea of simply capturing wind energy using a turbine is fairly straightforward, but it becomes more complicated when dealing with how to condition and store this energy once it is harnessed. The state-of-the-art HAWT turbines can be classified as either off-grid or on-grid. If a residence already receives its power from an electrical company, then it needs a turbine that be integrated into the grid. If a residence such as a remote cabin or RV is powered by a battery system, it needs an off-grid wind turbine. This in turn leads to categorizing the wind turbines into specific sizes and power ratings. Small turbines have been defined by an International Electrotechnical Commission (IEC) standard. These standards have been established based on design requirements, noise emission, and power performance. All small wind turbines by definition are required to have a power rating of less than 50 kW, or a swept area less than 200 m^2 (Wood, 2011). In some countries, the limit of 50 kW has been defined as the maximum amount of power that can be safely integrated into the grid from a residential application (Wind Energy, 2009). Large mega-watt turbines have been designed in conjunction with appropriate transformers by the industry. The complete categorization of small turbines can be seen in Table 2.3.

Table 2.3: Classification of small wind turbines (Wind Energy, 2009).

Rated Power	Rotor Swept Area	Sub-category
$P_{rated} < 1$ kW	$A < 4.9$ m^2	Pico-wind
1 kW $< P_{rated} <$ 7 kW	$A < 40$ m^2	Micro-wind
7 kW $< P_{rated} <$ 50 kW	$A < 200$ m^2	Mini-wind

The power rating of the small wind turbines is usually in conjunction with a design for an off-grid or on-grid application. Pico-wind turbines are almost always designed for off-grid applications to charge remote battery banks, while mini-wind turbines are most often designed to be integrated to the grid. The micro-wind category is the ambiguous transition from one category to the next. It is common in industry to design both off and on-grid turbines in the micro-wind category.

Another crucial item to take under consideration if a wind turbine is going to be purchased for residential applications is the power classification map in the installation area. Solar panels and PV cells are installed in areas with a large amount of sunlight in order to maximize the power outputs. Similar considerations apply for wind energy. As Figure 2.2 shows, it appears more beneficial to install wind turbines in the Midwest and plains states, rather than the southeast area of the country. Research should be conducted on whether or not it is makes economic sense to install wind turbines in a particular area. If it seems unfeasible, solar panels should be taken into consideration as another renewable resource.

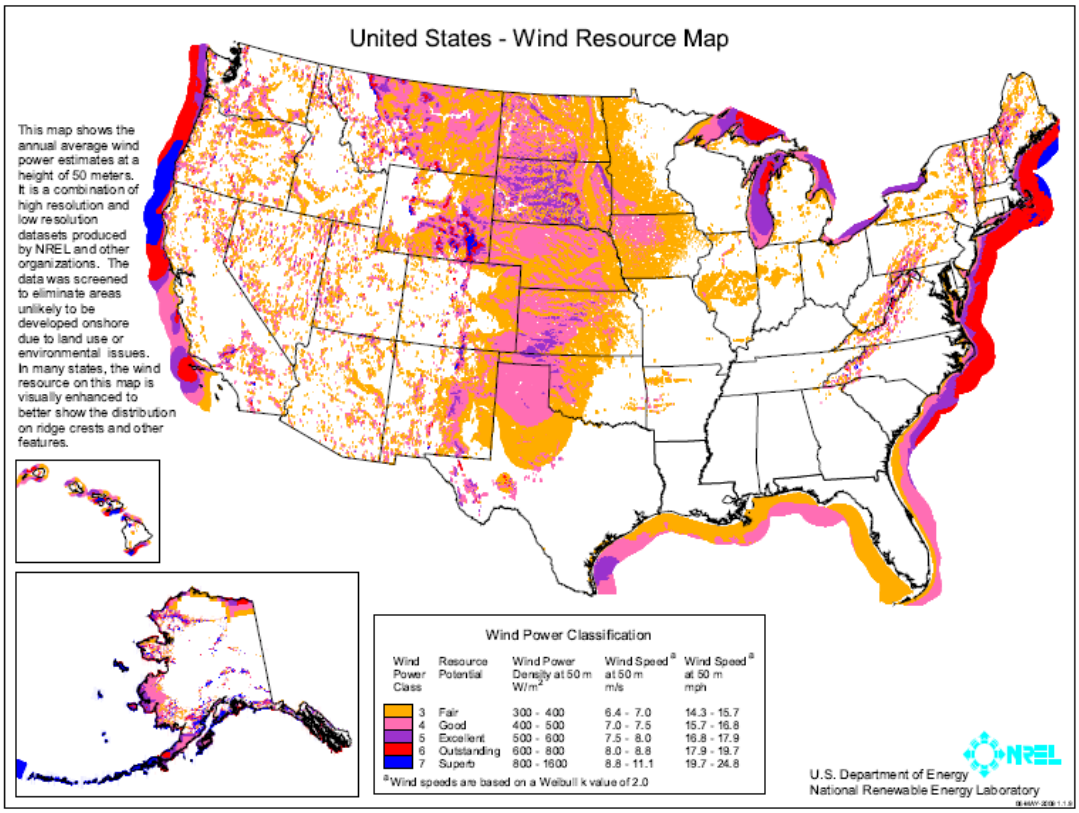

Figure 2.2: Wind power classification map of the United States (NREL, 2011).

Now that we have defined the type and scale of turbines most suitable for residential applications, we can introduce two great examples of HAWTs that are at the vanguard of their field. One is the *Skystream 3.7* and the other is the *AIR Breeze Marine 12V DC Wind Generator*, both sold and distributed by Southwest Wind Power (see Figure 2.3).

Figure 2.3: On-grid Skystream 3.7 (left) and off-grid AIR Breeze (right) wind turbines (Southwest Windpower, 2012).

The *Skystream 3.7* has a power rating of 2.4 kW, putting it in the micro-wind category; the *AIR Breeze* has a power rating of 300 W, putting it in the pico-wind category. The *Skystream 3.7*, which generates around 400 kWh per month, is used for on-grid applications while the *AIR Breeze*, which generates around 38 kWh per month, is used for off grid applications. The fact that they are off-grid and on-grid is directly associated with the amount of power they are capable of producing, as previously discussed. A typical American home consumes approximately 780 kWh of electricity per month (Four Seasons, 2012). The approximate energy outputs of the *Skystream* and *AIR Breeze* wind turbines are equivalent to around 50% and 5% of the typical consumption rate of an American household, respectively (Southwest Windpower, 2012). The assumption here is that both turbines experience an average wind speed of 12 mph. Therefore, two *Skystream* turbines can generate enough energy to power a house, and two *AIR Breeze* turbines can power most of the household appliances, such as televisions and microwaves, based on the pie chart in Figure 2.4.

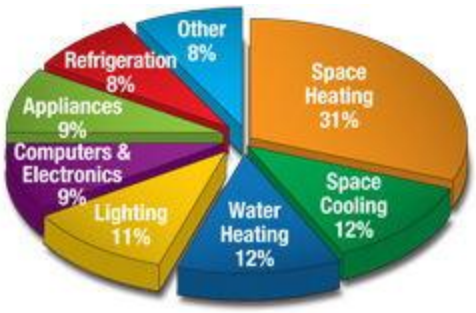

Figure 2.4: Average distribution of energy consumption in an American household (Energy Saver, 2012).

The fact that wind turbines can generate enough energy to power a household is a great step towards alleviating our dependency on non-renewable energy sources, such as oil and gas, but it comes with a price. The Skystream costs around $15,000. The average cost of electricity in the US is around 12 cents/kWh (Electric Power, 2012). As a result, a typical household spends around $1,120 per year on electricity. Assuming two *Skystream* turbines alone can power the average household, the money spent on purchasing the turbines will only start paying off after 25 years. This is the crucial statistic that is hindering residential use of wind energy. Therefore, people are more inclined to simply reduce their monthly electric bill by installing small scale turbines, such as the *AIR Breeze*, which only costs around $1,000. However, these wind turbines are also more useful for remote applications, such as camping or boating trips, in order to power crucial appliances when a grid source is not available.

Although there has been a significant improvement in wind turbine technology over the past 20 years, wind energy has made a relatively insignificant impact on the overall rate of renewable energy consumption in the US. Based on detailed logs kept by the US Energy Information Administration, residential sectors rely on geothermal, solar

and biomass (wood) as their main sources of renewable energy, while commerical sectors rely on the previously mentioned sources plus hydroelectric power and a very insignificant amount of wind energy. The respective data for energy consumption in trillions of Btu in 2010 is displayed in Tables 2.4 and 2.5.

Table 2.4: The renewable energy consumption of the residential sector in the US in 2010 (Renewable Energy, 2012).

	Residential Sector			
	Geothermal	Solar/PV	Biomass (wood)	**Total**
2010 Total (Trillion Btu)	37	97	420	**554**

Table 2.5: The renewable energy consumption of the commercial sector in the US in 2010 (Renewable Energy, 2012).

	Commercial Sector								
	Hydro-electric	Geo-thermal	Solar/ PV	Wind	Biomass				**Total**
					Wood	Waste	Fuel	Total	
2010 Total (Trillion Btu)	1	19	0.5	0.5	70	36	3	109	**129**

Wind energy, which is highlighted above, may play a small role as a renewable energy source, but as stated before it has enough energy potential to power America four times over. Although it is expensive to install turbines, wind is still a relatively untapped resource and should be made more prevalent around the US, especially in the residential sectors. The fact that it only takes 25 years to pay off the installment of a couple wind turbines to power a home signifies that wind energy can be extremely beneficial for

future generations. If the necessary steps are taken now, then our dependancy on oil and other soon-to-be depleted resources will greatly diminish.

2.4 Is it more optimal from an electricity generation and cost standpoint to have many smaller turbines or one larger one?

The wind turbine industry is continually exploring whether or not it is more beneficial from a cost and energy harvesting perspective to have many smaller turbines or one larger turbine. The assumption here is that the combined power output of the smaller turbines equals that of the larger turbine, and the smaller turbines are scattered over a widespread area. At first it seems more beneficial to have one large turbine from manhour and installation standpoints. However, during variant and stagnant wind conditions, the large turbine would fail to spin and produce electricity because of a lack of wind. Therefore, it might be more beneficial to have an array of small turbines with a couple of them spinning and generating power from areas that are experiencing better wind conditions, since they are scattered over a larger area. These postulations were investigated in this section.

First of all, the difference between a small and a large turbine needs to be revisited. The IEC standard (IEC 61400-2) for small turbines is a power rating of less than 50 kW (Wood, 2011). Almost all large turbines are used for strictly commercial turbines and are standardized for industry. Small turbines are used in two different applications. The first is off-grid, or autonomous applications where the turbines control their own voltage and power output and are used in remote locations without access to any electrical grid. The other is on-grid, or distributed generation applications, where the power generated by the turbine can be integrated, or "sold" back to the grid (Wind

Energy, 2009). Second of all, only HAWTs with three of more blades will be taken into consideration in order to avoid complications of comparing turbines across different domains.

One way to numerically quantify which set of turbines would be more beneficial is to note the cost per installed kW of power. Currently, the average costs for off-grid small turbines and on-grid small turbines range from $4000 - $8000 per kW, and $5000 - $10,000 per kW, respectively (Wind Energy, 2009). The increased cost for the on-grid small turbines is the power converter from DC to AC needed to connect to the grid. In stark contrast, large wind turbines have been perfected to be manufactured and produced at a cost of only $2000 per kW, which is a mere 30% of the average cost of the off-grid small turbine. The reason for this drastic difference in cost per kW is the technological advances that have been made for industrial sized turbines. Large turbines have a more "active" way of harnessing wind energy. First, they have stall control or blade pitch control to be able to continuously capture energy at very high wind speeds (Wind Energy, 2009). An advanced smaller turbine typically has an electromechanical system that stops the turbine from spinning in order to prevent damage, which significantly reduces the power efficiency. Secondly, large turbines also have active yaw control systems that detect changes in wind direction and rotate the turbines accordingly. Smaller turbines have passive yaw control with vanes, making them more unstable with rapidly changing directions. Lastly, large wind turbines are built much taller than small turbines. This is because there is significantly more energy available in the wind at increasing heights,

making larger turbines more productive and increasing their useful lifespans (Green, 1999). These become significant hindering factors for small wind turbines.

For increasingly smaller turbines, additional problems arise. It becomes more detrimental to use permanent magnet generators, which is the most common generator used in pico-wind category. The reason for this as an increase in the ratio of cogging torque to the rated torque, as will be discussed in Section 2.6. A decrease in size of the turbine itself will also cause a decrease in swept area and ability to overcome the cogging torque of the generator. This implies that an induction generator is needed for smaller turbines, but this consequently requires supporting electronics to induce a voltage output as the induction generator is not self-exciting. Furthermore, no wind turbines in industry with a power rating less than 1 kW (pico-wind turbines) use an induction generator (Wind Energy, 2009). Therefore, it appears to be more beneficial to install one large turbine as opposed to many smaller ones.

2.5 What efforts have been made to optimize blade design for a given wind turbine?

There have been numerous efforts to optimize wind turbines in order to increase their efficiency. Most of the recent significant have improved the electromechanical systems that maximize power output, such as stall and blade pitch control. However, there have been many experiments and simulations that attempt to optimize the basic mechanical aspects of wind turbines, such as the quantity and shape of the blade, for both HAWTs and VAWTs.

One crucial parameter that governs the efficiency of a wind turbine system is the aspect ratio. For HAWTs, the aspect ratio is the ratio between the radius and thickness of

the blade. It is essentially the slenderness of the blades: the higher the aspect ratio, the more slender the blades. For VAWTs, the aspect ratio is the ratio of the height to the radius (Jamieson, 2011). Ideally, an infinite aspect ratio is desired to minimize the amount of induced drag caused by the aerodynamic forces of the blades, as well as to minimize the amount of turbulent flow, which is essentially unusable wind energy. A comparison of a realistic and theoretical aspect ratio is shown below for a two-bladed Darrieus VAWT, and an actual HAWT.

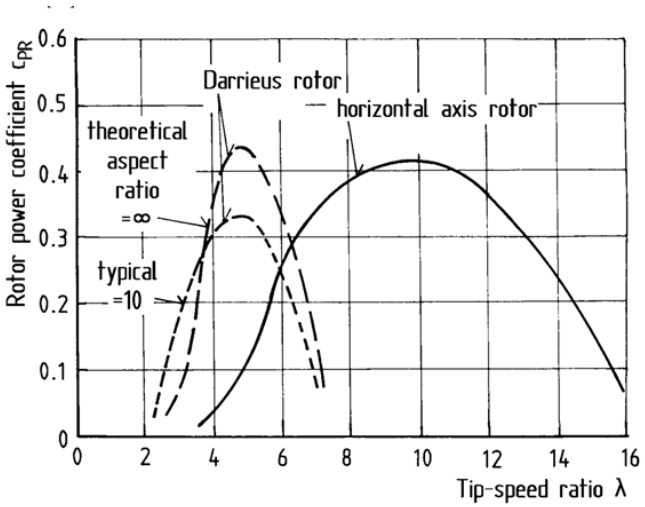

Figure 2.5: Power coefficients for two bladed Darrieus VAWTs and standard HAWTs (Hau, 2011).

Figure 2.5 shows that the power coefficient increases by 57% from an actual to a theoretically infinite ratio between the length and thickness of the blade. However, it should be noted the TSR, or essentially the angular speed, is nearly half of a HAWT, meaning that it needs more torque in order to generate the same amount of power. To achieve this, the size of the blades would need to be increased for a larger swept area, thereby increasing their weight and cost, further proving an earlier discussion point that

VAWTs need significant improvement before they reach the level of maturity of HAWTs.

An experiment completed at the University of California at Berkeley came to same conclusion that blades with thinner airfoils designs exhibited better power characteristic curves (Inamdar, 2009). This is because thicker blades create more turbulence closer to the airfoil. Turbulence absorbs some of the energy available in the fluid and consequently decreases the amount of energy transferred to the rotor (Inamdar, 2009). A thinner blade causes separation of the boundary layers further downstream from the rotor.

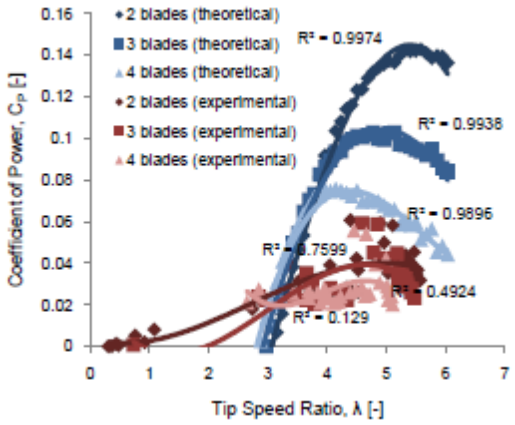

Figure 2.6: Theoretical effect of the number of blades on the power characteristic curve (Inamdar, 2009).

Theoretical simulations also indicated that the number of blades on a HAWT has a significant effect on the power characteristic curve, as can be seen in Figure 2.6. It is more beneficial to have fewer blades at higher TSRs and more blades at lower TSRs (Inamdar, 2009). The reason for this is that mroe blades will be able to capture more energy at lower speeds due to the fluid buildup at the front of the rotor. On the other

hand, fewer blades will inherently have less inertia and will be able to spin faster by capturing a more laminar flow.

For the purposes of the bridge monitoring project, attempts to optimize small scale Savonius style VAWTs are discussed from this point forward. There has not been nearly as much effort dedicated to improve the design of Savonius VAWTs as opposed to HAWTs based on Savonius turbines' inherently low rotational speeds. However, previous experiments have been conducted to try to optimize the design of the Savonius in order improve upon its efficiency. One such attempt was to insert an obstacle that shields the returning Savonius blade in order to reduce the amount of drag that the blade experiences rotating against the wind. A series of simulations were run using computational fluid dynamics, and the results proved that an obstacle shielding the returning the blade significantly increased the power characteristic curve of the Savonius turbine by 39%, seen in Figure 2.7 (Mohamed et al, 2010). The only problem with inserting the shield is that it would only work for wind coming from a certain direction.

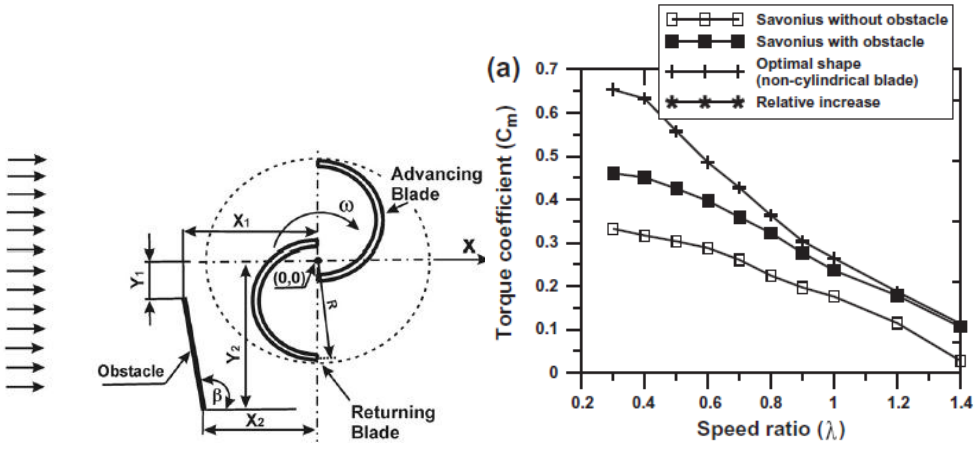

Figure 2.7: Schematic of the Savonius setup with an obstacle, along with the results from the simulated experiments (Mohamed et al, 2010).

Saha et al. (2008) have also conducted a thorough simulation of numerous variations of Savonius turbines. The three variables included in these experiments were the number of stages, the number of blades, and the blade geometry. The number of stages varied between single, two, and three-stages; the number of blades varied between two to three blade; the shape varied between semicircular to twisted. Once again, simulations like these were conducted for the purpose of achieving a simple, low cost and reliable Savonius VAWT design with a higher efficiency. The results indicated that the optimal turbine configuration consists of a twisted, two-bladed, two-stage rotor (Saha et al, 2008). Normally, a two-bladed turbine would not always be self-starting. However, introducing a second stage with differently aligned blades eliminates this problem. Furthermore, increasing to three stages or three blades decreased the efficiency due to a relative increase in inertia, while a twisted rotor decreases the torque ripple of the system.

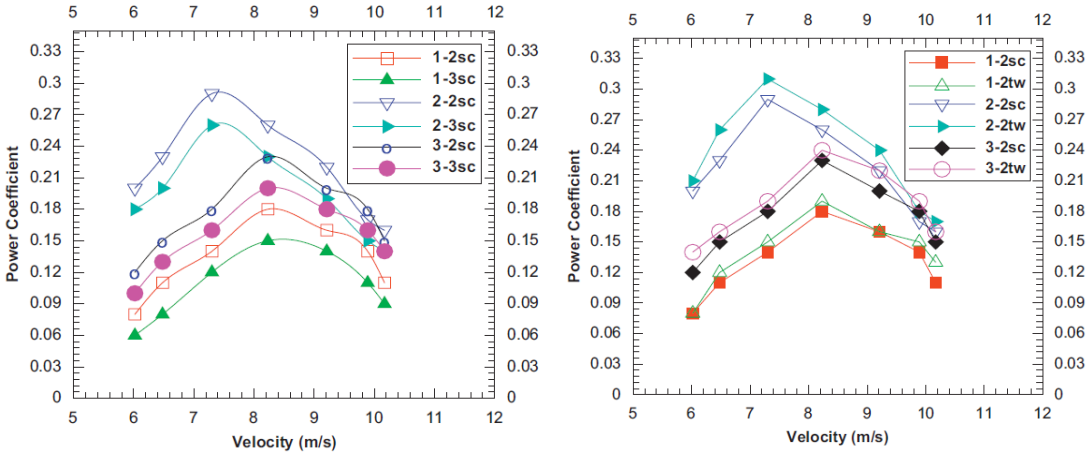

Figure 2.8: Power coefficients of different Savonius combinations with respect to wind velocity (Saha et al, 2008).

Furthermore, combinations of different VAWTs have also been tested for an improved efficiency. As previously discussed, a hybrid design could improve the overall

efficiency and reliability. Through the design of an experimental hybrid Darrieus-Savonius turbine, Alam and Iqbal used a two-stage, two-bladed Savonius rotor as was proposed by Saha et al. (2008) to be the most optimal Savonius design. Their experiment proved that a hybrid design has an improved power coefficient compared to the traditional counterparts (Alam & Iqbal, 2010). It can be observed that there are continuous efforts being made to improve the highly reliable, yet inefficient Savonius turbine for small scale wind applications.

2.6 How does one decide upon the type and size of generator for wind turbines? What is used in conjunction with different generators?

There are many crucial events that occur downstream from the generator once the wind turbine start spinning. For small scale turbines, it could be as easy as connecting the generator to a simple charge controller and a battery, or in some occasions such as do-it-yourself turbines, simply using motors run backwards as generators. However, this process increases in complexity for larger turbines with different type of generators. Once these turbines are connected to a grid, they also have to abide by International Electrotechnical Commission (IEC) requirements as well. The most important requirements are outlined in Table 2.6 below.

Table 2.6: Requirements of grid-connection of large wind turbines (Hau, 2011).

Prevention of motor operation (reverse-power protection)
Rapid disconnection of generator from the grid if grid voltage or frequency exceeds or drops below certain limits
Compensation for the reactive-power requirement to a power factor $cos\ \varphi = 0.9$
Connection of the induction generator only within a range of about 95% to 100% of the synchronous speed

Large turbines most frequently use induction generators (IGs), whose voltage is rectified in the nacelle and inverted again in the base of the tower in an AC-DC-AC fashion (Hau, 2011). This power is then transformed and transmitted back into the grid. However, additional voltage must be supplied to comply with the requirements above. Feedback control systems must be implemented to stop the generator from acting as a motor when regulating voltage is applied, to connect the generator during synchronous periods, and to disconnect the generator from the grid during potentially dangerous events. Furthermore, the reactive power from connecting to the grid must be a balanced to a factor of 0.9, which requires controlling the output of the generator. These complex solutions are mostly used for large scale wind energy applications. However, it is common for small scale turbines to combine the control and monitoring system into one switchbox because of the lower voltage outputs. When it comes to a question of scale, choosing the right generator becomes the more critical issue in order to improve the effectiveness of the turbine.

One key specification to consider when choosing generators is whether or not to mount a gearbox. The original intent of gearboxes on motors when a voltage is applied is to decrease output speed and increase output torque. A higher torque defines a higher acceleration applied to a given load on the motor in order to be able to handle larger load sizes (Hughes, 2005). The intent of a gearbox on a generator is to increase the alternator RPM and therefore increase the voltage generated when an external torque is applied from the coupled wind turbine. However, this purpose is not always reflected when the motor is run backwards as a generator. Gearboxes are not common on smaller rated

turbines and are losing popularity on larger rated turbines. For reference, the IEC standard (IEC 61400-2) for small turbines is defined to have a power rating of less than 50 kW (Wood, 2011). Anything more than this standard is considered a large turbine. The reason for this is because gearboxes introduce mechanical failure modes and losses in efficiency that have a significant effect on the maximum power that can be drawn from smaller turbines (Wood, 2011). These losses become more negligible at a larger scale, but are still nevertheless losses.

Gearboxes are also used in conjunction with different type of generators and different sizes of wind turbines. Permanent magnet generators (PMGs) are more common on small turbines, because they are more efficient at low RPM and therefore have no need for a gearbox. On the other hand, induction generators (IGs) are more common on large turbines because they are inexpensive, mass produced, and easy to replace (Wood, 2011). PMGs are also more suitable for smaller turbines because they are self-exciting. Once the PMGs overcome the start-up torque due to the mechanical and magnetic inertia inside, they conveniently produce a DC voltage once they start spinning (Hau, 2011). IGs require additional equipment and electronics, such as encoders in order to properly adjust the excitation capacitance at different speeds and successfully produce a rectified and usable voltage (Wood, 2011). These induction generators also need to be individually customized because the cable length between the generator and the controller has a significant impact on the excitation capacitance. Furthermore, if a stagnant turbine connected to an induction generator suddenly experiences a gust of wind, the induced acceleration may be too high to properly excite the generator. A study

was also completed with various IGs, and it was shown they lose their efficiency as their power rating decreases (Wood, 2011). The reason IGs are used in large commercial turbines is because the location has been carefully based on wind speed characterizations. As discussed earlier, large turbines already have additional electronics that control the yaw, mechanical breaking to prevent failure, and the blade pitch angle. Therefore, an additional control system that properly excites the IG by adjusting the generator speed can easily be integrated into the turbine. Small turbines are meant to be placed in remote locations where the wind speed characterizations are not necessarily known, which justifies the need for a PMG that can be excited at any speed to produce a DC voltage. This can be convenient for off-grid or residential applications that simply need to recharge batteries. The supporting electronics, customization issues, and decreasing efficiency indicate that it becomes difficult to use induction generators on small turbines.

PMGs are most beneficial for small scale turbines. PMGs are convenient in that they can produce a DC voltage, but one of their disadvantages is that they have an inherent start-up torque, or referred to as "cogging torque" in literature (Kikuchi & Kenjo, 1998). Mounting a gearbox to PMGs only increases the cogging torque and therefore the amount of wind required to overcome it. PMGs are already highly efficient at low RPMs, so there is no need to install a gearbox on a smaller turbine. Furthermore, mounting a PMG on a larger turbine requires large and very expensive magnets to be constructed for that PMG. This causes an increase in cost and a non-beneficial return on investment. That is why the most common generators in large, industrial turbines are IGs. Most are also coupled with one or more sets of gearboxes because of their lack of

cogging torque. Nevertheless, both PMGs and IGs are used in large scale turbines. Studies have shown that IGs are still the most attractive in terms of cost per kW. Polinder et al. (2006) have compared the energy yields over the total cost of different generators used in large scale commercial turbines. The five generators that were compared were a double-fed induction generator with a three-stage gearbox (DFIG3G), a direct-drive synchronous generator with electrical excitation (DDSG), a direct-drive permanent magnet generator (DDPMG), a permanent-magnet generator with single stage gearbox (PMG1G), and a doubly-fed induction generator with single-stage gearbox (DFIG1G). Table 2.7 shows that the induction generator with a single-stage gearbox is the most attractive in terms of cost per kW.

Table 2.7: Annual energy yield over total cost for the five generators (Polinder et al., 2006).

Generator	DFIG 3G	DD SG	DD PMG	PMG 1G	DFIG 1G
kWh/Euro	4.13	3.72	4.05	4.16	4.25

The fact that PMGs themselves are more costly at large scale is not the only reason for their lower kWh cost ratios. They pose a significant problem when used in large numbers and high voltage grid applications. This has to do with meeting the IEC standards for reactive power, which is the power supplied from the grid. A power factor ($cos\ \varphi$), must compensate for this reactive power when connecting to the grid. For synchronous IGs, the power factor can be controlled with capacitors, supporting electronics, and by regulating the terminal voltage (Hau, 2011). However, because PMGs self-excite an uncontrolled DC voltage, the power factor becomes very poor and

must be compensated for using inverters and filters that control this reactive power, therefore increasing the cost of wind turbines.

Now that we have established that PMGs should be used for small scale turbines we can theoretically construct smaller and smaller PMGs to mount on smaller and smaller turbines, but this is not the case. It becomes difficult to harvest energy from PMGs if we further decrease their scale. PMGs have a disadvantage in that as they become smaller, the ratio of their cogging torque to their nominal torque increases (Wood, 2011). This can be verified through an empirical study completed in industry. Figure 2.9, whose vertical axis is logarithmic, displays an increase in the ratio of the cogging torque over the rated torque as the rated power decreases. Furthermore, it has been shown that in order for a turbine to start at a low cut-in wind speed—around 6 mph—the cogging torque should be around 1% of the generator's rated torque (Tudorache et al., 2010). These two factors create a limitation for not only how small PMGs can be before they become detrimental, but also for how small the turbine can be to initiate electricity generation in the PMG. With both PMGs and IGs losing their efficiency as they become undersized, it becomes very difficult to construct complementary wind turbines on smaller and smaller scales with a beneficial and realistic power output.

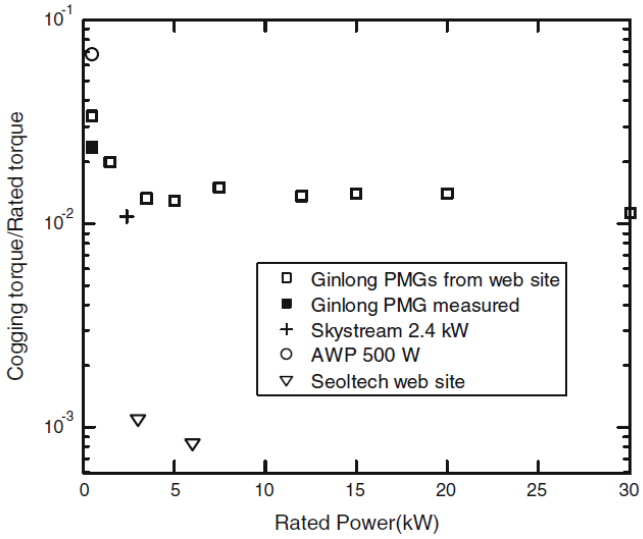

Figure 2.9: Ratio of cogging torque to the rated torque for various PMGs (Wood, 2011).

In order to achieve a desirable voltage output for small scale turbines, it becomes a question of designing the right generator for the specific application. Efforts have been made to design a low speed PM generator specifically for wind turbine applications. Madescu et al. (2011) have analyzed electromagnetic design elements, such as number of coils, inductances, and magnetic pole combinations in order to minimize detrimental effects such as cogging torque. The bridge monitoring project could be expanded into designing such a generator in the future. However, it should be noted that the generator specifications will be unknown until tested and efficiencies will not be as high as commercially available generators.

2.7 DISCUSSION

The insights gained from the literature review successfully answered the questions posed at the beginning of this chapter. The design space of wind turbines is ever-expanding into their respective vertical and horizontal domains, with promising

improvements of the efficiency of both types. Current state-of-the-art wind turbine technology for residential applications can have many benefits for future generations to reduce dependency on ever-depleting resources. Fewer, larger turbines seem to be more promising than many smaller ones from a cost and electricity generation standpoint. There are continuous efforts to improve on the design of VAWTs, but they are still not at the level of commercial maturity of HAWTs. Finally, the advantages and disadvantages of different generators on different sized turbines have also been discussed. This knowledge will be carried out through the subsequent phase of the project, which will be the analytical modeling and testing of a first generation prototype.

Chapter 3: Analytical Modeling of a Wind Turbine

3.1 MOTIVATION

In this chapter, a detailed analytical model was developed in order to assess the dynamic behavior of wind turbines and properly decide upon the blade size and generator specifications necessary to achieve a high enough voltage. The difference in behavior between VAWTs and HAWTs was also analyzed to determine which turbine would be more feasible for this project.

There are many analytical models that simulate the behavior of large-scale commercial wind turbines systems, but most of them are focused on the generators and the electrical conditioning downstream from the generator. There have been many efforts to model different types of electricity generation subsystems, from double fed induction motors to permanent magnet motors, as well as the behavior of inverters and dynamic rotor resistance of wind power plants (Singh, 2011). Although the aforementioned analytical models are extremely well constructed and helpful in modeling wind turbines from an electricity generation standpoint, for the purposes of this research it was more desirable to model wind turbine behavior at a system level in order to properly size the blades of the turbine as well the generator. The requirement for this project is to power a 6V battery, so we can simplify the electricity generation portion of the model by acknowledging the fact that a voltage greater than 6V is all that is needed from the generator, assuming sufficient current is generated as well. The analytical model will also be used to solve a coupled design problem: sizing the generator and sizing the blades.

3.2 IDENTIFYING KEY REQUIREMENTS, ASSUMPTIONS AND EQUATIONS

Requirements

The requirements for the wind energy harvester are the specific needs that the system will satisfy. These requirements have been previously quantified in the project and are explicitly stated in Table 3.1 below:

Table 3.1: Electrical and power requirements for the wind energy harvester (McEvoy, 2011).

Requirement	Specification
Provide DC voltage	> 6V DC, constant
Provide DC current	200 mA, max pulse
Generate long term energy level	> 104 Wh/year (375 kJ/year)
Provide power level continuously for 2 weeks	> 61 mW

The bottom line is that the wind turbine needs to harness enough energy to continuously provide charge to a battery in order to extend the service and maintenance life of the bridge health monitoring system. The analytical model will verify if the wind turbine will satisfy these electrical requirements.

Assumptions

Some key assumptions were made before the model was created. First of all, the generator will be a direct-drive permanent magnet motor run in reverse. This simplifies the way electricity is conditioned, as a permanent magnet motor will generate an already rectified DC voltage. This voltage will simply have to connect to a charge controller, which in turn monitors the voltage of the 6V battery.

The second assumption is that the motor works just as well running backwards as forwards. The specifications of the motor, specifically the speed constant, have to be assumed to work both ways. In other words, the same speed constant is used to output the rotor speed when a voltage is applied as when an input rotor speed is applied to generate voltage. The justification for these two assumptions can be illustrated through an experiment later in this section.

Finally, the last assumption deals with modeling the power coefficients of the wind turbines. Betz's law states that no turbine can capture more than 59.3% of the energy available in the wind, using conservation of energy and mass equations (Khaligh & Onar, 2010). The power coefficient varies with different types of turbines and wind speeds, but it can never exceed .593. Savonius style VAWTs, for example, have a maximum power coefficient of 0.2. The most accurate way to achieve power coefficients is to measure them experimentally, but because an analytical model is being created, power coefficient curves and values have to be used from previous empirical studies and literature.

Parameters and Equations

One of the key parameters to consider from the motor standpoint is the voltage to RPM ratio that governs how much electricity is generated. This can either be achieved by inverting k_n, the speed constant, or by dividing the nominal voltage by the nominal speed, which can be accessed from any motor specification sheet. If there is a gear system on the motor, then the gear ratio also needs to be considered. A gear system increases the

input RPM, but it also increases the input torque required. The final ratio with a gear system becomes:

$$Ratio = \frac{Voltage*Gear}{RPM} = \frac{Gear}{k_n} \qquad (3.1)$$

A key equation that governs the turbine in this analytical model is the wind torque equation, which is simply derived from the power that can be obtained from a fluid by a turbine (Patel, 2006).

$$P = \frac{1}{2} C_p \rho A_s v^3 \qquad (3.2)$$

where C_p is the power coefficient, ρ is the density of the fluid, A_s is the swept area, and v is the velocity of the fluid. This can be combined with the definition of power below:

$$P = T\omega \qquad (3.3)$$

where T is the torque and ω is the angular velocity, yielding the following equation:

$$T_w = \frac{1}{2} C_p \rho A_s R v^2 \qquad (3.4)$$

where T_w is the torque applied to the turbine by wind, and R is the radius of the turbine. Equation 3.4 essentially converts energy in the fluid domain to the mechanical domain, and is crucial in modeling wind turbine behavior.

Another key motor parameter is the start-up torque, which is the amount of torque required to initialize rotation of the generator. Because this parameter is typically not found on specification sheets, it has to be found empirically. This is an important aspect of the motor to consider because the torque applied due to wind discussed earlier has to be greater than the start-up torque of the motor. Otherwise, the turbine would never reach a dynamic state and electricity generation would never commence.

Only the most important equations and parameters to model wind turbine behavior were highlighted in this section. The other governing equations are discussed in the following section.

Justifying Assumptions

The assumption justified in this section is that the speed constant of a commercially available motor does not change when the motor is run in reverse as a generator. A small, commercially available, toy wind turbine from Pitsco (see Figure 3.1) was purchased in order to validate the assumption stated above. A permanent magnet DC motor that was coupled to the turbine was run in reverse and compared to the speed constant of the actual specifications in Table 3.2. It should be noted that the no load speed was used for the ratio calculations because although the turbine is considered a mechanical load on the motor when it is run forwards, the turbine becomes the energy source and does all the mechanical work when it is run in reverse.

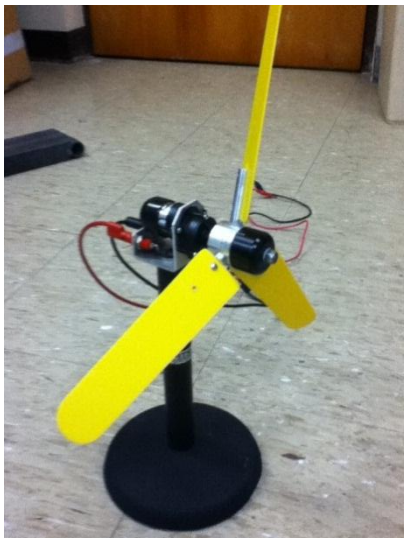

Figure 3.1: Small, toy wind turbine used in the experiments.

Table 3.2: Specifications of the motor mounted on the turbine

Power Rating	Voltage	No Load Speed	Gear Ratio
12 W	6 V	14200 RPM	3.75

During the test, various wind speeds corresponding to an input RPM were applied and the output voltage of the generator was measured. This test was repeated for four different wind speeds. The corresponding voltage to RPM ratio and speed constant were averaged over all of the tests and compared to the given specifications. The percent variation was found to be 1.69% when the experimental ratios were averaged, indicating a satisfactory level of repeatability. It should also be noted that the gear ratio of the motor was taken into account in all of the calculations. The result from the experiments can be seen in Table 3.3.

Table 3.3: Voltage to RPM ratios and speed constants from the experiment with respect to actual motor specifications.

	V/rpm ratio	k_n, speed constant
Experimental	0.00141	707.18
Actual	0.00158	631.11
% Difference	10.7%	12.1%

The results indicate a relatively low percentage difference between the experimental and actual ratios, indeed indicating that the speed constant can be used for a permanent magnet DC motor to calculate voltage outputs from a given RPM. The limitation of this experiment is that a no “mechanical” load speed is assumed, but this value can change if there is an electrical load attached to the motor when it is run backwards as a generator. Furthermore, Equation 3.1 can also be used to calculate the voltage output of the generator. Although this was only demonstrated for one motor, it

will be assumed that most commercially available motors will behave in a similar fashion when run as generators.

Given the results above, a follow-up experiment was conducted to calculate the minimum RPM input needed to generate 6V for this particular turbine. The minimum input was then converted to the TSR and compared with the observed values as well as those in literature. For the TSR calculations, it was assumed that the wind turbine should start producing a desirable amount of energy given an above average wind speed in Austin of 12 mph. The results are shown below.

Table 3.4: Minimum RPM needed and TSR to achieve 6V for the small, toy turbine.

Minimum Input	**Wind Speed**	**Turbine Radius**	**TSR**	**Observed TSR**
3787 RPM	12 mph	7 in	14.14	1.7

Table 3.4 indicates that a TSR of 14 would be needed to generate 6V from the turbine. However, this value is much higher than the observed TSR during the experiments, and does not correlate with empirical models. A three bladed turbine starts losing its efficiency after a TSR of around 6. A TSR of 14 can only be achieved with a single-bladed rotor, as illustrated in Figure 2.1 in Chapter 2. A couple of observations can be made from these results. Firstly, it appears unfeasible to produce the nominal voltage rated on the motor when it is connected to a turbine and run in reverse; the TSR indicates that it is limited by the RPM input and aerodynamics of the turbine. One alternative would be increase the radius of the turbine in order to harness more energy from the wind, but this simply increases the TSR. These results seem to imply that a

higher rated motor should be used to produce the desired amount of voltage. The idea of sizing generators and turbines is explored throughout the rest of this Chapter.

3.3 MODEL SIMULATION

Our ultimate goal for the analytical model is to predict the voltage output of the system. This voltage is implicitly defined by the RPM input to the generator, directly coupled to the wind turbine. Therefore, the most significant parameter that needs to be modeled is the angular velocity of the turbine. The bond graph method was used to develop the model (Beaman & Paynter, 1993). The bond graph for this system is shown in Figure 3.2 In this model, the input wind velocity, on the extreme left, is transformed to a torque that is applied to the wind turbine. The turbine experiences an inertial load, I_t, a friction resistive load, b, and ultimately the motor resistive load, R_{eff}.

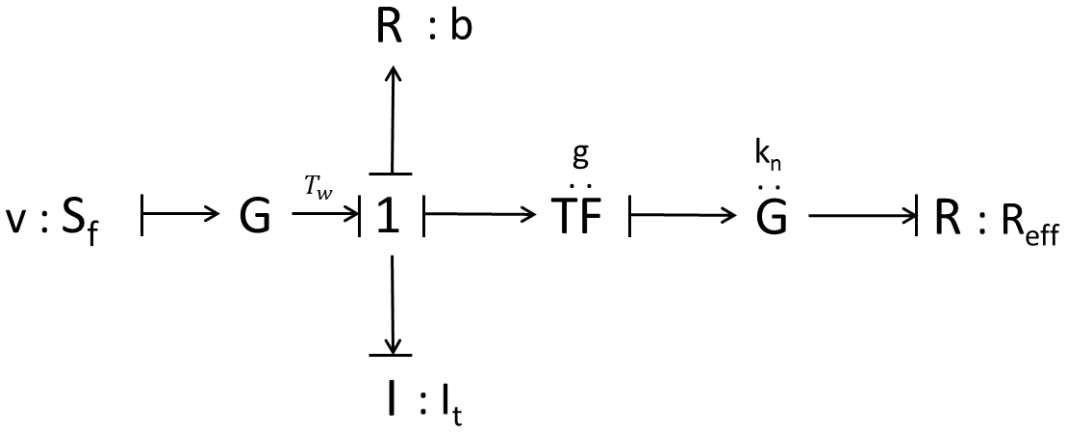

Figure 3.2: Bond graph of the wind turbine

The key parameter that we want to monitor is the angular velocity, which can be expressed through the angular momentum p_t of the turbine, described by $p_t = I_t\dot{\omega}$. The

state equation of the system derived from the bond graph is the single order differential equation shown below (Beaman & Paynter, 1993):

$$\dot{p_t} = T_w - T_f - T_m \quad (3.5)$$

Equation 3.5 describes the derivative of angular momentum in terms of the torques applied in the system: T_w, the torque applied due to wind; T_f, the torque applied due to friction; T_m, the torque applied due to the motor. These torques are defined below:

$$T_w = \frac{1}{2} C_p \rho A_s R v^2 \qquad T_f = \frac{b}{I_t} p_t \qquad T_m = \frac{g^2}{k_n^2 I_t R_{eff}} p_t \quad (3.6)$$

where b is the friction coefficient, I_t is the inertia of the turbine, g is the gear ratio, k_n is the speed constant, and R_{eff} is the terminal resistance of the motor. This set of state equations was used to compute the state variable of the system, the angular velocity. The angular velocity was then multiplied by the V/rpm ratio described in Equation 3.1 to yield voltage of produced by the generator, which is the most important output parameter of the system. The entire analytical model was implemented in MATLAB code and can be seen in Appendix A.

The bond graph model above is similar to previous efforts to model the behavior of a wind turbine. Neammanee et al. (2007) developed a block diagram of the output generator speed based on three torques: turbine, friction, and generator (see Figure 3.3). However, their overall goal was to also model how accompanying software controls the variable speed of an induction generator in order to maximize power output. For the purposes of this model, we are using a direct drive permanent motor in a stand-alone system, so no controller is needed.

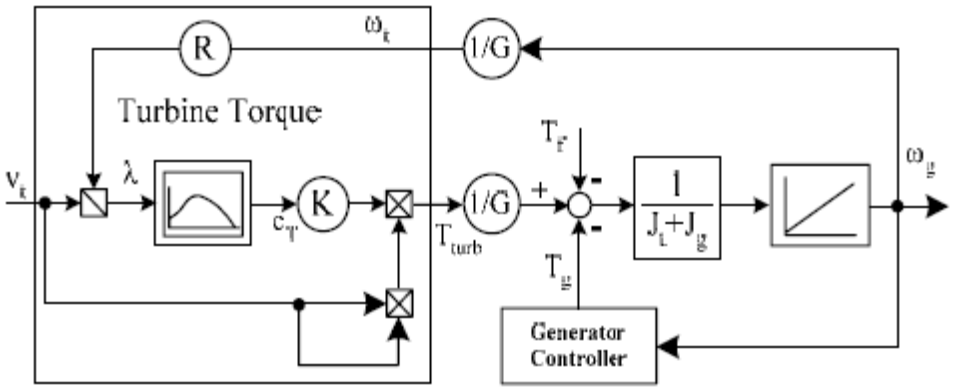

Figure 3.3: Block diagram model of a wind turbine with various input torques that govern the output generator speed (Neammanee et al., 2007).

3.3.1 Coupled Design Problem

The analytical model was used to solve a coupled design problem. To provide the context for this problem, consider the proposed design and already constructed proof-of-concept by McEvoy (2011), shown conceptually in Figure 3.4. In this design, the Savonius wind turbine (B) has a blade size with a cross-sectional area of around 10” x 4”, resulting in a swept area of 80”. The generator (D) has a nominal voltage of 6V, a nominal speed of 6110 rpm—which result in a motor constant of 1380 rpm/V—and a gear ratio of 15:1. These parts are mounted in a commercially available wire frame (A) (McEvoy, 2011).

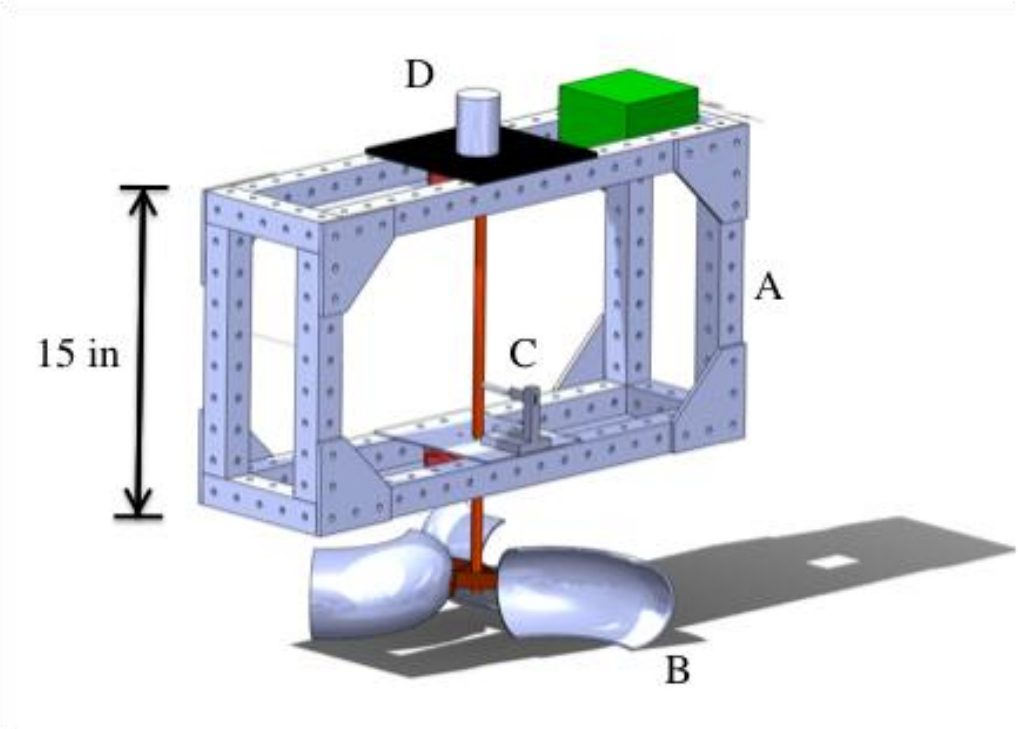

Figure 3.4: Embodiment of the proof-of-concept and proposed design (McEvoy, 2011).

Although this is only a proof-of-concept and there are clear improvements that can be made, the motor and turbine dimensions chosen for this design were used as benchmarks for the analytical model.

The first step of this problem was to verify the motor parameter values required to successfully provide enough power to charge a 6V battery, given the size of the current proof-of-concept. The second step was to verify the size of turbine required, given a motor whose parameters are effective in providing a 6V DC output.

Sizing the Motor

For the first phase of the design problem, the nominal voltage, nominal speed, and gear ratio, which are available on any motor specification sheet, were varied. These are

the crucial parameters that directly influence the voltage produced based on a given input speed. The blade size of the current design was maintained constant at a cross-sectional area of 10” x 4”, resulting in a swept area of around 80”.

A parametric study was completed that varied the key specifications of the motor (nominal voltage, nominal speed, and gear ratio). These three specifications were combined to form the V/rpm ratio, and were used to execute the analytical model derived above. The resulting voltage produced by the generator was graphed against to determine which values crossed the 6V threshold, also shown in the graph. An example of one of the graphs is shown in Figure 3.5, for three different RPM values.

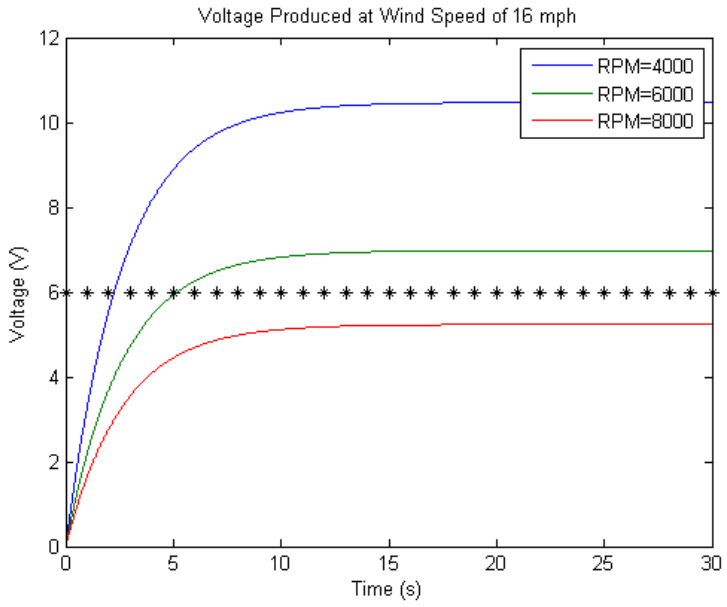

Figure 3.5: Voltage produced with varying RPM value of the generator

Each parameter was varied individually while the others were kept constant. This resulted in three different motor parameter combinations that reflected the minimum

specifications needed to successfully produce more than 6V at a given wind speed. The three motors and their values are shown in Table 3.5.

Table 3.5: Motors with different specification combinations

Motor	Voltage	RPM	Gear Ratio	V/rpm Ratio
1	72	4000	40	0.72
2	48	2000	40	0.96
3	48	4000	60	0.72

The results indicated that the minimum motor specifications needed to have a nominal voltage of at least 48V, a gear ratio of at least 40:1, and a nominal speed of at most 4000 RPM. The current motor that was chosen for the proof of concept had values of 4.5V, 6010 RPM, and 15:1 gear ratio, indicating the need for a much larger motor.

To determine if a motor is suitable to be used as a generator for a wind turbine, the V/rpm ratio must be calculated from Equation 3.1. The resulting value must be greater than 0.035 (WindyNation, 2010). A ratio smaller than this means that the wind turbine must rotate at unrealistically high speeds to produce sufficient voltage. Turbines with smaller ratios will work only in areas of very high winds. This guideline was used to determine if the chosen motor was feasible after the parametric study was completed. All three motors modeled with the simulation exhibited ratios higher than 0.035, at 0.72, 0.96, and 0.72 respectively. However, the motor previously chosen for the proof-of-concept had a value of 0.011, indicating that it was not suitable to be used as a generator in this application. This ratio is useful only for determining if the motor can produce the desired output voltage at a given RPM. It does not indicate the mechanical effort needed

to produce the required rotational speed. Generally, the larger the motor becomes, the higher the mechanical and electrical inertia (GotWind.org, 2010). Therefore, the ability of the wind turbine of the given size to spin the chosen motors must be verified.

The approach used to determine if the chosen motor was feasible was to calculate the minimum wind speed needed to overcome to start-up torque T_m of the motor by rearranging the wind torque equation previously described:

$$v = \sqrt{\frac{2T_m}{\rho C_p A_s R}} \quad (3.7)$$

In order to estimate the start-up torque of a motor, an empirical study was conducted of a wide variety of PMDC motors. The start-up torques was physically measured by hanging weights from the motor shaft. Weights were incrementally added the shaft started to rotate. The torque was the final weight multiplied by the respective shaft radius. Torques for multiple motors were plotted against their respective V/rpm ratios.

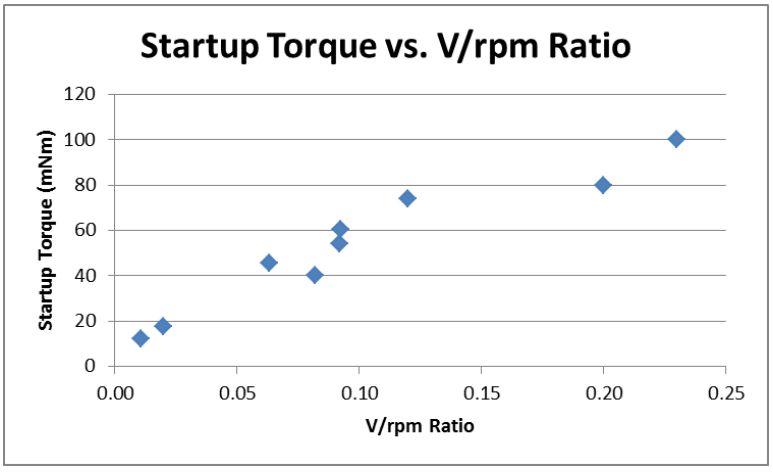

Figure 3.6: The start-up torques of various motors plotted against their V/rpm ratios.

As Figure 3.6 shows, there is a noticeable trend that the start-up torque of a motor increases with higher V/rpm ratios. Using this trend, we can extrapolate this data to predict the start-up torque of one of the motors we previously chose that would be suitable to power the 6V battery.

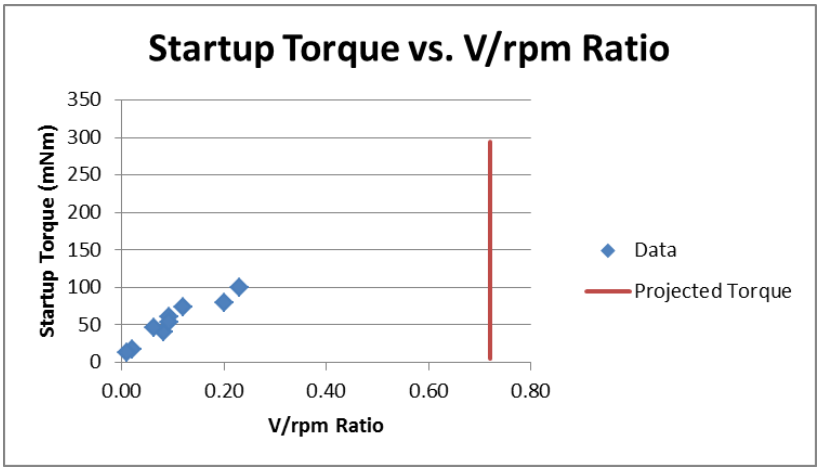

Figure 3.7: The projected torque based on the calculated V/rpm ratio.

As can be seen in Figure 3.7, the start-up torque of the motor was projected to be around 300 mNm. Assuming the turbine is coupled directly to the generator, the minimum wind speed needed to initiate rotation of the turbine was calculated to be 45 mph. This high start-up torque is unfeasible as only infrequent large wind gusts would even begin to spin the VAWT. It was therefore determined that locating a motor would be unfeasible for the current size of the wind turbine.

Sizing the Turbine

The second phase of the design problem was to quantify turbine dimensions necessary to provide enough power for the battery given the current specifications of the

motor. Rearranging Equation 3.6 shows that two variables describe the turbine dimensions.

$$A_s R = \frac{2T_m}{\rho C_p v^2} \quad \text{(x)}$$

To simplify the design problem, the turbine was assumed to be a square. The startup torque T_m was determined to be 12 mNm, and was found the same way as in the empirical study previously described. The wind velocity was assumed to be the Austin yearly average of 8 mph (NCDC, 2008). It was found that the minimum swept area needed was around 260 in^2. The current prototype has a swept area of 80 in^2, meaning that the turbine would need to be redesigned. A more in-depth study of the redesign of the VAWT was conducted, as described in the next section.

3.3.2 Vertical Axis Wind Turbines

Using the results obtained from the coupled design problem, it was determined that the current proof-of-concept could not provide enough power to charge a battery based on the given motor and turbine dimensions. Furthermore, using the same results, sizing a turbine rather sizing a motor would be the more feasible and realistic approach of creating the next-generation design. Therefore, a parametric study was conducted in order to more thoroughly study the behavior of VAWTs. The parameters that were varied were the height and radius of the Savonius VAWT, or essentially the swept area, which governs the amount of power that can be harnessed from the wind as well as the input torque.

Because the previous motor chosen for the proof-of-concept was deemed infeasible to use as a generator, a motor was chosen with specifications that could effectively provide enough power, assuming a realistic input speed that would not damage the turbine. There were many possible solutions for that generator, but after speaking with Maxon motor representatives and consulting their literature, a 24V, 5190 RPM, 217 rpm/V, and 20:1 geared motor was chosen (Maxon Motors, 2011).

The justification for this decision was a simple calculation using the back EMF of the motor. Measurements showed that the turbine in the previous proof-of-concept rotated at a range from 90-150 RPM. Assuming an average of 120 RPM input from the turbine, the motor constant needed is:

$$k_n = \frac{120\ rpm}{6\ V} = 20\frac{rpm}{V}$$

However, Maxon motors and other motor manufacturers do not make motors with such small speed constants. Therefore, a gearbox was needed to increase the speed of the motor. With the given motor specifications, the output voltage can now be obtained by subtracting the electrical loss from the generated back EMF voltage, assuming a 200 mA current draw:

$$EMF = \frac{(20{:}\,1)(120\ rpm)}{217\frac{rpm}{V}} = 11V$$

$$Voltage\ Out = EMF - R_{motor}I = 11V - (7.3\ ohm)(.2A) = 9.54V$$

Now that a motor has been chosen, the next step in the process was to define the turbine inertia, mass, and swept area in order to properly model the VAWTs. The inertia

is simply the mass moment of inertia, and the mass was calculated by multiplying the material density by the volume of the annulus-shaped Savonius style VAWT. The swept area is simply the cross sectional area of the turbine.

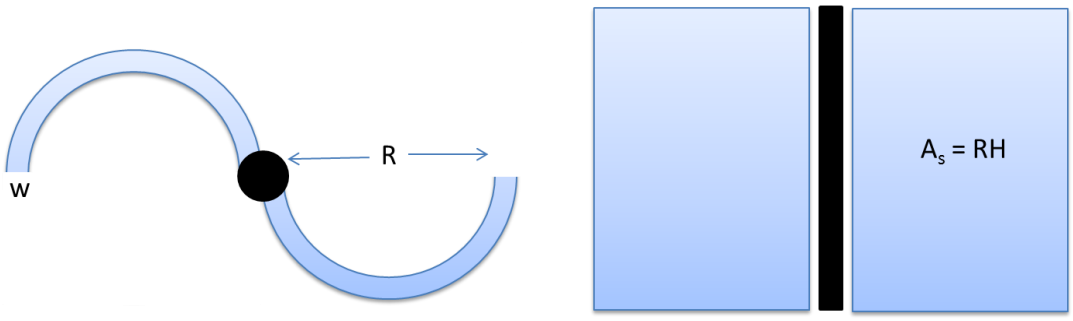

Figure 3.8: Dimensions and swept area of a Savonius VAWT.

The equations for the inertia and mass were calculated using Equations 3.9 and 3.10 below, with the dimensions defined in Figure 3.8.

$$I_t = mR^2 \qquad (3.9)$$

$$m = N\frac{\pi}{2}\rho_m H[(R+w)^2 - R^2] \qquad (3.10)$$

where N is the number of blades, ρ_m is the blade material density, R is the radius, H is the height, and w is the width of the blades. Now that everything in the model has been clearly defined, the only step left was to determine the minimum swept area needed to overcome the start-up torque of the new motor using the Austin yearly average wind speed of 8 mph. Using the empirical study in Figure 3.6, it was determined that the start-up torque was 40 mNm, resulting in a minimum swept area of 169 in^2 or a 13" x 13" square. Because there are many levels of experiments that could be performed, a parametric study was performed by keeping two variables constant while varying the

third in order to simplify the number of iterations. The three variables in question are the radius, height, and wind speed. The results of the parametric study are shown below:

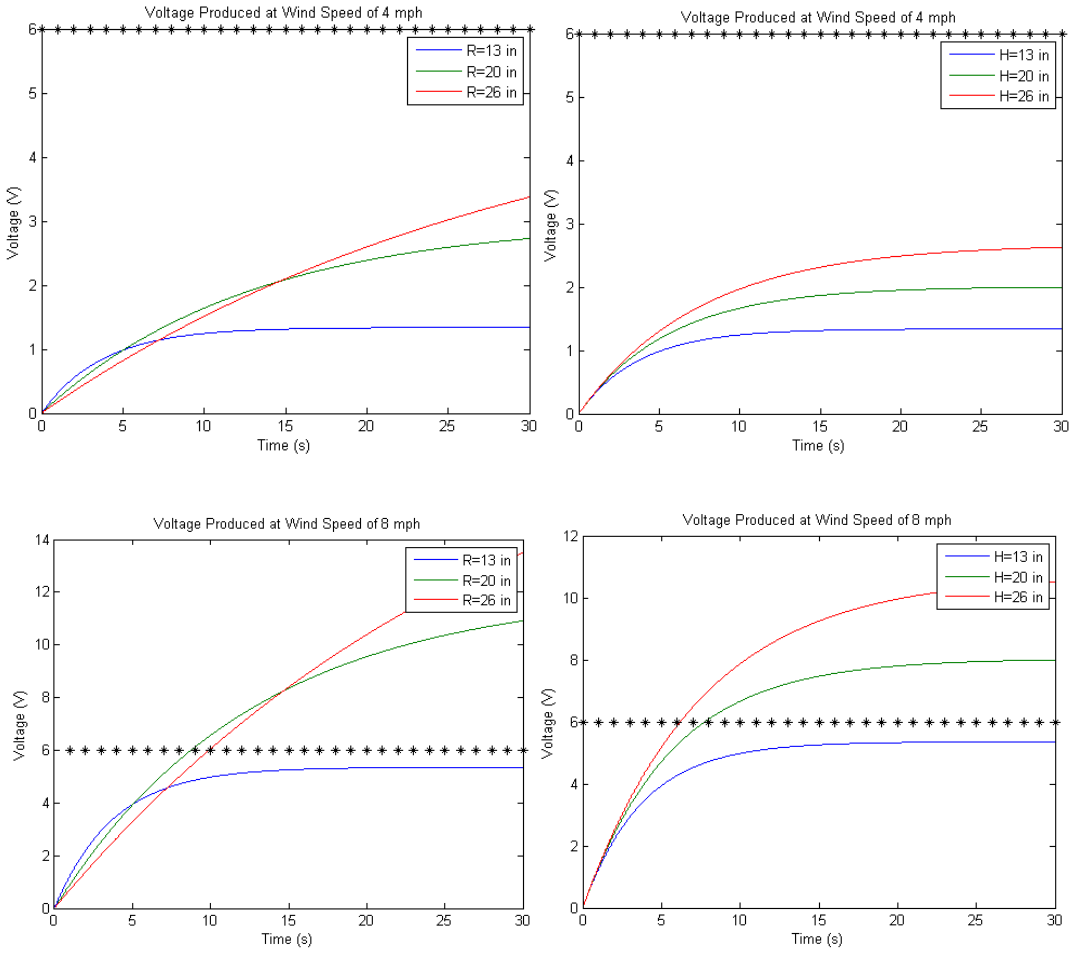

Figure 3.9: Voltage produced of a vertical axis turbine with varying radius, height and wind speed.

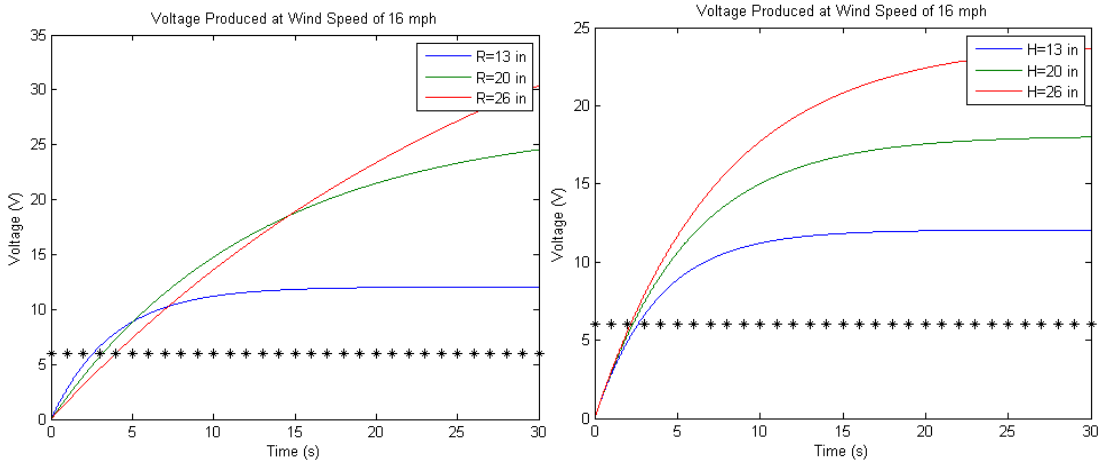

Figure 3.9: Voltage produced of a vertical axis turbine with varying radius, height and wind speed (cont'd).

As can be seen from Figure 3.9, the wind speed was varied from half to double that of the average wind speed of 8 mph, while both the radius and height were separately, yet incrementally increased. For a wind speed of 4 mph, none of the sizes could produce a high enough voltage. As the wind speed increased, more and more of the turbines could spin at a fast enough rate to produce the required amount of voltage. A couple of insights were gained from the results. Firstly, increasing the radius produces more voltage than increasing the height at the same rate; at the same time, increasing the radius also has a drastically larger effect on the time to reach steady-state. This makes sense because the radius has a cubic term and a square term defining the inertia, while the height only has a single order term. This can be seen if we substitute Equation 3.10 into Equation 3.9:

$$I_t = N\frac{\pi}{2}\rho_m H(2R^3 w + w^2 R^2) \qquad (3.11)$$

In order to further quantify this observation, a simple design of experiments using the analytical model was performed. The three variables that were used were the defining parameters of the mass and inertia of the turbine: the radius, height and width. The two outputs were the voltage and the time to reach a steady state (see Table 3.6).

Table 3.6: The variables associated with the parameters.

Variable	x_1	x_2	x_3	y_1	y_2
Parameter	Radius	Height	Width	Voltage	Time

A 2^3 factorial design was performed, calculating the main effects but assuming all second and higher order effects were negligible. The reason for this assumption is because the second order effects are interaction effects; the focus of this design of experiments is to analyze the main effects, not the interaction effects. The appropriate mathematical models for both outputs were constructed:

$$y_1 = 9.11 + 5.51x_1 + 3.04x_2 \qquad (3.12)$$

$$y_2 = 70.38 + 57.11x_1 + 25.86x_2 - 20.86x_3 \qquad (3.13)$$

One item we can notice from Equation 3.12 is that the width has no effect on the voltage produced because it is not included in the swept area equation. On the other hand, it has a pretty negative effect on the time to reach a steady state in Equation 3.13, because it contributed to the mass of the blades. Therefore, we naturally want to minimize the width of the blades.

The more significant finding is that the model shows that the radius (x_1) has a greater effect on the voltage produced than the height (x_2), but it has a 50% larger effect on the time to reach a steady state. Therefore, it is more beneficial to increase the height

of the Savonius VAWT rather than the radius. However, an increase in the height causes problems with the proposed design of mounting it under the bridge. One of the requirements set by the Texas Department of Transportation for this project is that no part of the energy harvester can extend below the lowest part of the bridge, because of the clearance needed for passing vehicles. Since it was deemed disadvantageous to increase the swept area by increasing the radius, increasing the height of the turbine would likely interfere with the traffic below. The next generation turbine would have to be mounted on the concrete side of the bridge. This mounting option would be more beneficial anyway because there is a larger amount of energy available in the wind above the bridge as opposed to underneath it.

After further analysis of the results, there were a couple of additional problems that were encountered with the results of the model. The first was the amount of time required for the wind turbine to reach a steady-state speed. As can be seen from the figure above, it takes more than 20 seconds for either simulation to reach a steady state, and an average of 70 seconds from the mathematical model shown above. The required increase in size and inertia of the turbine to provide enough power consequently hinders its maximum wind harvesting capability. Another problem was that the tip-to-speed ratios (TSR) calculated from the results were physically impossible. Recalling Figure 2.1 from Chapter 2, wind turbine aerodynamics from empirical studies dictate that Savonius style turbines never reach TSRs higher than 1 without significantly losing efficiency (Alam & Iqbal, 2010). However, the larger sized turbines would exhibit TSR larger than 1, as shown in Figure 3.10.

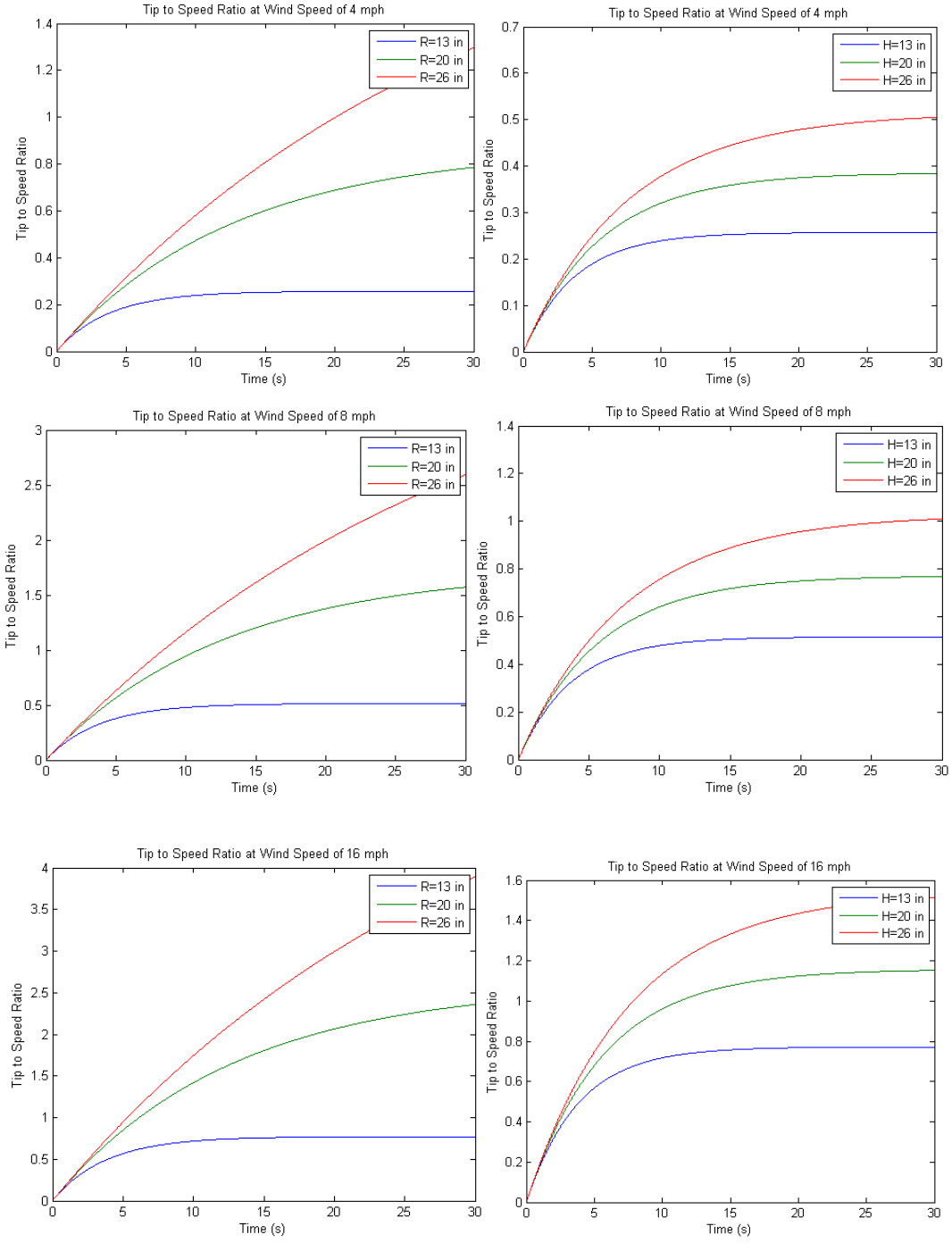

Figure 3.10: Tip to speed ratios of a vertical axis turbine with varying radius, height and wind speed.

Therefore, a larger VAWT would likely not perform as well in the field as predicted analytically. These results led to the hypothesis that VAWTs are **not** the most feasible turbines for this project. This hypothesis was tested through the design and experimentation of an alpha prototype, as described in Chapter 4.

3.3.3 Horizontal Axis Wind Turbines

The more prevalent turbines in the commercial and residential fields are horizontal axis turbines, as discussed in Chapter 2; therefore, their behavior was simulated to compare them to vertical axis turbines. Before running the simulation, some slight changes to the analytical model were required. First, the mass and inertia were recalculated. Although most HAWT blades are triangular-shaped and twisted in order to catch the oncoming wind, it was assumed that the blade shapes for this model were rectangular prisms. The mass was calculated to be:

$$m = N\rho_m Rwt \qquad (3.14)$$

where N is the number of blades, ρ_m is the density of the material, w is the width, R is the radius, and t is the thickness. Secondly, the swept area of a HAWT is considerably different, giving it significant advantages over the VAWT. Not only is the swept area increased by a factor of π from the area of a circle, but it is also considerably larger in proportion to the physical cross-sectional area of the wind blades, as demonstrated in Figure 3.11.

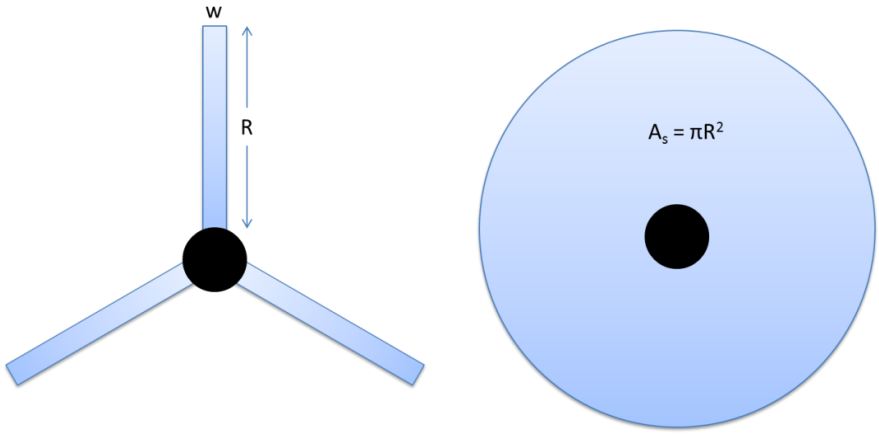

Figure 3.11: Dimensions and swept area of a HAWT.

If we assume that the radius is 10 times larger than the width, then the ratio of the swept area to the physical cross-sectional area is more than 10 to 1. This ratio for a VAWT is simply 1. It is ideal to minimize the cross sectional area and volume to decrease inertia and maximize swept area to increase wind energy harvesting capability, which is exactly what the HAWT does. These advantages were immediately noticeable in the results once the simulation was run. The voltages produced and tip to speed ratios of varying blade radii and wind speeds are displayed in Figure 3.12:

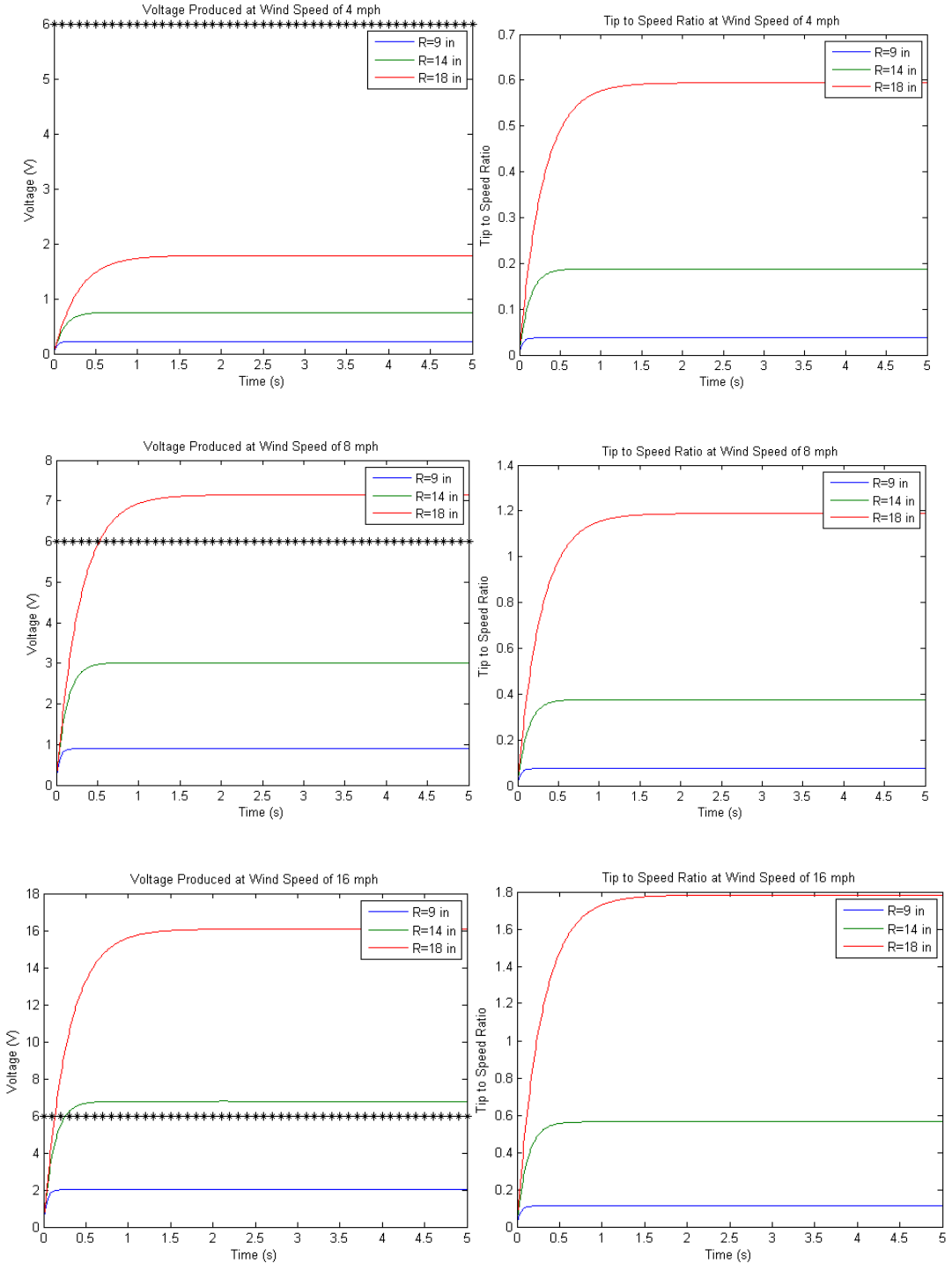

Figure 3.12: The voltage produced and tip to speed ratios of HAWT with varying radii and wind speeds.

The greatest difference between the two turbine results is the time to reach steady state. The HAWT simulation indicates that it reaches steady state within no more than 2 seconds, significantly increasing its efficiency. Note that there is also reduction in the dimensions of the turbine design that can exceed the threshold of 6V. These results further added to the previous hypothesis that HAWTs are better suited for this application.

3.4 DISCUSSION

The results achieved from the VAWT model were verified by a review of the geometry and dimensions of actual commercial turbines. Both the simulation and mathematical model proposed that an increase in the height is more beneficial than an increase in the radius. The time to reach steady state was much more sensitive to an increase in the radius, because it has a greater influence on the mass moment of inertia than the height. A great number of the commercial turbines available on the market—both Darrieus style and Savonius style VAWTs—are built to be much taller than they are wider.

Figure 3.13: Darrieus style VAWT (left) by Windspire (Windspire, 2012) and a helical Savonius style VAWT (right) by HelixWind (HelixWind, 2012).

The examples in Figure 3.13 are among many that support the preference for increasing the height as opposed to the radius. Therefore, it would be much more advantageous to abandon the idea of mounting the energy harvester below the bridge for this specific project and instead mount it on the side of the bridge on the concrete barriers where it will not interfere with bridge traffic.

Another reason why the wind turbine should be mounted in the side of the bridge rather than underneath it is the fact that the 8 mph yearly average wind speed is the best case scenario. The wind speeds have been previously characterized through experimentation for different locations under the bridge, and only come close to reaching that threshold, as seen in Figure 3.14. The wind under a bridge is also much more

turbulent and it would be difficult to harness an uninterrupted amount of wind energy for an extended period of time.

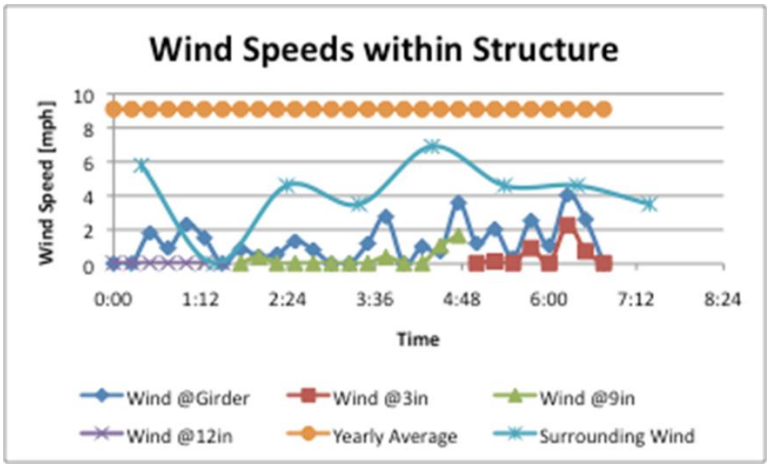

Figure 3.14: Wind speeds within the structure (McEvoy, 2011).

Not only was the analytical model successful in determining the more beneficial location for the wind harvester, but it also suggested that a different type of turbine would have better performance metrics. There were some significant differences between the results of the two wind turbines. First and foremost, the geometry of the HAWT proved to be a defining advantage. The problem with the VAWT is that its dimensions and size of the blades are directly proportional to the swept area of the turbine, unlike the HAWT. The maximum possible swept area of a VAWT is essentially the cross-sectional area of the blades, but this is only the maximum possible area. One key assumption made in the analytical model is a constant swept area. During certain parts of its rotation, the VAWT swept area actually decreases to half of its original size, as illustrated in Figure 3.15.

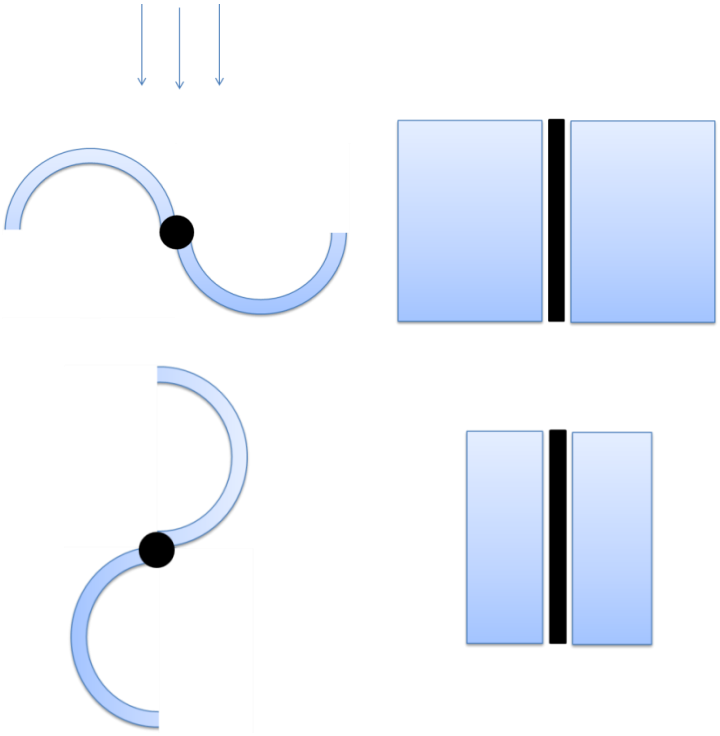

Figure 3.15: The two extreme cases of the swept areas of a Savonius style VAWT

If we assume that the actual swept area is an average of the two scenarios, then the model demonstrates a decrease in efficiency of the turbine. Another deterrent observed from modeling the VAWT is the force balance during certain positions of its rotation. When the swept area is at half of the original area, as shown in the figure above, then the geometry of the Savonius does not actually capture any of the wind energy. At this instant in, the moments of the system are balanced. Therefore, a stable equilibrium can be reached if the turbine does not have enough momentum to overcome this situation. Thus, the results obtained in the analytical model were only the best case scenario results for the VAWT.

One way to solve this problem is to add another blade to the system (see Figure 3.16). Even though this increases the inertia, it increases the rate of energy acquisition

because there will never be a point in time where the turbine is not exposing one of its blades directly into the wind. Furthermore, the swept area of a three-bladed system does not decrease as significantly during certain parts of its rotation. Therefore, as discussed in Chapter 2, three-bladed VAWTs appear to be more advantages than two-bladed ones. This hypothesis was tested experimentally, as described in Chapter 4.

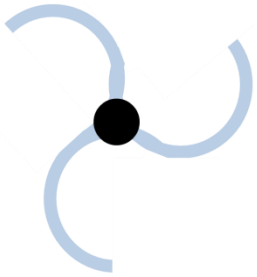

Figure 3.16: Three-bladed Savonius style VAWT.

On the other hand, the performance of a HAWT is not hindered through different positions of its rotation. The swept area of a HAWT is constantly modeled as the entire circle through which it spins, because the blades are always experiencing the force of the wind. This gives a significant advantage to the HAWT because the swept area can be increased to harness more wind without significantly increasing the dimensions and therefore the mass and inertia of the blades. In order to increase the swept area of a VAWT, the entire cross-sectional area must be increased. This consequently takes a heavy toll on the mass and inertia of the system, significantly reducing the performance capability of the VAWT.

Another advantage that the HAWT has is that it can reach TSRs much higher than 1 according to empirical studies, which is ideal for electricity generation. A higher input speed will yield a higher voltage. The steady state speed is reached at a much faster rate

with the HAWT, and the dimensions of the turbine are smaller than the VAWT yet yield just as much voltage. These differences give the HAWT significant advantages in terms of wind harvesting capability, so it appears that it would be more beneficial for this project.

Finally, the results obtained from the simulation also satisfied the requirements stated in the previous section of this chapter. Assuming a HAWT with a radius of 18 inches and a wind speed of 8 mph, the average power output of the wind turbine was calculated to be 140 mW using the voltage shown in Figure 3.12. For the calculation of the long-term energy level, it was conservatively assumed that 25% of the days in a year have a high enough wind speeds to provide energy to the battery. The basis for this claim can be observed in Chapter 5 for available versus usable energy. The results are shown in Table 3.7 below.

Table 3.7: Power requirements and their respective simulation results

Requirement		**Simulation Result**
Provide power level continuously for 2 weeks	> 60 mW	140 mW
Generate long term energy level	> 104 Wh/year	306 Wh/year

Therefore, according to the analytical model, a HAWT can harness enough energy to satisfy the power requirements. Verification of this analytical model and its results is completed in the next chapter through the design and experimentation of an alpha prototype.

Chapter 4: Prototype Development and Experimentation

4.1 MOTIVATION

In the previous chapter, an analytical model was constructed and executed to simulate the behavior of vertical and horizontal wind turbines. The results concluded that VAWTs cannot reach speeds high enough to generate the required voltage from a motor without significant trade-offs, such as an increase in blade size leading to an extreme increase in time to reach steady state. The hypothesis that VAWTs are not suitable for this application was tested through the design and experimentation of an alpha prototype. This chapter describes the prototype design and testing and analysis of the results.

4.2 IDENTIFYING REQUIREMENTS AND CONSTRAINTS

The requirements and constraints delineated in this section are metrics that identify the overall structure and functionality of the design. If the alpha prototype were to perform better than expected in a controlled environment, then the next step in the experimentation process would be to test it on an actual bridge. Therefore, the prototype was designed with the constraints and requirements necessary to implement the prototype for field testing and for possible future iterations into a final product.

The requirements delineate the needs of the system. The ultimate goal of the system is to deliver charge to a battery; therefore, the most important requirements are to create an electro-mechanical system which meets the need of 200 mW and 6V DC. However, there are also physical requirements having to do with the service life, safety and maintenance of the system. These are explicitly stated in Table 4.1:

Table 4.1: Requirements for the energy harvester in a bridge environment

Requirement	Specification
Service Life	10-15 years
Weatherproof	Rain, ice, etc.
Maintenance Interval	5 years
Force needed to detach from bridge	> 100 lbs

The constraints were previously established in the energy harvesting project with the idea of the harvester being mounted underneath the bridge. However, due to the results indicating that this would be infeasible in the previous chapter, these constraints are subject to change. For prototyping purposes only, these constraints will be applied in order to compare the performance capabilities of the VAWT with the analytical model results and verify the hypothesis established at the end of Chapter 3.

Table 4.2: Constraints for the energy harvester (McEvoy, 2011).

Constraint	Specification
Volume	< 1 ft3
Largest Surface Area	< 4 ft2
Prototype Cost	< $600
Weight	< 20 lb
Time to Install System	< 1.5 hours
Number of inches that the harvester can extend below the lowest part of the bridge	0
Number of permanent alterations to metal parts of bridge, such as welds and holes	0

One of the constraints for the energy harvester was to non-destructively integrate with the existing architecture of the bridge. Table 4.2 explicitly states that no permanent

alterations can be made to any metals part of the bridge, which includes the I-beams, girders, and angles. However, drilling into the concrete is acceptable if necessary. This would enable an attachment mechanism on the outer portion of the bridge. The bottom line is to inflict the least amount of damage to the parent structure—or in this case—the bridge. An attachment methodology that describes non-destructive principles is discussed in Chapter 6, and a list of these attachment principles can be seen in Appendix F.

4.3 DESIGN AND CONSTRUCTION OF THE ALPHA PROTOTYPE

Once the requirements and constraints were clearly established, the design process and construction of the prototype began. The first step was to select an appropriate location for mounting the prototype to create a foundation for its design. Next, an iterative design process was employed to model all of the key features of the prototype. Finally, the appropriate materials were purchased and machined to construct the prototype model.

4.3.1 Choosing an Appropriate Location

The first phase in the design process was to examine the geometry and architecture of bridges around Austin in order to determine an appropriate location for mounting the alpha prototype. The two bridges previously examined for the energy harvesting project—the 183-71 and the 410-I35—were also chosen for this prototype, so the underlying architecture of each bridge was observed (see Figure 4.1). The dimensions associated with the bridges can be seen in Appendix B.

Figure 4.1: Underlying architecture of the 183-71 (left) and 410-I35 (right) bridges in Austin.

Both bridges have nearly identical geometries and are classified as I-Girder bridges, based on the long I-beams that extend along their lengths. These I-beams are connected by L-shaped angles to stabilize and reduce the bending moments of these beams. The angles were chosen as the most suitable location for mounting the prototype (see Figure 4.2).

Figure 4.2: L-shaped beams chosen as the attachment location for the alpha prototype are common two both types of bridges.

The basis for the decision was not only the fact that these angles can be used for a variety of different clamps or hooks as the attachment mechanism (see Figure 4.3), but also because there is enough free space to fit the prototype so that no part extends below the lowest part of the bridge.

Figure 4.3: Depiction of the hook or clamp attachment method that will be used for the prototype.

Once the angles were chosen as the appropriate location, their architecture was modeled using CAD and the design process quickly followed.

4.3.2 Prototype Modeling

Framework and Attachment Mechanism

Using the angles as the basis for the design, the previously constructed proof of concept was used as a benchmark for the next generation prototype. The brainstorming process first began with modeling the appropriate attachment mechanism, followed by choosing the appropriate framework or enclosure once the mechanism was chosen. The first mechanism type chosen was the clamp that attaches to the bottom flange of the angle. Two different versions of clamps are shown in the models (A) and (B) of Figure 4.4. These first iterations were abandoned because model (A) is too cumbersome and the prototyping cost is too high and model (B) will experience an excessive bending moment

due to the nature of the clamping mechanism. The next two iterations use hook mechanisms by attaching to the other side of the angle so that the bottom flange does not interfere with the wind harvester. Model (C) is acceptable in terms of the force requirements, but it still uses the rudimentary framework of the proof of concept and has too much unused space. However, the hook is a much more feasible attachment mechanism, so the consequent step was to model the enclosure. Model (D) completely abandons the framework and uses a slider to allow access to the components on the inside, but it still is not completely weatherproof and is not the most elegant way to enclose the electronics.

A. 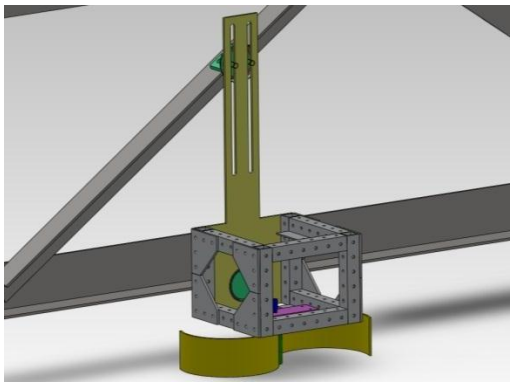 B. 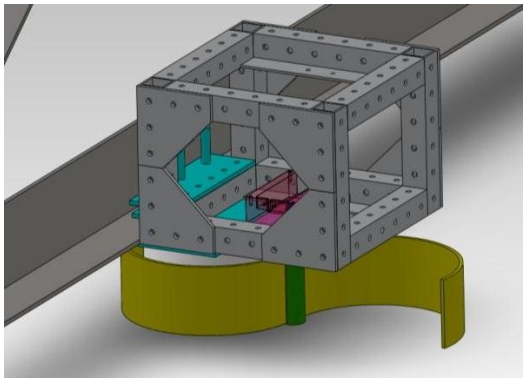

C. 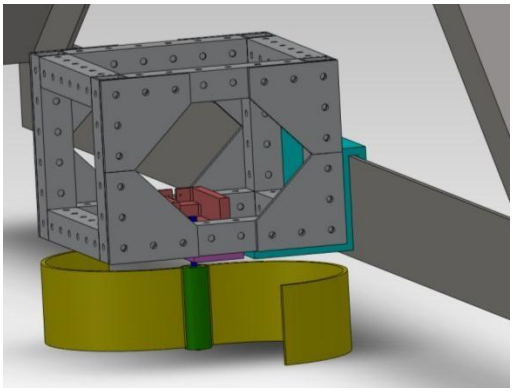 D. 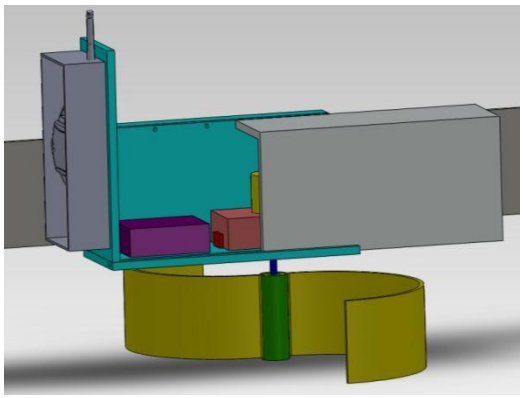

Figure 4.4: Four design iterations of the alpha prototype in chronological order: (A), (B), (C) and (D).

In order to create a fully weatherproof prototype, precision machining was required. Therefore, the final version of the prototype uses an off-the-shelf weatherproof encasing in which all of the electronics are stored and protected. Once this was chosen as the foundation for the prototype, a hybrid hook and clamp attachment mechanism was constructed around it. As can be seen in Figure 4.6, an L-shaped beam is machined to mechanically attach to the casing with bolts. The other side of the hook includes adjustable rubber clamps that can fasten to the bridge angle. This combination of hook and clamp has a couple of advantages: the clamps reduce the mechanical vibrations due

to the damping nature of the rubber and the hook over the bridge angle acts as a safety factor to protect the harvester from dislodging if the rubber clamps ever became loose. Figure 4.5 displays the full model of the prototype, but the generator and turbine design are explained in the next section.

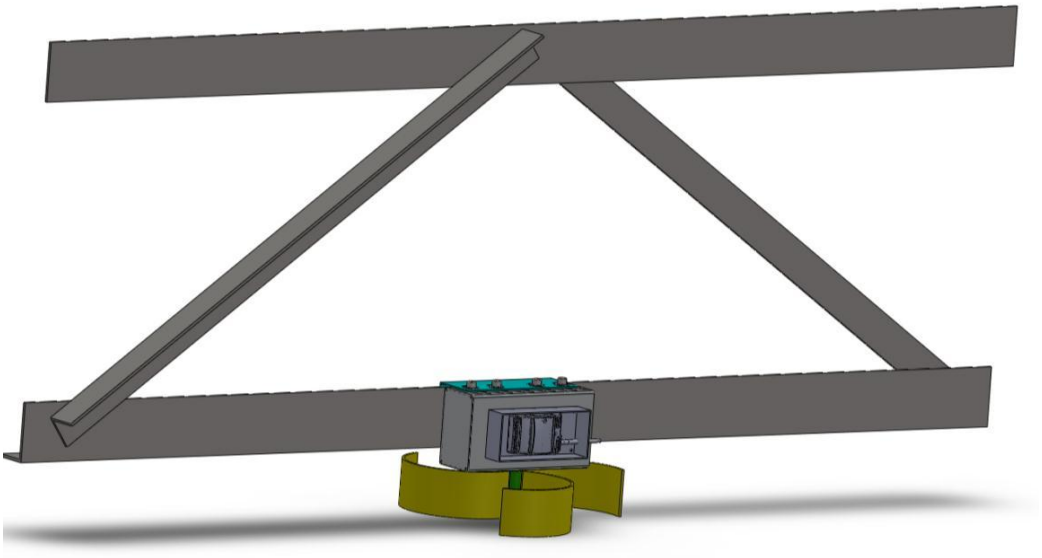

Figure 4.5: The alpha prototype mounted on the L-shaped angle under the bridge.

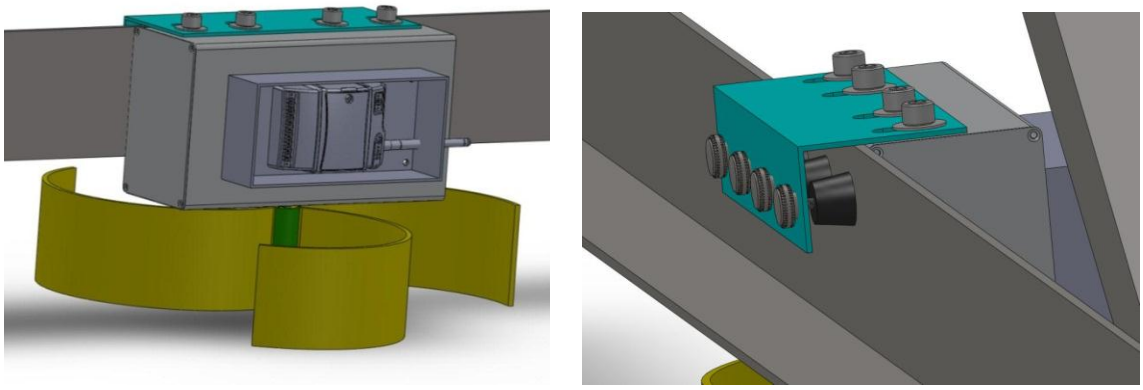

Figure 4.6: Close-up of the alpha prototype and the Wireless Sensor Node (left) and the attachment assembly of the alpha prototype.

Generator and Turbine Assembly

Once the framework and the attachment mechanism were completed, the next step was to design the generator and turbine assembly. The foundation for this assembly was the Maxon motor chosen in Chapter 3, so the constraints were based on the geometry of this motor. Referring to Figure 4.7, the motor (1), which is coupled directly to the wind turbine by a shaft (5), is also attached to a hollow generator mount (2) such that the rotor spins freely inside the encasing. The shaft is press fit into a plastic bearing (4) to allow free rotation and also to reduce bending moments. The material chosen for the bearing is acetal to minimize friction. The system is assembled using screws that can be accessed from the bottom of the prototype and tightened through the aluminum base (3).

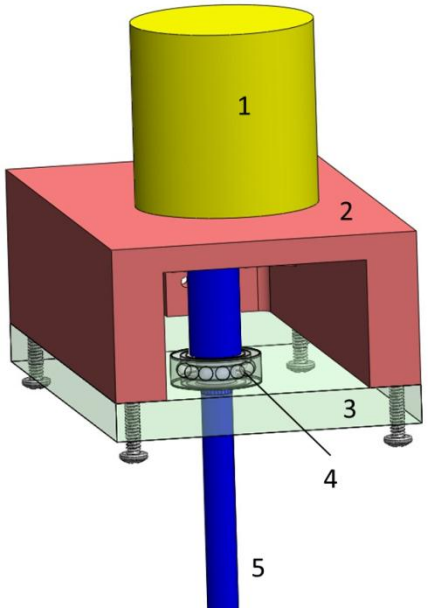

Figure 4.7: Inside view of the motor, shaft, and bearing assembly.

Because there were two motors to test—the proof of concept motor and the new Maxon motor—an insert was later added to the generator mount (2) and a small coupler

was constructed to be placed inside the shaft (5) so that both motors could be tested without a complete redesign of both parts.

The turbine, which was seen in previous figures, was designed concurrently with the other assemblies. Because of the desired shape, weight, and assembly requirement, the turbine was fabrication using Selective Laser Sintering (SLS), specifically using Nylon 12 PA, which was the least brittle of all of the possible materials and was chosen to reduce bending stress. The turbine blades and connecting axes were designed in a modular fashion so that the blades could be assembled and disassembled an unlimited number of times without any alterations to the parts. This way, only two axes and three blades had to be manufactured to create both sets of turbines (see Figure 4.8).

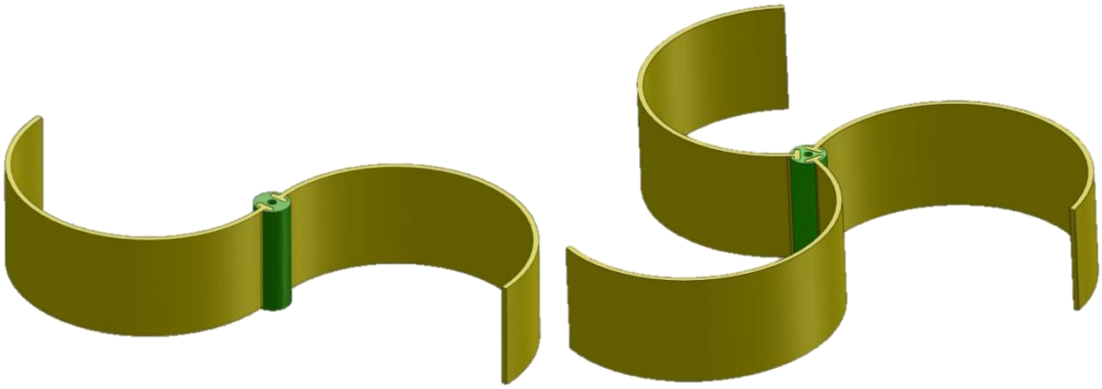

Figure 4.8: Two-bladed and three-bladed Savonius wind turbine design.

The blade was designed as a thin semi-circular shape, with a T-shaped protrusion that can be inserted into the axis that has a slightly larger, yet similarly shaped slot. One axis has two of these slots, and the other has three; each one is used as the foundation for a two and three-bladed turbine, as can be seen in Figure 4.9.

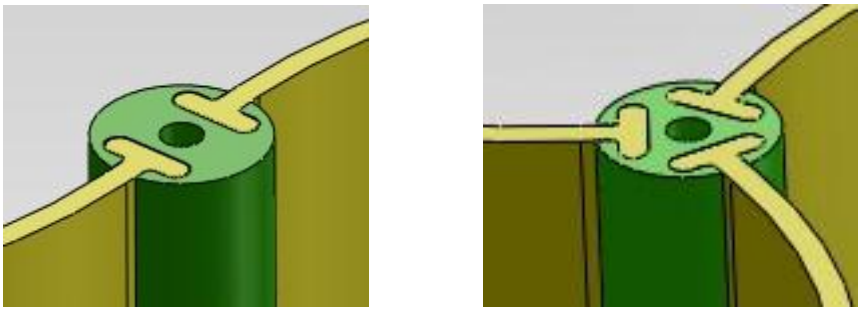

Figure 4.9: Close-up view of the assembly blade and axis assembly.

The axis of each turbine was also designed to mate with the shaft. The through hole in the axes has enough clearance for the shaft to snugly pass through and attach to a threaded insert that is press fit into the bottom of the axis. This assembly can be more clearly seen in the following section.

4.3.3 Construction of the Prototype

Before construction of the wind harvester prototype commences, appropriate complete bill of materials was compiled. Aside from the electronics and the weatherproof enclosure, everything was machined from aluminum stock. This bill of materials can be seen in Appendix C. The prototyping cost met the constraint of $600 stated earlier in this chapter.

Once all the parts were machined and the SLS turbines arrived from Solid Concepts, Inc. located in Austin, the assembly process took about 30 minutes to complete. The finished prototype was mounted on an aluminum stand that was created to accurately simulate the actual attachment location, as well as the time to install the system. The full system can be seen in Figure 4.10 with a National Instruments (NI) Wireless Sensor Node (WSN) mounted on the outside; the individual parts and

assemblies can be seen in Appendix D. The newly constructed alpha prototype was mounted in less than 2 minutes by hooking over the angled beam and was tightly secured using the rubber clamps. This was well below the constraint of 1.5 hours described in Table 4.2.

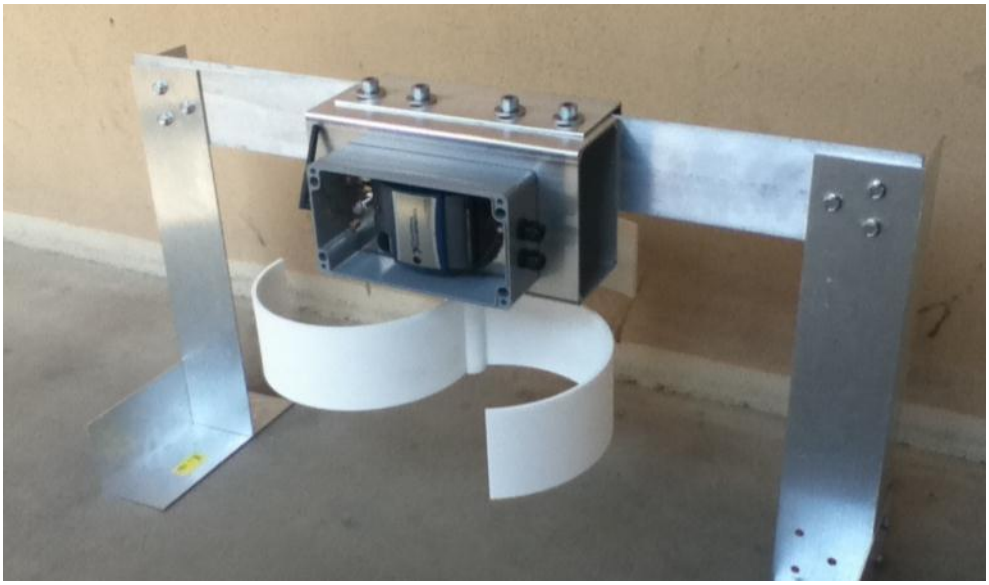

Figure 4.10: Completed alpha prototype of the next generation wind harvester.

4.4 TESTING OF ALPHA PROTOTYPE

During the testing phase of the alpha prototype, a detailed experimental plan was formulated and carried out in order to monitor key outputs of the system. Furthermore, it should be noted that another goal of running these experiments was to compare them with the results achieved from the analytical model in the previous chapter.

4.4.1 Experimental Plan

A plan was created in order to give structure to the experiments that were meant to prove or disprove various hypotheses. These hypotheses were formulated from design issues in previous chapters, dealing with turbine type, motor specifications, and ability to charge a battery. A total of three distinct experiments were executed and repeated with a set number of trials. The design, noise, and performance variables were clearly defined for each experiment. The experimental plan and hypotheses are explicitly stated bellow:

HYPOTHESES

A. The 2-bladed system will be stagnant at certain points during its rotation.
B. The 3-bladed system will have a higher TSR ratio due to more blades harnessing energy.
C. The weaker, proof-of-concept motor will not be able to produce enough voltage to charge a 6V battery.
D. The stronger, recently acquired Maxon motor will be able to produce enough voltage to charge a 6V battery.

EXPERIMENTS

I. Measure the Rotational Speed

1) Run the 2-bladed system, mechanically decoupled from the motor, and determine the response.
2) Repeat for a 3-bladed system.

	Variable	**Measurement Device**
Design	Wind speed (mph)	Anemometer
	Number of blades	N/A
Noise	Air environment	Fan in controlled environment
Performance	Rotational speed (rpm)	Piezo hits
	Tip to Speed ratio	Anemometer & Piezo hits

II. Measure the Voltage Produced from the Weaker Motor

1) Run the 2-bladed system, mechanically coupled with the weaker motor, but electrically decoupled, and determine the response.
2) Repeat for a 3-bladed system.

	Variable	Measurement Device
Design	Wind Speed (mph)	Anemometer
	Number of blades	N/A
Noise	Air environment	Fan in controlled environment
Performance	Voltage (V)	NI DAQ Board
	Rotational speed (rpm)	Piezo hits
	Start-up torque (mNm)	Weight pulley

III. Measure the Voltage Produced from the Stronger Motor

1) Run the 2-bladed system, mechanically coupled with the stronger motor, but electrically decoupled, and determine the response.
2) Repeat for a 3-bladed system.

	Variable	Measurement Device
Design	Wind Speed (mph)	Anemometer
	Number of blades	N/A
Noise	Air environment	Fan in controlled environment
Performance	Voltage (V)	NI DAQ Board
	Rotational speed (rpm)	Piezo hits
	Start-up torque (mNm)	Weight pulley

Each experiment and sub-experiment was performed three times to avoid bias due to random error. The wind speed was varied for each trial, and each performance variable was measured and averaged over a 10 second span once the turbine reached steady state. The noise variable was minimized by performing the experiments in a controlled environment with a fan that produces a consistent, laminar air flow. It should also be noted that the rotational speed was measured by the number of times the turbine axis hits a piezoelectric strip with a protruding set screw. Each time contact is made, a voltage spike can be measured by the DAQ board, and the rotational speed can be calculated.

4.4.2 Testing the Hypotheses

Experiment #1

The 2 bladed and 3 bladed systems were mounted on the alpha prototype and tested over various wind speeds. The purpose of this experiment was to examine any difference in the performance capability between the two turbines, as well as to test Hypotheses A and B stated above. The results for the rotational speed and tip to speed ratios for both turbines are shown in Figures 4.11 and 4.12.

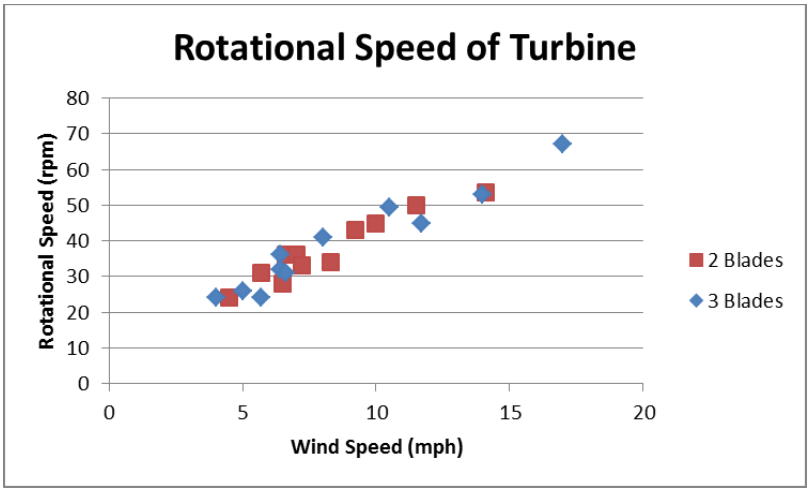

Figure 4.11: Rotational speed of the 2 and 3-bladed turbines.

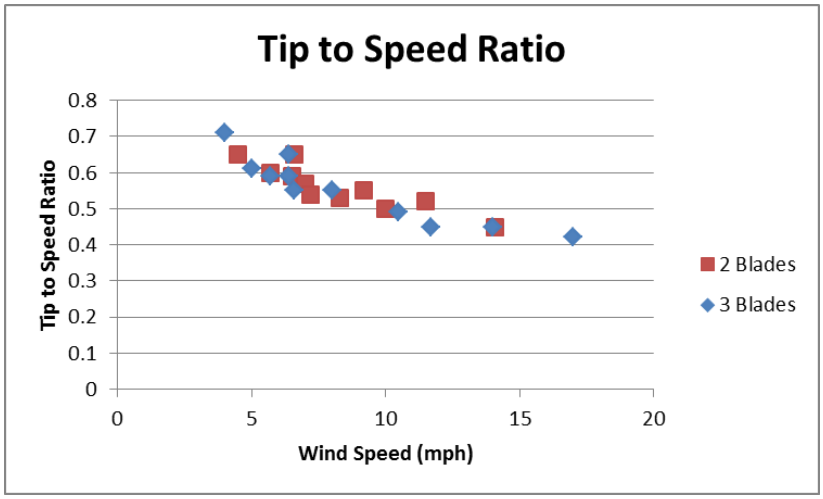

Figure 4.12: Tip to speed ratio of the 2 and 3-bladed turbines.

There is very little if no variance in the rotational speed and tip to speed ratios between the two types of turbines. Adding another blade seemed to have no significant influence over the performance of the turbine. This disproved Hypothesis B; a 3-bladed system will ***not*** have a higher TSR ratio due to more blades harnessing energy. However, an observation made during the tests was that the 2-bladed system was in fact stagnant at certain points during its rotation. This verifies the assumption stated in Chapter 3 that the wind flowing on both sides of the turbine can cause equal moments and a point of equilibrium. The results in the figures above only indicate the times when the 2-bladed system reached steady state operation, although there were many occasions where it was simply stagnant and could not begin rotating because of its specific orientation. This proves Hypothesis A to be true; a 2-bladed system ***will*** be stagnant at certain points during its rotation. Given this result, we can amend the conclusion made about Hypothesis B. Even though a 3-bladed system does not reach a higher TSR than a 2-bladed system, it will be more advantageous to use because it truly does not depend on the wind direction and will never become stagnant.

Experiment #2

The first performance variable measured was the start-up torque of the motor, which was determined by hanging weights from the shaft. This torque was approximately 13.5 mNm. The motor was then mechanically coupled to the shaft and its voltage output was measured through the DAQ board, along with the associated rotational turbine speed. Figure 4.13 displays the voltage output versus the rotational

speed to verify the V/rpm ratio discussed in Chapter 3. Likewise, Figure 4.14 shows the voltage output versus the design variable: wind speed.

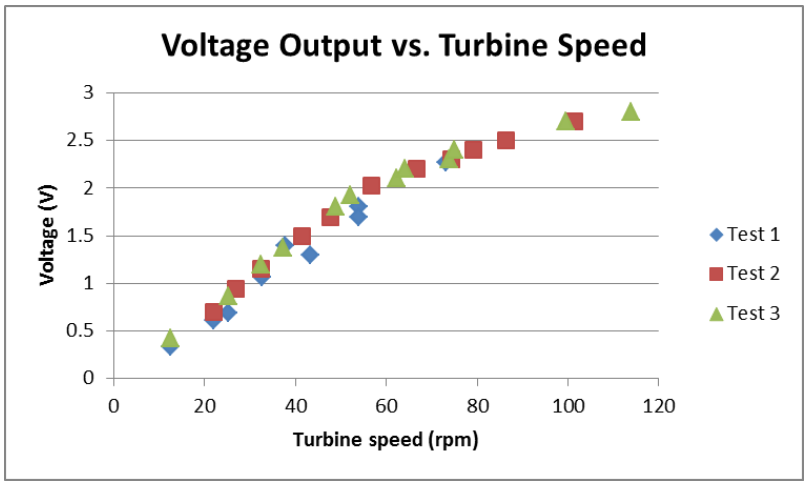

Figure 4.13: Voltage output versus turbine speed of the alpha prototype.

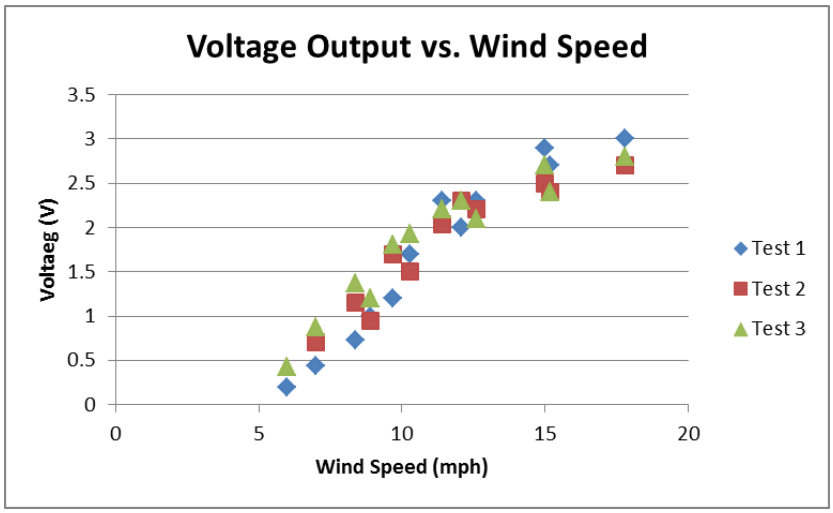

Figure 4.14: Voltage output versus wind speed of the alpha prototype.

Figure 4.14 shows a trend that never reaches a voltage above 3 V, so we can safely say that Hypothesis C is true; the weaker motor will not be able to produce enough voltage to charge a 6V battery. Even though Figure 4.14 possibly shows a non-linear trend, we maintain our assumption that the voltage output is linearly proportional to the

rotational speed to simplify the calculation of the V/rpm ratio, based on an R^2 value of .89. The justification for this assumption is that the motor is not limited by the RPM input, but that the wind turbine itself is limited by a decreasing efficiency as wind speed increases due to the Savonius design, with its maximum TSR value below 1. This will be demonstrated later in this chapter.

Based on the linearity assumption, the linear trend displays that the V/rpm ratio for this weaker motor is 0.0237. Even though it is larger than the motor specifications indicated (0.011), it is still smaller than the recommended value of 0.035, further disproving Hypothesis C. The voltage produced in this experiment is compared to the analytical model in a later section.

Experiment #3

The start-up torque of the stronger motor was measured to be 40.1 mNm, which is around 3 times the value of the weaker motor. The motor was then mechanically coupled to the turbine system. The same strategy for measuring the performance variables was employed for this experiment. However, there were some problems that were immediately noticed from trying to measure the voltage output and rotational speed. For the two-bladed turbine, the system would not rotate at any of the preset wind speeds from the previous experiment. This system was then replaced by the 3-bladed turbine to repeat the test, but it would not begin spinning until wind speeds reached around 20 mph. Even then, the turbine rotated at an extremely slow rate—around 20 rpm—nowhere near high enough for electricity generation. This result disproved Hypothesis D; the stronger motor will ***not*** be able to produce enough voltage to charge a 6V battery. Of course, it could

potentially produce enough voltage at higher wind speeds, but it is implied that electricity generation should occur at reasonable wind speeds.

The results from Experiments #2 and #3 also led to conclusions that concur with the hypotheses made at the end of Chapter 3. The size and type of turbine were not suitable for this application: firstly, the turbine is too small and does not have enough swept area to overcome the start-up torque of the motor; secondly, the Savonius style turbine is limited by its aerodynamic properties and can never reach speeds high enough for a beneficial amount of electricity generation. In the next section, the experimental and analytical results are compared to prove that the Savonius is not the right type of turbine to be used for this application.

4.4.3 Experimental vs. Analytical Results

Verifying the Power Coefficient

Before comparing the voltages and tip to speed ratios, one key verification that needed to be completed was the power coefficient of the Savonius turbine. The power coefficient used in the calculations for the analytical model was acquired from previous empirical studies. To determine the validity of this value, the actual power coefficient was calculated from the experimental results using simple power ratios. The power coefficient C_p by definition is the ratio of the electricity produced by the wind turbine over the total energy available in the wind (Kindwind, 2012). This ratio can be broken down into two components. The first is the fraction of energy that can be harnessed from the wind, for which the maximum amount is Betz's limit of 59.3%. The second component is the fraction of energy that can be converted into electricity, which is

governed by the efficiency of the system. Using the data from the experiments performed, the power coefficient was calculated by assuming that the power harnessed by the wind turbine is equivalent to the power delivered by a laminar fluid to a flat plate (Munson et al., 1998).

$$P_{plate} = \frac{1}{2}\rho A(v - U)^2 U \qquad (4.1)$$

where v is the fluid (wind) speed and U is the tangential velocity of the plate. The tangential velocity can be expressed in terms of the measured TSR in the experiments.

$$U = \lambda v \qquad (4.2)$$

where λ is the TSR. Using Equation 3.2 from Chapter 3 that explicitly states the amount of power P that can be delivered by the wind, we can form the following ratio:

$$C_p = C_e\left(\frac{P_{plate}}{P}\right) \qquad (4.3)$$

We can substitute Equations 4.1 and 4.2 into the ratio above to form the final equation to calculate the power coefficient.

$$C_p = C_e(\lambda - 2\lambda^2 + \lambda^3) \qquad (4.4)$$

The efficiency coefficient C_e in Equation 4.4 is unknown, so it will be assumed that the total system efficiency of converting rotational energy to electrical energy is around 80%. Equation 4.4 has been verified through algorithms previously conducted to estimate the power coefficient using more complicated algorithms (Mok, 2005). However, the power coefficient was still estimated as a function of the TSR:

$$C_p\big(\lambda(t)\big) = [a_3\ a_2\ a_1\ a_0]\begin{bmatrix}\lambda^3(t)\\ \lambda^2(t)\\ \lambda(t)\\ 1\end{bmatrix} \qquad (4.5)$$

Using this equation and the gathered TSR data, the power characteristic curve of the wind turbine prototype was constructed, as shown in Figure 4.15.

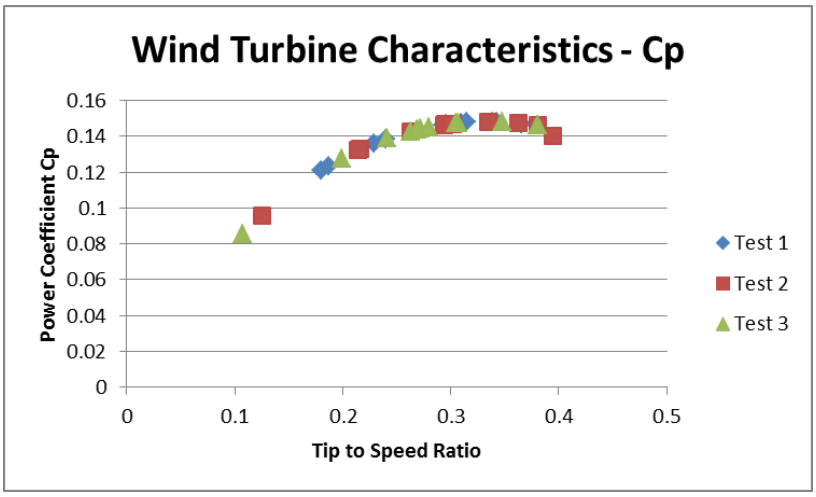

Figure 4.15: Power coefficient C_p of the wind turbine from empirical data with respect to TSR.

The power curve generated from the experimental results indicates that the maximum coefficient achieved was 0.15, at a TSR between 0.3 and 0.4. If we recall Figure 2.1 from Chapter 2, the Savonius turbine can experience a maximum power coefficient of 0.2 at a tip to speed ratio of less than 1. As soon as the Savonius turbine experiences a TSR greater than 1, its efficiency is extremely hindered. This parabolic curve is reflected in the results of Figure 4.15, as the power curve steadily increases and then begins to exhibit a slight decrease once the maximum is reached. The results were also compared to experiments conducted by other researchers at the Indian Institute of Technology at Bombay. A power curve was constructed from the results of an experiment with varying Reynolds numbers to determine the differences between single stage, two stage and three stage Savonius turbines (Kamoji et al., *Energy Research* 2008).

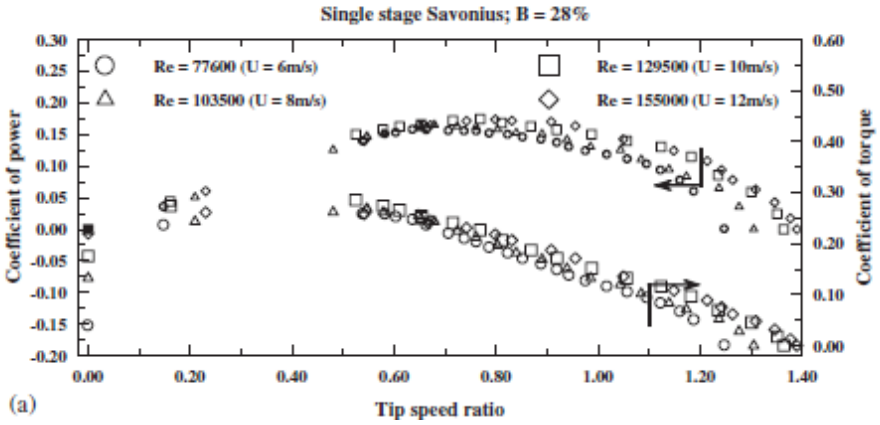

Figure 4.16: Experimental results of a single-stage Savonius rotor with varying power coefficients compared to the tip to speed ratio (Kamoji et al., *Energy Research* 2008)

As can be seen from Figure 4.16, the power curve exhibited the same behavior as the power curve constructed from the experiments reported in this chapter, resulting in a maximum between 0.15 and 0.20. This supports the conclusion that the constructed prototype embodies the performance capabilities of other Savonius turbines and previously conducted experiments. Furthermore, the results indicate that the power coefficient used in the analytical model was a correct assumption.

Voltage Produced and Tip to Speed Ratio

Once the power coefficient was verified, the voltage output and TSR from the experimental and analytical results were compared. A parametric study was completed with the analytical model by incrementally varying the wind speed and taking the maximum voltage produced once the system reached steady state. The maximum rotational speed was also noted, and divided by the respective wind speed to achieve the tip to speed ratio. The results are shown below in Figures 4.17 and 4.18.

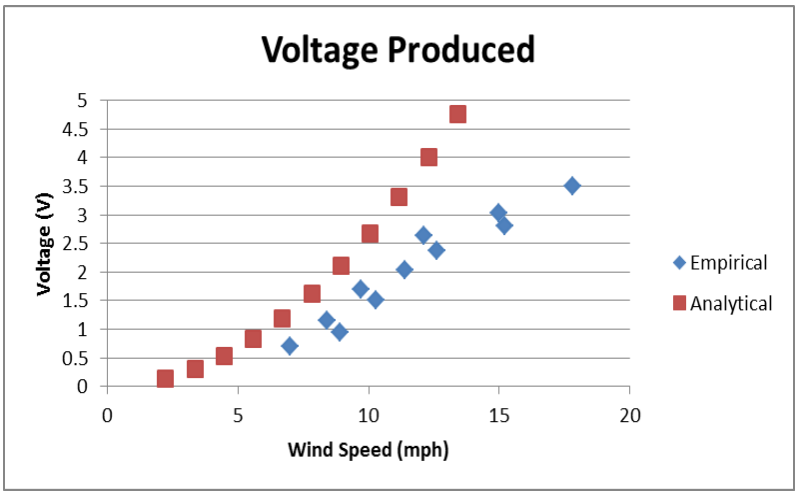

Figure 4.17: Empirical and analytical data of the voltage produced.

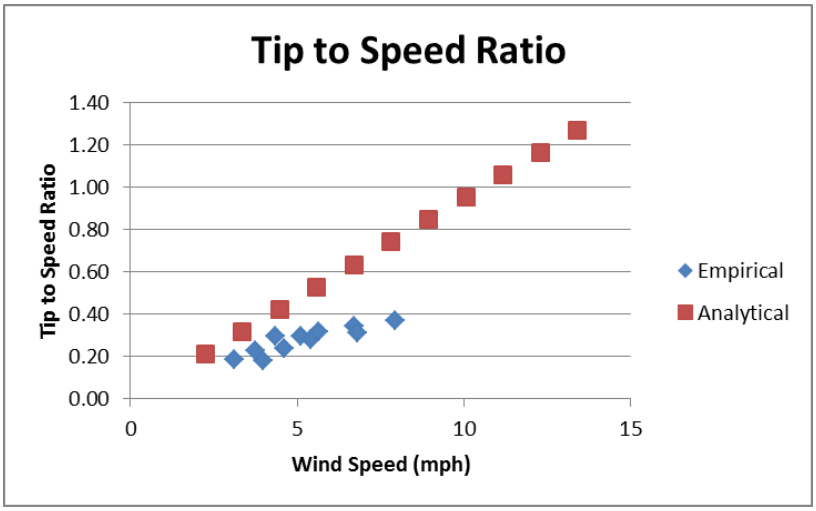

Figure 4.18: Empirical and analytical data of the tip to speed ratios.

Even though both the empirical values for the voltage and tip to speed ratio were below the predicted values, the analytical model is a good representation of the experimental results based on the correlations from the figures above. The analytical voltage increases exponentially based on the fact that the amount of energy available in the wind is a function of the square of velocity. The empirical voltage does not exhibit

the same behavior because the analytical model does not account for the performance limitations of the Savonius turbine when the wind speed and TSR ratio are increased, as previously discussed in this chapter. The difference between the two results can also be due to more friction inherent in the system, a less than perfect conversion from mechanical to electrical energy, as well as other mechanical losses that were not accounted for in the analytical model.

4.4 DISCUSSION

This chapter described tests of the hypothesis that VAWTs are not suitable for this application. In particular, details of the design and experimentation of an alpha prototype are reported. Furthermore, the results from the experiment also verify the results from the analytical model.

The original problem statement asserts that the current proof of concept does not produce a desirable voltage level. The results achieved from the analytical model indicate that the current size of the motor and turbine from the proof of concept VAWT need to be altered in order to produce enough energy to charge a battery. With the idea in mind of being mounted on a bridge for field testing if lab testing proved otherwise, the alpha prototype was constructed to the dimensions of the proof of concept to verify this hypothesis. The experimental results indicated that the system indeed never reached voltages higher than 3 V, well below the required amount of 6 V for the WSN. Even with the new, more powerful motor coupled to the turbine, it was observed that the size of the turbine could not produce enough torque to overcome the cogging torque of the generator with wind speeds less than 18 mph.

The design results in Chapter 3 show that it is infeasible to redesign the motor for the given size of the turbine, so the turbine was parametrically optimized to be large enough to harness a sufficient amount of energy. However, increasing the size of the turbine had severe consequences on the turbine's weight and the time it took for the system reach steady state. Furthermore, once it did reach steady state, the results did not reflect the actual behavior of VAWTs, which have TSRs less than 1. The experiments in this chapter verified that the TSR never even exceeded 0.5 even with increasing wind speeds, proving that this limiting factor of Savonius VAWTs was detrimental to electricity generation. Savonius VAWTs are more suitable for high torque applications, such as water pumps, due to their inability to reach high enough speeds and their low power coefficients (Hau, 2011).

In addition, the hypothesis that the three bladed system is more advantageous that the two bladed system was also verified in this chapter. During the experimentation phase with the new, more powerful motor, the three bladed system could begin rotation from any position because of its universal angle of attack. Further, it was observed that the two bladed system became stagnant at certain positions during its rotation because it was experiencing a balance of moments and equilibrium.

Finally, the results of the analytical model were compared and verified through the experiments conducted in this chapter. Therefore, the postulations made at the end of Chapter 3 as a result of the findings from the analytical model can be established as accurate and in accord with the findings from the literature discussed in Chapter 2. In

conclusion, the VAWT is not the most suitable turbine for this project and a HAWT should be implemented for the next generation design.

Chapter 5: Next Generation Wind Turbine Design

5.1 MOTIVATION

In the previous chapter, a prototype was designed, constructed and tested to verify the hypothesis that Savonius VAWTs are not suitable for the scope of this project. It was concluded through the findings that in fact the prototype performed as expected from the analytical model, and that a HAWT should be pursued for the next generation system. This chapter discusses the benchmarking of a commercially available turbine, the design of the next generation system, and the methodology and design of non-destructive attachment systems.

5.2 COMMERCIAL TURBINE BENCHMARKING

To help determine the proper size for a wind turbine for our bridge health monitoring applications, a commercially available wind turbine was purchased for benchmarking its performance. The smallest state-of-the-art HAWT was desirable for experimentation. After a thorough search, the 12V 400W AIR-X turbine from Southwest WindPower was purchased. The specifications of the AIR-X turbine are given in Table 5.1.

Table 5.1: Performance specifications of the AIR-X wind turbine (Air X, 2012).

Model	AIR-X
Rated Power	400W @ 28 mph
Weight	13 lbs
Diameter	46 in
Start-up Wind Speed	8 mph
Killowatt Hours/month	38 kWh/month

Experiencing the Product

One key observation made while experiencing the state-of-the-art wind turbine was the start-up torque of the generator. It was noticed during assembly that the generator shaft spins rather easily. Using the same techniques as the empirical study discussed in Chapter 3 the start-up torque was measured to be 38.1 mNm. Recalling the two values of 13.5 mNm and 40.1 mNm from the previous generators, it was noted that the start-up torque of the commercial turbine was actually slightly smaller than one of the previous generators used in the alpha prototype. The question quickly arose was how the larger generator could have a smaller start-up torque than one of the prototypes.

The answer was in the gearboxes. The previous generators both have gear boxes, while the specification sheet of the commercial turbine indicated that the generator inside was a permanent magnet DC alternator with no gearbox. After a more in-depth investigation, it was concluded that gearboxes actually significantly hinder the performance capability of wind turbines—especially at smaller scales—because they add a detrimental amount of start-up torque to the motor. The complete explanation can be seen in the literature review section of Chapter 2.

Without using gearboxes for generators, the only way to achieve the desired output is to optimize the two parameters left: voltage and RPM. The overall size of the generator needs to be increased in order to have a beneficial V/rpm ratio without introducing a gear ratio. The previous two generators chosen for the proof of concept and the alpha prototype had gear ratios in order to increase the alternator RPM from the relatively slow input speed of the Savonius VAWT. However, the turbines did not have a large enough swept area to overcome the start-up torque of the generator once a gearbox

was introduced. The AIR-X has a larger generator to produce enough voltage, but it also has a relatively smaller start-up torque because it has no gearbox. Assuming we had a generator with an acceptable V/rpm ratio and no gearbox, such as the one in AIR-X, using a Savonius VAWT would still be detrimental because of its low TSR and relative RPM, based on the results seen in the analytical and empirical studies in previous chapters. This further proves the need to use a HAWT for this project.

5.2.1 Experimental Plan and Set-up

A series of experiments was performed to benchmark the performance of the AIR-X commercial wind turbine. The AIR-X was mounted on the rooftop of the ETC building on The University of Texas at Austin campus using a solar panel mount available from previous experiments. The wind turbine has three output leads: a positive voltage, a negative voltage and a ground terminal for protection against lightning strikes. The AIR-X already has a built-in charge controller that monitors the voltage of the battery and charges it appropriately, so the positive and negative leads were directly connected to a 12V 40A-h deep cycle lead acid battery. A load was also necessary to dissipate the energy accumulated in the battery, so the NI Gateway, which consumes around 10W, was connected to the battery terminal with an intermediary charge controller. The additional charge controller disconnected the battery from the load when there was not enough wind energy and the battery voltage dropped below a threshold level. This prevented the battery from completely discharging. The battery voltage was monitored every minute using the NI Compact Real-time Input and Output (cRIO)

system and could be accessed at any time from any remote location using a cellular modem.

Figure 5.1: AIR-X commercial turbine mounted on the rooftop.

The experimental set-up shown in Figure 5.1 monitored only the battery voltage. Additional equipment was required to record the wind speed and correlate it with the battery voltage. A wireless weather monitoring station was purchased from Urban Green Energy to record wind speeds, wind gusts, and wind direction, although it also has the capability of monitoring pressure, temperature, and rainfall (see Figure 5.2). The fastest monitoring frequency of this station is every 5 minutes, so the battery voltage was averaged over a 5 minute period. The station was mounted on the roof as well at the same level as the AIR-X wind turbine.

Figure 5.2: Urban Green Energy wireless weather monitoring station (UGE, 2012).

The experimental plan consisted of monitoring certain aspects of the system over a short period of time as well as over a long period of time. The motivation for this is to benchmark important features for the next generation prototype design. The complete experimental plan is as follows:

EXPERIMENTS

I. Monitor system over a short period of time (1 hour)

1) Estimate the V/rpm ratio
2) Determine average start-up wind speed
3) Determine an average TSR

II. Monitor system over long period of time (1 week)

1) Monitor battery voltage, wind speed, and charging periods
2) Determine wind speed to start charging battery

5.2.2 Results

Short Term Monitoring

The V/rpm ratio is difficult to measure because of the built-in charge controller, so it was estimated based on the specifications from its manual. The AIR-X is supposed to produce 12.75V when the blades reach a speed of 400-500 RPM, which corresponds to an average V/rpm ratio of .029 (Air X, 2012). If the generator were a motor used in reverse, then the appropriate speed constant would be 34.9 rpm/V, which is an excellent speed constant for generator use based on the research findings from previous chapters. The start-up wind speed was found to lie somewhere between 8 and 9 mph by averaging wind speeds monitored by an anemometer held close to the wind turbine, which also correlates to the AIR-X specification sheets. Finally, the TSR was calculated by measuring the rpm of the wind turbine using a tachometer at various wind speeds. The average TSR was found to be 4.6 at wind speeds between 15-20 mph, which are optimal charging speeds. Although each turbine has a slight variance, this TSR also correlates to the performance curves of most 3-bladed HAWTs, which have the highest power coefficients at TSR between 4 and 6.

Long Term Monitoring

The battery voltage and wind speed were monitored and graphed over an 8 day period at the end of February 2012. The cut-in wind speed was also graphed to indicate the points at which the turbine began spinning. The results are shown below in Figure 5.3.

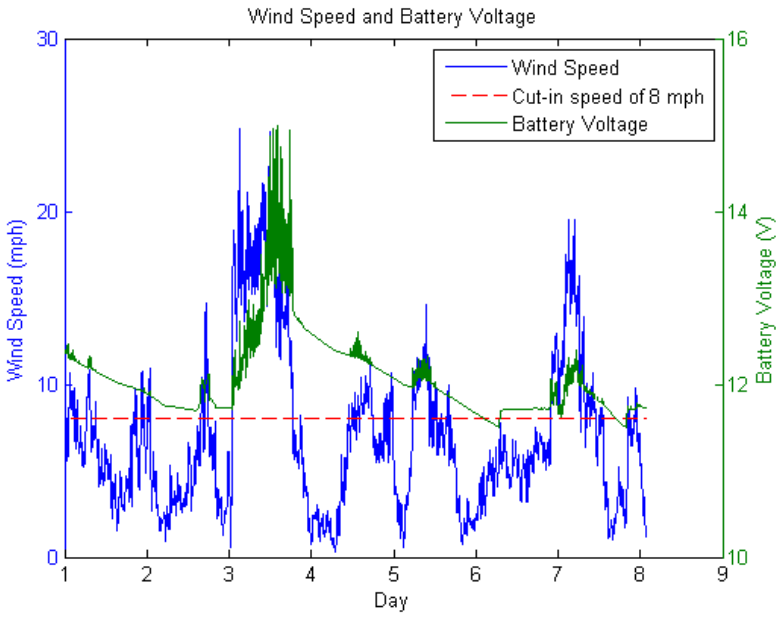

Figure 5.3: Wind speed and battery voltage over an 8-day period.

The turbine started to trickle charge the battery as soon as it reached the cut-in wind speed of 8 mph. This indicated that the wind turbine was producing more voltage than the battery voltage in order to commence charging, meaning that there is enough power in the wind given the size of the turbine at the specified cut-in wind speed of 8 mph. These facets of the AIR-X provide good benchmarks, but more information was required to size the next generation turbine. Specifically, the available power for a given wind speed is needed. In order to perform this prediction, the power coefficient was calculated by measuring the power produced and dividing by the theoretical available power in the wind.

$$C_p = \frac{P_{elec}}{P_{wind}} = \frac{V*amp}{\frac{1}{2}\rho A v^3} \qquad (5.1)$$

A Hall-effect sensor was attached to one of the leads from the turbine while the battery voltage was being monitored. The wind speed was also recorded at the instant the voltage and current were measured. A series of ten measurements were taken, and the average power coefficient was found to be C_p = 0.44. This value was higher than expected, but it was soon discovered that the power coefficient was skewed because of imprecise voltage measurements. The voltage monitored from the system is the battery voltage, not the true voltage, so it does not indicate the true voltage produced for lower wind speeds. Therefore, the power coefficient was recalculated for wind speeds higher than the cut-in speed, and the average was found to be approximately C_p = 0.34.

Once the power coefficient value was estimated, a simple analytical model was created to compare the results to the AIR-X power curve provided in the specification sheet using the following equation:

$$P = \frac{1}{2} C_p \rho A v^3 \qquad (5.2)$$

The performance specifications give a "bandwidth" of power that should be expected from the AIR-X turbine based on whether or not the input wind is steady or non-steady (Air X, 2012).

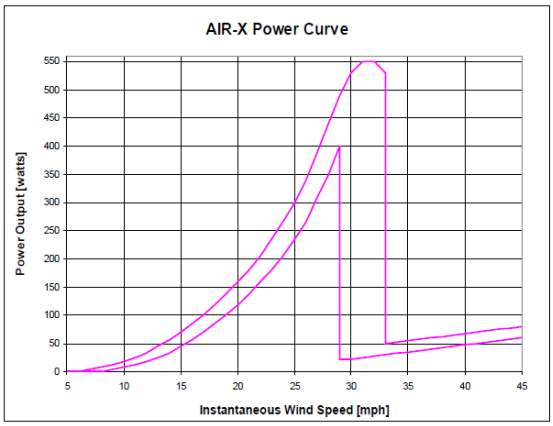

Figure 5.4: AIR-X power curve for steady and non-steady wind conditions (Air X, 2012).

The power curve shown in Figure 5.4 follows a steady power curve up until the cut-out wind speed where the turbine begins to regulate and slow its speed. Because it would be difficult to model this behavior, the power curve up until the cut-out wind speed was compared to the analytical model using the lowest value of the power coefficient found. The code for this model can be seen in Appendix E.

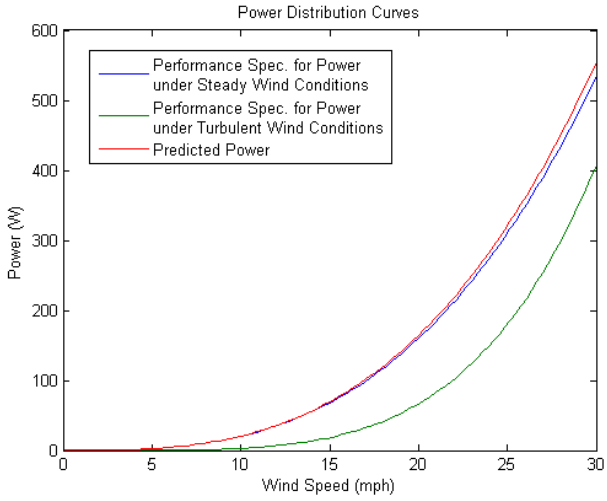

Figure 5.5: Power curves for steady and non-steady wind conditions, compared with the analytical model for predicted power.

As can be seen in Figure 5.5, the predicted power from the analytical model more closely follows the steady wind power curve rather than the non-steady wind power curve. This will have to be taken into account for the next generation design. Based on the bandwidth given by the specifications, non-steady wind conditions produced around 20% less power for optimal charging conditions between 10 and 20 mph, as can be seen in Figure 5.6. The reason why there is 80% less power for the cut-in speed is because the wind can fluctuate in and out of the cut-in speed and therefore sometimes will not produce any power at all.

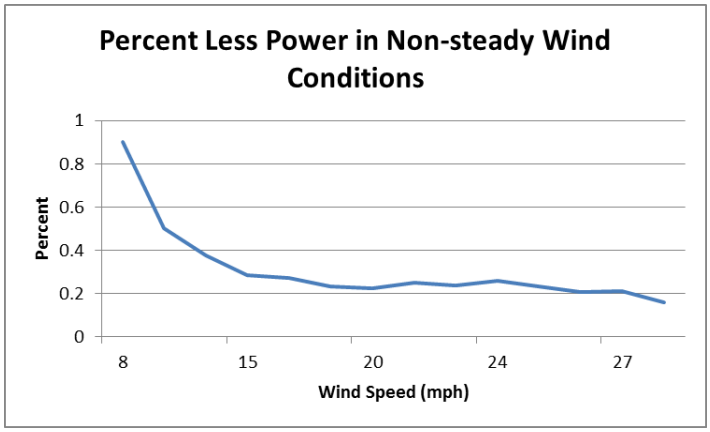

Figure 5.6: Percent less power in non-steady wind conditions.

It will be assumed that the wind profile acquired by the wireless weather station is a steady wind speed based on the fact that it averages the wind speed over a 5 minute period. Based on this assumption, the expected power was plotted along with the power associated with the cut-in wind speed in Figure 5.7 below.

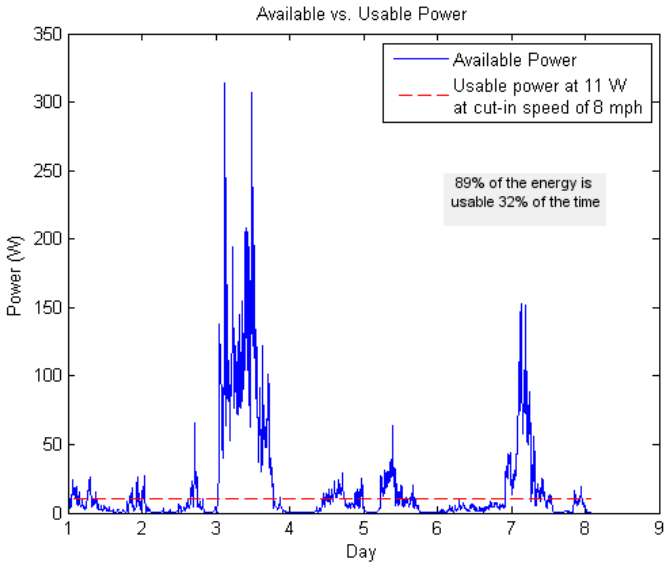

Figure 5.7: Available and usable power based on a given wind profile for the AIR-X.

Based on these results, the power associated with the cut-in wind speed for the AIR-X is 11W, which is just more than the power dissipated by the connected load (Gateway) at 10W, meaning that there is more power going in than out. This correlates with the data from Figure 5.3 with the battery starting to charge at the cut-in speed as well. These findings reveal that the specifications of this turbine (size, cut-in speed) are well-suited for powering the designated load, which gives a good benchmark for designing the next generation turbine.

Figure 5.7 also indicates that 89% of the energy available in the wind is usable only 32% of the time. This indicates that wind turbines only harness energy a fraction of the time when wind speeds become high enough and they should be optimized for the lowest cut-in speed possible. This also gives a clue about appropriately sizing a battery for energy storage, presented in the next section.

5.3 DESIGN OF NEXT GENERATION WIND TURBINE SYSTEM

5.3.1 Sizing the Next Generation System

The experiments completed in the previous section provided a good benchmark of the appropriate size for turbines based on their applications. The analytical model for predicted power was verified to correlate with the commercial turbine specifications and was used to size the next generation turbine. The end goal was to design a turbine to successfully produce enough energy to power the required load—or in this case—the router. The following flow chart in Figure 5.8 illustrates the steps taken to properly size the wind turbine for the next generation system.

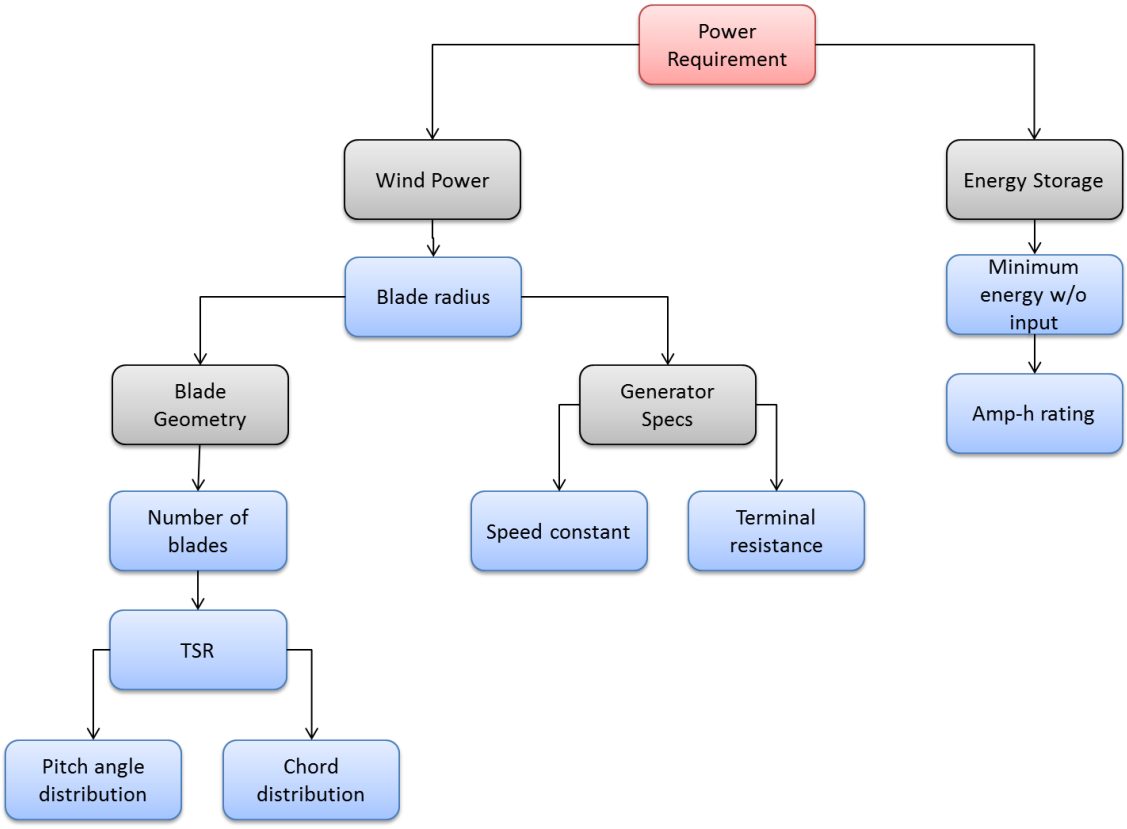

Figure 5.8: Wind turbine design flow chart.

Power Requirement

1. Assume a power coefficient and minimum cut-in speed
2. Find minimum blade size to achieve enough power for load at cut-in speed

The first step in designing a wind turbine is to determine the minimum swept area needed to harness enough power from the wind, assuming a given power coefficient and cut-in speed. In order to achieve this goal, a parametric study of varying radii and power coefficients was performed. The radius was varied to determine the minimum radius needed to produce enough power, while the power coefficient was varied to detect its sensitivity to expected power.

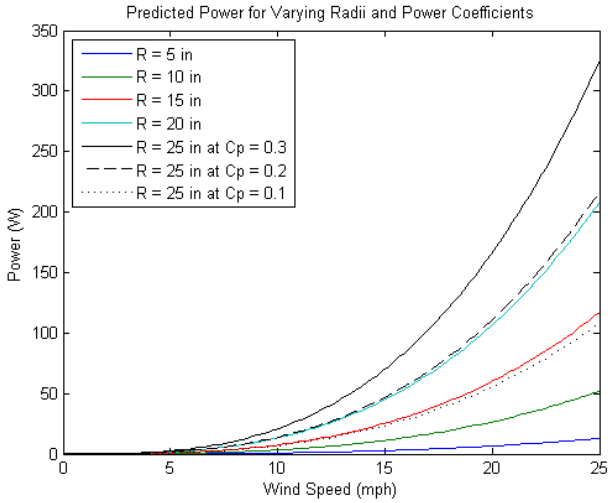

Figure 5.9: Predicted power for varying radii and power coefficients.

Figure 5.9 shows that the 25 in turbine produces around 325W, while a 5 in turbine produces around 13W in 25 mph winds. However, both of these scenarios are for a power coefficient of 0.3, and this coefficient varies according to different TSRs and corresponding wind speeds. The power curve for the 25 in turbine was plotted for power

coefficient values of 0.2 and 0.1. The plot shows that lower values of power coefficient are fairly detrimental to power produced. In fact, a drop of 0.1 in the power coefficient corresponds to about a 5 in decrease in turbine size. This simply indicates that the turbine prototype should be overdesigned at a power coefficient of 0.1 in case it underperforms.

Another parametric study was completed for a range of smaller radii in order to find the minimum size needed to produce enough power for a given load. In this case, the given load is the router, which dissipates around 300 mW. The power coefficient was assumed to be 0.1, while the minimum cut-in speed to start producing enough power was assumed to be 10 mph. Additionally, the predicted power was reduced by 20% to account for non-steady wind conditions using the findings from Figure 5.6. The results are shown below.

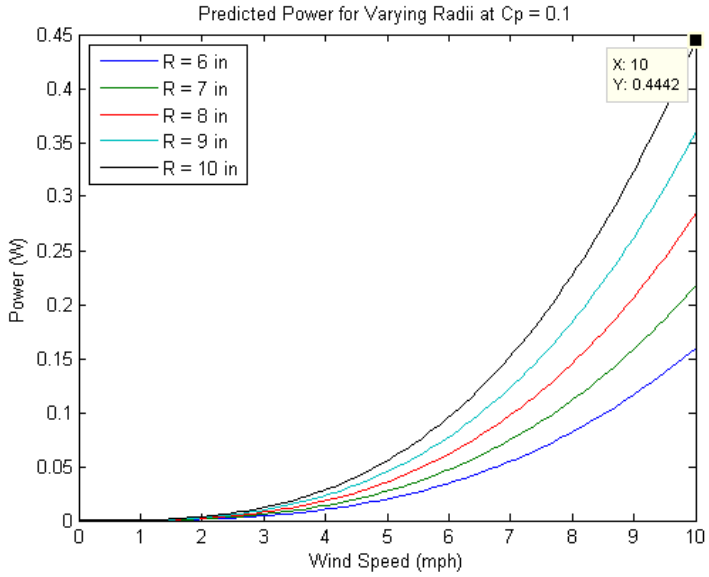

Figure 5.10: Predicted power for varying radii at a power coefficient of 0.1

The results from Figure 5.10 indicate that a power level of around 400 mW can be produced with a turbine blade radius of 10 in, meaning the power going into the system is just equal to the power leaving the system. This radius was then used to measure the predicted power based on the previously acquired wind profile. The usable power was calculated for speeds over 10 mph, along with the amount of total usable energy harvested over the time period.

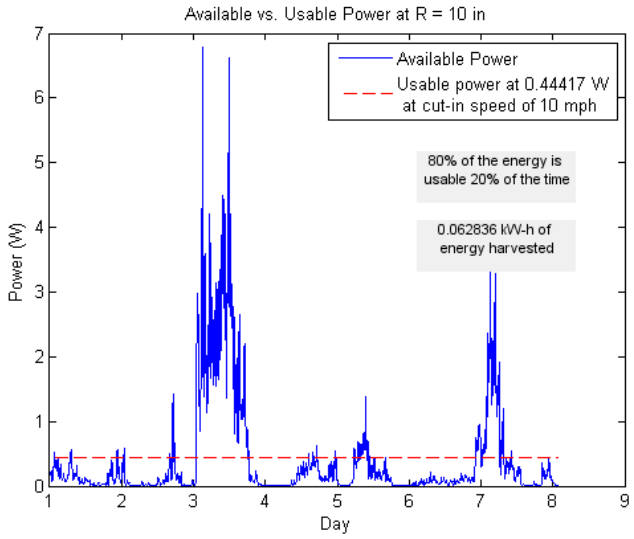

Figure 5.11: Available and usable power based on a given wind profile for the next generation turbine.

Figure 5.11 shows that usable power begins at .44 W based on a cut-in speed of 10 mph. Additionally, around 62.8 W-h were harvested given this wind profile, which is more than the router would consume over 7 days—around 50.4 W-h—suggesting that a 10-inch wind turbine can supply enough energy for the router. This figure also indicates that 80% of the energy is available 20% of the time based on the higher cut-in wind speed. This is used in sizing the battery in a later section.

Blade Geometry

1. Find optimal number of blades
2. Find optimal TSR
3. Calculate optimal pitch angle distribution
4. Calculate optimal chord length and thickness distribution

It is important to carefully consider the blade geometry when building a HAWT. A well designed blade means the difference between a high and low power coefficient, and governs its overall performance. HAWT blades are designed like the airfoils of airplanes in order to take advantage of lift forces that increase their rotational speed. Lift forces give HAWTs a significant advantage over Savonius turbines, which are governed by drag forces as previously discussed. The difference between wind turbine blades and plane airfoils is that turbines have an added velocity component due to their rotation. Therefore, the total effective velocity U_T changes with respect to the rotational speed of a given blade element. The angle that governs the direction of the total effective velocity is defined as the blade inflow angle ϕ. Figure 5.12 is a schematic of the different velocities and angles at which they occur at.

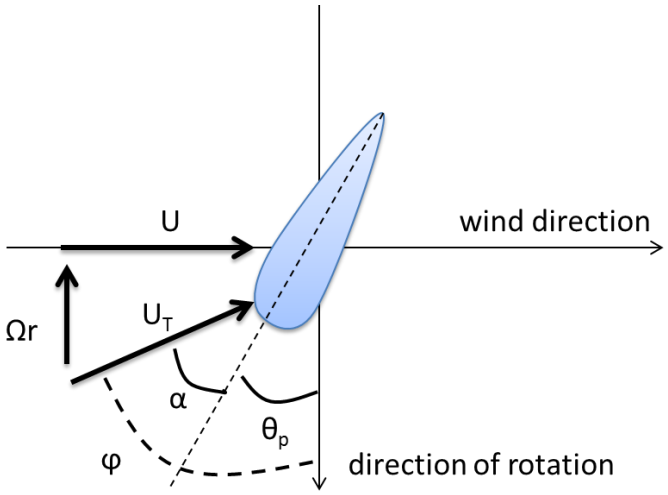

Figure 5.12: Velocities and angles for a blade element at a given radius (Wood, 2011)

U is the wind speed, Ωr is the rotational speed, while α is the attack angle and θ_p is the pitch angle of the blade. The blade inflow angle ϕ decreases with respect to an increase in radius or rotational speed. This relationship can be reduced to the angle being inversely proportional to the local tip to speed ratio given in the following equation.

$$tan\varphi = \frac{2}{3\lambda_r + \frac{2}{\lambda_r}} \qquad (5.3)$$

where λ_r is the local TSR as a function of radius, whose maximum value is the optimal TSR value of λ. This indicates that the blade inflow angle decreases with respect to an increase of the local TSR. If we consider the following equation, the blade inflow gives us an indication of which pitch angles are needed for different radius distances from the rotor.

$$\varphi = \alpha + \theta_p \qquad (5.4)$$

However, before we solve to find the pitch angles, the number of blades and optimal TSR must be chosen. It is important for maximum power extraction to achieve

the highest power coefficient possible. If we define the time for a blade to move into its predecessor's position as t_s and the time it takes for a disturbed wind profile to reestablish itself into a steady state as t_w, then the maximum power extraction occurs when these two times are equal to each other (Ragheb *Optimal TSR*, 2011).

$$t_s = \frac{2\pi}{N\omega} \qquad t_w = \frac{s}{V} \qquad (5.5)$$

This can be reduced to a direct function of the number of blades in any given wind turbine.

$$\lambda_{opt} \approx \frac{4\pi}{N} \qquad (5.6)$$

The most common number of blades used commercially in both large and small turbines is three, based on the fact that this provides a good balance between power and torque coefficients. Consulting Figure 5.13 below, a larger number of blades results in a high torque coefficient, meaning that it can start spinning with a low wind speed, but it has a low power coefficient based on the fact that it is limited by its TSR. On the other hand, fewer blades results in a higher power coefficient but lower torque coefficient. Therefore, the optimal number of blades is three, which results in an optimal TSR between 4 and 5.

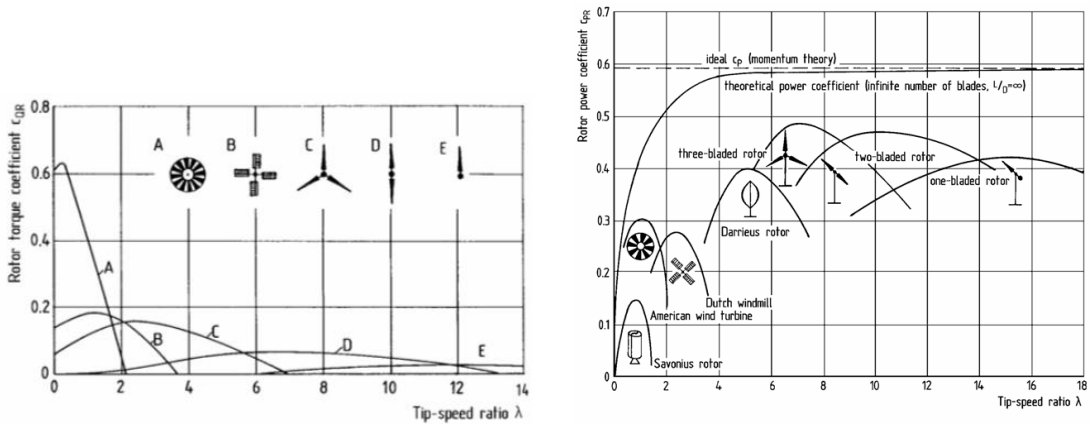

Figure 5.13: Torque coefficient (left) and power coefficient (right) as a function of TSR (Hau, 2011).

Now that the optimal TSR and number of blades have been defined, the next item to address is the angle of attack α. The Wind Energy Handbook indicates that the optimal angle of attack is somewhere in the range of 3-10 degrees (WE Handbook, 2012). There have been many experiments and empirical studies of optimal angles of attack for wind turbines with varying blade shapes and number of blades. Kim et al. (2001) indicate the optimal angle of attack is around 6 degrees for their particular experiment, while GotWind indicates an optimal angle of attack of around 5 degrees. An experiment at the Suranaree University indicated optimal angles of attack between 9-10 degrees for moderate wind speeds of 15-25 mph (Thumthae, 2008). The same experiment indicated that the optimal angles of attack increase with increasing wind speeds. Larger and more complex turbines can dynamically vary their pitch angles in order to optimize their angles of attack. However, for our application, the angle of attack will be maintained constant, and an attack angle of 5 degrees will be assumed. Therefore, Equations 5.3 and 5.4 can be combined to achieve the optimal pitch angles at varying radii. Figure 5.14 below

indicates an exponentially decreasing curve ranging from 20 to 5 degrees over a normalized radius.

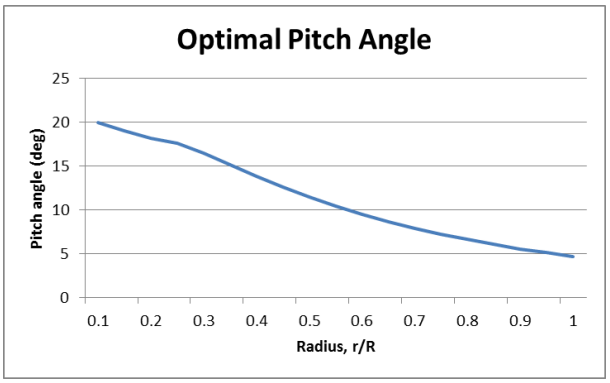

Figure 5.14: Optimal pitch angles of an airfoil as a function of radius.

The next design issue is to determine the actual geometry of the airfoil. Airfoils are governed by two dimensions, the chord length *c* and the thickness *t* as can be seen in Figure 5.16. There is also a third design variable called the camber, which is the length from the perpendicular chord length to the top or bottom of the airfoil. The National Advisory Committee for Aeronautics (NACA) has examined different shapes of airfoils, with varying thicknesses and cambers. Figure 5.15 illustrates four different airfoils associated with 4-number codes. The first number denotes the camber percentage, the second denotes location of maximum camber, while the last two numbers indicate the thickness to chord percentage. If we take 6412 as an example, a 6% camber occurs at 40% of the distance, with a 12% thickness to chord ratio. In this figure, the airfoils have successively increasing cambers, but all the same thickness.

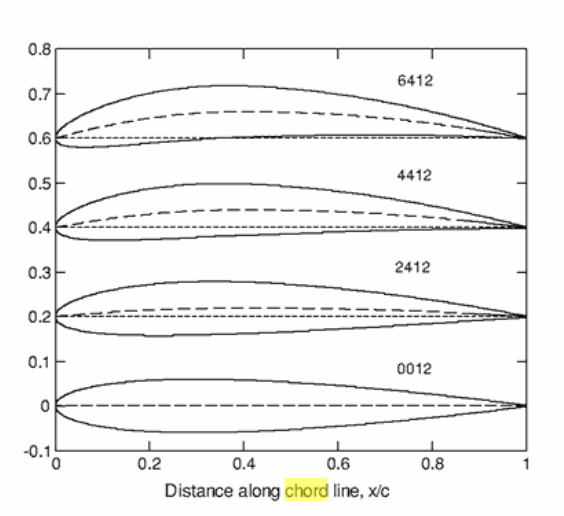

Figure 5.15: Four examples of NACA airfoils, with successively higher cambers (Wood, 2011).

It is common practice to assume a thickness based on the chord length. Thickness can vary anywhere from 10-20% of the chord length (Wood, 2011). If the turbine will experience larger stresses, then the thickness should be increased. The most commonly used and extensively studied airfoil in history is the NACA 0012 shown in Figure 5.15, which has been tested and used for a variety of applications (McCroskey, 1987). Therefore, a thickness of around 12% of the chord length is assumed in this research for designing the turbine blades. For the purposes of simplifying the design process, a symmetrical airfoil without any camber will also be assumed.

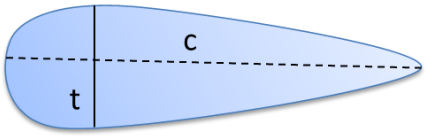

Figure 5.16: Geometry of an airfoil.

Similar to the behavior of the pitch angle, there is optimal chord length to create the maximum amount of lift based on the maximum TSR and the local TSR. The equation is given below:

$$c = \frac{16\pi}{9N\lambda\sqrt{\frac{4}{9}+\left(\lambda_r+\frac{2}{9\lambda_r}\right)^2}} \qquad (5.7)$$

This gives a non-dimensional value which can be appropriately scaled according to the size of the turbine. The idea here is to base the governing behavior of the chord length on location from the center of the turbine. Using Equation 5.7, the optimal chord length was plotted as a function of fractional distance away from the center rotor, as shown in Figure 5.17.

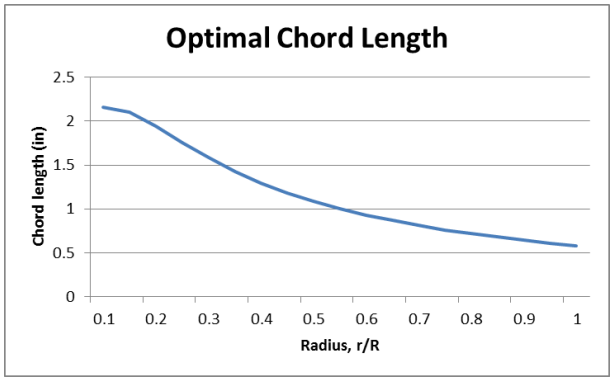

Figure 5.17: Optimal chord lengths of an airfoil as a function of non-dimensional radius.

These guidelines were used in designing the next generation blade. The finalized model was compared to the geometry of the AIR-X turbine blade used in previous experiments. The AIR-X pitch angles were measured to be similarly distributed as in Figure 5.14, ranging from 25.4 to 5.9 degrees, while the proposed design will vary from around 20% to 5%. The chord lengths of the AIR-X were also measured for reference.

They ranged from a maximum of 4.5 in to a minimum of 0.91 in. If we recall that the AIR-X (23 in) is larger than the next generation turbine (10 in), the larger chord lengths correlate with the model indicated in Equation 5.7. The AIR-X chord lengths also showed a similar distribution to Figure 5.17. The thicknesses of the AIR-X used in previous experiments were measured to vary between 9.4% and 11%, close to the assumed 12% thickness. The similar shapes of the two blades can also be seen in Figure 5.18.

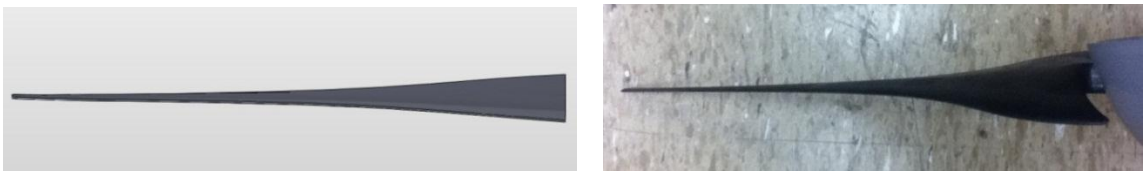

Figure 5.18: Next generation blade and AIR-X commercial blade.

Generator Specifications

1. Determine minimum speed constant to achieve required voltage based on angular speed of turbine
2. Determine current produced based on power available in the wind
3. Choose minimum terminal resistance possible
4. Calculate final voltage produced based on electrical losses and resize speed constant if needed

The most crucial specification for a generator is the speed constant, or the voltage it can produce based on a given rotational speed. Generators should be designed and constructed specifically for their given application, but for the purpose of prototyping, permanent magnet DC motors run in reverse will be used as generators. Therefore, another crucial parameter to consider is terminal resistance. There may be many motors that have speed constants in the range of 50 rpm/V, but their wiring can lead to drastic

differences in terminal resistances. Thick wires and few turns indicate low terminal resistance, while thin wires and many turns indicate high terminal resistance (Maxon Technology, 2012). The higher the resistance, the higher the losses from generated current. Ideally, the smallest terminal resistance is desirable to minimize losses, but larger motors tend to have higher terminal resistances (Maxon Technology, 2012). The analytical model from Chapter 3 was modified to perform parametric studies for the minimum speed constant required to produce enough voltage to start charging the battery based on the given blade radius. In the first study the speed constant was varied while assuming zero terminal resistance, as summarize in Figure 5.19.

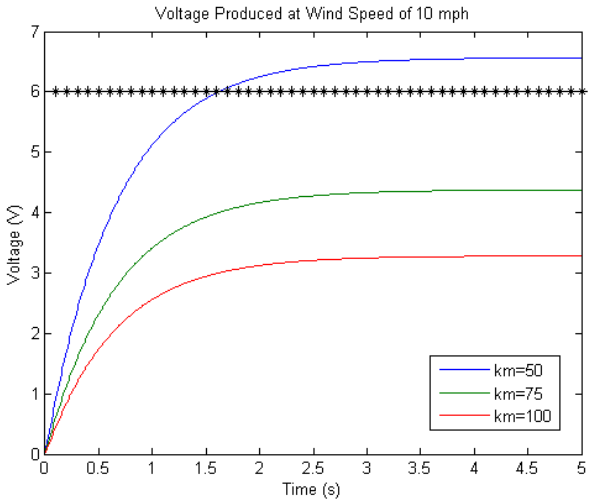

Figure 5.19: Parametric study of generator speed constants.

Figure 5.19 indicates a voltage of around 6.5 V produced at a 10 mph wind for a speed constant of 50 rpm/V. The next parametric study performed varied the terminal resistances of the generator using the 50 rpm/V speed constant. The results in Figure 5.20 indicate that higher terminal resistances result in a higher loss of voltage, further proving

that the terminal resistances should be as minimal as possible once an acceptable speed constant has been chosen.

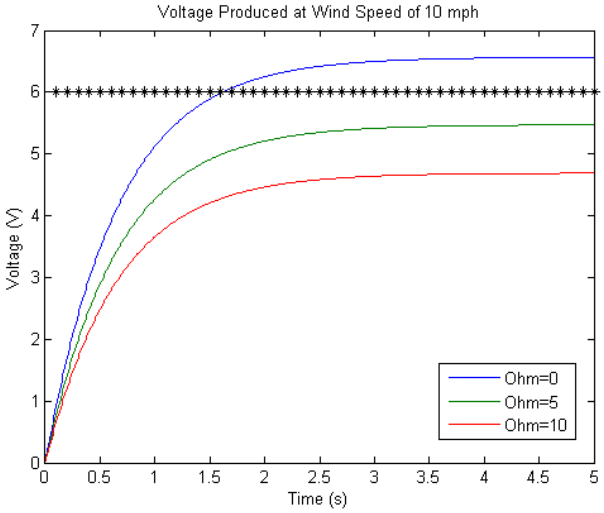

Figure 5.20: Parametric study of generator terminal resistances.

The recommended generator specifications acquired above were thoroughly searched among commercially available motors. Maxon Motor #370357 was found to have a speed constant of 39.5 rpm/V and a terminal resistance of only 3.9 Ω. Assuming power is conserved throughout the system, the maximum amount of current that can be generated from the harnessed wind power of 0.44 W is around 68 mA. Therefore, the losses from the generated current are only around 0.2 volts, which results in a generated voltage of around 6.3 V at a cut-in wind speed of 10 mph.

Energy Storage

1. Determine minimum energy storage required without input
2. Choose appropriate Amp-h rating based on required voltage of load

Finally, an important aspect of energy harvesting systems is proper battery sizing. For this specific application, it is important to consider that 80% of the energy is only available 20% of the time. Therefore, the worst case scenario for continuous days without energy input must be considered in order to size the battery. If we assume that 20% of the days in a month have enough energy to recharge the battery, then the other 80% of the days dissipate that charge. However, spring is traditionally a windy season, and February is one of the months with the highest average wind speeds at 9.7 mph, so this must also be taken into consideration (NCDC, 2008). The months with the lowest wind speeds are August and September at 7.7 mph. Therefore, there is approximately 21% less energy available in these months, leading to the conclusion that only 16% of the days in a month have enough wind energy to recharge the battery. Considering this worst case scenario, the battery must provide 300 mW for a maximum of 7 straight days, or around 50.4 W-h. Therefore, the minimum size of the battery needed is a 6V 9A-h battery in order to provide at least 54 W-h of continuous energy.

5.3.2 Design of the Next Generation System

All of the features calculated in the previous sections were aggregated into the design of the next generation turbine. The most critical components of the wind turbine resulting from the flow chart in Figure 5.8 were compiled into a spreadsheet. Because of their complex geometry, the three turbine blades can be fabricated using selective laser sintering to accurately produce the precise geometrical features. The generator will be a 200W motor run in reverse with an appropriate speed constant and terminal resistance to achieve enough voltage. A 6V 9 Ah rechargeable sealed lead acid battery will be used as

the energy storage device, with its 54 Whr rating exceeding the maximum amount of time for the energy dissipation rate of the router without input power.

Table 5.2: Key components for the next generation wind turbine.

WIND TURBINE PROTOTYPE KEY COMPONENTS					
Part #	Name	Quantity	Material	Specifications	Price
Blades					
1	Turbine Blade	3	SLS - Nylon	10 in radius	$210
Generator					
2	Permanent Magnet DC Motor #370357	1	Maxon Motors	200W, 70V, 39.5 rpm/V, 3.9 Ω	$351
Energy Storage					
3	Sealed Lead Acid Battery #HR9-6	1	Zbattery	6 V, 9 Ah, 54 Whr	$20
				TOTAL	**$581**

Table 5.2 delineates the main components for wind turbine functionality, but there are additional features required for an appropriate wind turbine assembly in order to optimize performance. The wind direction can be considered a noise variable, so the turbine needs to be able to rotate in order to perpendicularly face the wind for any wind direction. Large wind turbines can actively change their yaw angle using internal wind direction feedback sensors. However, for this prototype, the yaw angle will be changed passively using a vane, as can also be observed in commercially available small scale turbines, such as the AIR-X. The vane will be mounted to the metal casing and will allow the turbine to rotate into the wind supported by a bearing mounted between two metal sleeves. The top sleeve will be welded to the turbine mount while the bottom sleeve will be secured to the attachment system (to be addressed in a later chapter), allowing for

free relative motion between the two. The full assembly will require a casing to protect the generator, which will be secured to a metal plate with U-bolts and dampened from internal vibrations with a rubber sheet. The bill of materials for the necessary framework is outlined in Table 5.3.

Table 5.3: Bill of materials for necessary framework material.

FRAMEWORK BILL OF MATERIALS					
Part #	Name	Quantity	Material	Specifications	Price
1	Casing	1	Aluminum	3” x 4” x 6” bar	$55
2	U-bolts	2	Steel	2” OD	$7
3	Vane	1	Aluminum	6” x 6” x ¼” sheet	$50
4	Sleeves	1	Aluminum	3” OD, 3 ft. rod	$130
5	Bearing	1	Acetal	1” ID, 2” OD	$15
6	Rubber sheet	1	Rubber	6” x 6” x 1/8” sheet	$10
7	Mounting plate	1	Aluminum	6” x 6” x 1/8” sheet	$30
8	Connector	1	Aluminum	4” x 12” x ¼” sheet	$10
				TOTAL	**$307**

The full model of the next generation turbine prototype with all of the included features can be seen in Figures 5.21 and 5.22 below.

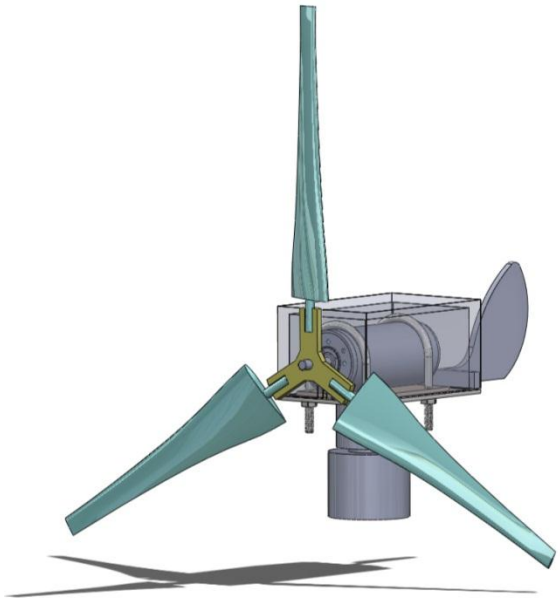

Figure 5.21: The next generation turbine.

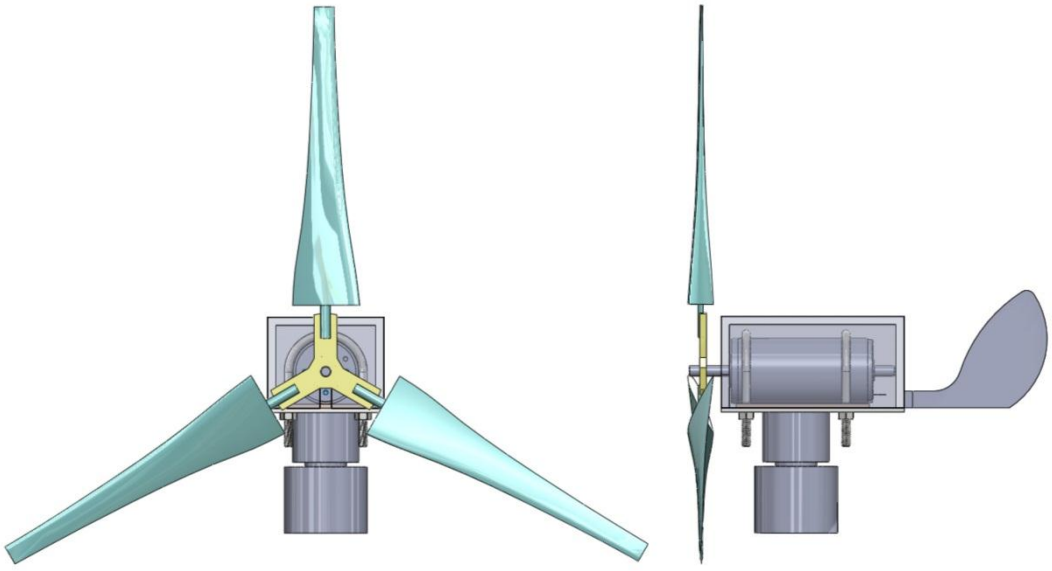

Figure 5.22: Front and side views of the next generation turbine.

5.4 DISCUSSION

In this chapter, a small scale commercially available turbine was purchased to be benchmarked for performance once the decision was made to pursue a HAWT for the

next generation design. A series of experiments was executed to monitor the system and benchmark key components of the turbine, such as the average cut-in speed, TSR, and power coefficient. An analytical model was then created to compare the experimental results to the specifications given by the manufacturer. Once proven to correlate well with the specifications, the model was appropriately scaled for the design of the next generation turbine. A flow chart was also developed to help organize the hierarchy of HAWT design. The key features addressed were minimum blade size to achieve required power, blade geometry to optimize aerodynamic performance, and generator and battery specifications to meet the power and energy storage requirements. The final design was modeled and the defining features were found to be akin to those of the commercially available turbine. The next step is to non-destructively integrate the newly designed turbine into the architecture of highway bridges, which will be addressed in the next chapter.

Chapter 6: Next Generation Attachment System

6.1 MOTIVATION

In the previous chapter, the next generation turbine was appropriately designed for bridge health monitoring applications. The next step in this project is to integrate it into the architecture of the bridge by designing an attachment system. Instead of using a haphazard approach by choosing a random location to mount the wind harvester, an attachment methodology was developed not only to increase the quantity, quality, variety and novelty of ideas, but also to structure and justify the design of the new attachment system. This was coupled with case studies of generated concepts as well as design experiments to test the validity of the methodology.

6.2 ATTACHMENT METHODOLOGY

6.2.1 Background

The design problem we are faced with is to integrate a new device or subsystem onto an existing system while meeting design requirements. There are numerous engineering design problems where the selection of the attachment method is vital. A good example is a wall-climbing robot that can attach to a variety of slopes existing in nature or structures. There have been parallel solutions to this design problem, spanning a great variety of attachment mechanisms, including electrostatic attraction, magnetic fields, and vacuums (Yamamoto et al., 2007; Berengueres et al., 2007; Elliot et al., 2006). Another good example is a project completed at Northwestern University involving the design of a robust quick-release mechanism for a paint roller holder (Ostman, 2011). It is

apparent from these and countless more examples that an attachment methodology would be useful in conceptualizing a design that satisfies the appropriate requirements.

Previous literature concerning attachments reveals that there are different classifications for these connections. It has been proposed that the various attachment methods be classified into three categories of fastening: material, form, and force (Roth, 2000). Another proposal suggests that the categories be termed mechanical, chemical, and physical (Brandon & Kaplan, 1997). Connections can also be characterized as one of fourteen physical effects that restrict movement, define the materials involved, or describe the geometry of the connection (Koller, 1984). Existing work reveals that there have been efforts into developing an attachment methodology and categorizing attachment principles, but not in the realm of non-destructive integration. The attachment methodology described in this chapter was developed for the purpose of non-destructively mounting energy harvesters onto highway bridges.

6.2.2 Research Approach

It is important to define a few key terms when dealing with attachment systems before the research approach is delineated. The device or subsystem to be attached is termed the "child", while the existing device or system is termed the "parent." The important characteristic that distinguishes the two is that the parent is always independently designed of the child, while the child may or may not be designed with the parent in mind. A couple of examples of products that exhibit this parent and child relationship can be seen below in Figure 6.1.

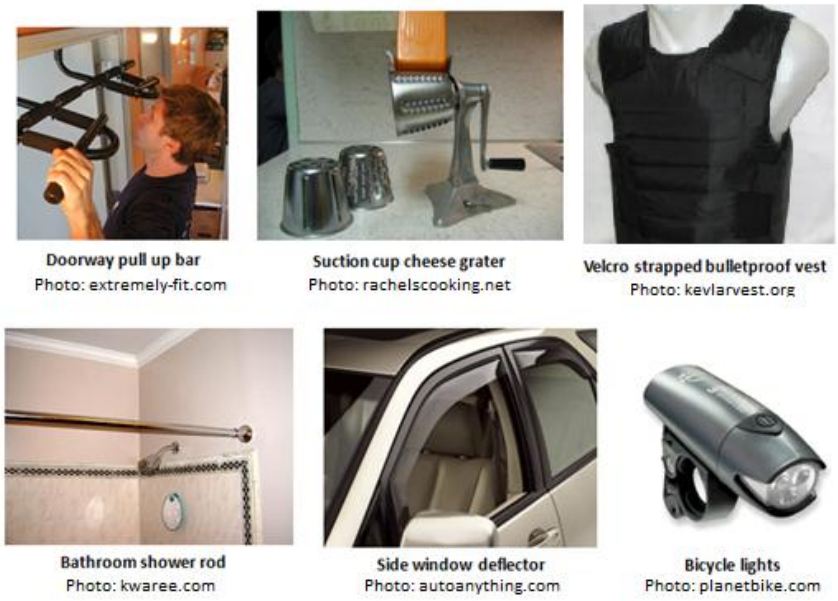

Figure 6.1: Examples of products that exhibit the parent and child relationships.

Products like these as well as patents and biological representations were used as the basis for an empirical study to define a list of attachment principles. For each example studied, the parent and child components were identified as well the geometric characteristics that enable the attachment to exist. In order to justify capturing the majority of attachment principles, the number of unique principles encountered was graphed with respect to the number of examples studied. A total of 50 examples were studied. As shown in Figure 6.2, no new principles were discovered after the first 25 examples were examined. Thus, it was assumed that the majority number of attachment principles was discovered.

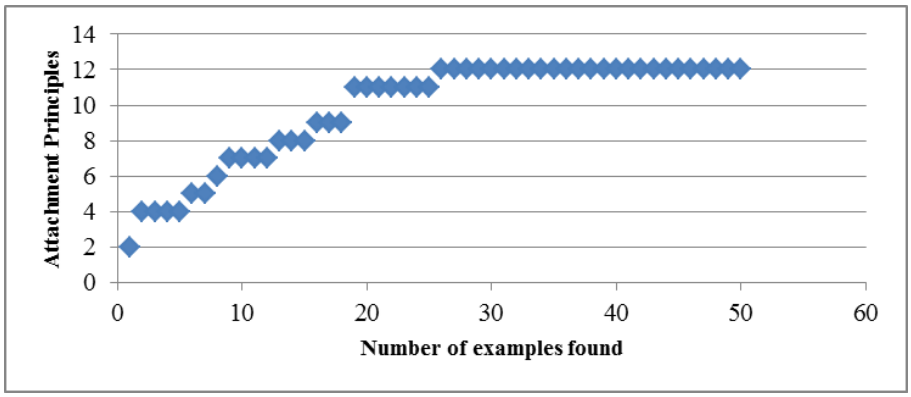

Figure 6.2: Number of unique attachment principles found.

The attachment principles were categorized into their respective domains, as previously defined in literature. The mechanical attachment principles were generalized to be independent of their original design purpose. For example, a shower rod is attached between bathroom walls to enable curtains to be hung, while a car jack is used to elevate a vehicle. However, both are defined as axially expansive attachment devices. The principles can be seen in Table 6.1 below.

Table 6.1: Attachment principles categorized into different domains

Attachment Principle Domains	Attachment Principles	Definition	Examples
Mechanical	Radial Expansive	Applies a radially outward force within a hole	Anchor bolts, Threaded inserts
	Radial Compressive	Applies a radially inward force on an extrusion	Zip ties, Hose clamps
	Axial Expansive	Applies axially outward forces perpendicular to two surfaces	Shower rod, Car jack
	Axial Compressive	Applies axially inward forces perpendicular to two surfaces	Table clamp, Doorway pull up bar
	Hook	Object is suspended through the contact interface between the upward facing surfaces of an extrusion and the downward facing surfaces of an object	Hangers, Backpack
Material	Adhesive Bonding	Reactive: Adhesives that chemically react to harden.	Epoxies, Light-curing materials
		Non-reactive: No chemical reaction required	Drying adhesives, contact adhesives, hot adhesives
	Coalescence	Attachment where two or more components merge and form a singular part	Concrete, Welding, Soldering, Brazing
	Cohesion	Attachment describing the natural attraction of similar materials	Water molecules, Surface tension
	Chemical Adhesion	Attachment where the two surfaces form ionic, covalent, or hydrogen bonds	Gecko, Wet paper on glass
Fields	Magnetic	The components are locked through the attraction of opposing magnetic fields. Magnetic field can be supplied through a permanent magnet or electrically generated.	Magnetic base dial indicator, fridge magnets
	Vacuum	The component interfaces are locked through the difference between ambient pressure and the pressure in the contact cavity	Suction cups, GPS windshield mount
	Electric	Attachment through the attraction between two electrically charged bodies	Electrostatic chuck, static balloon

For the purpose of non-destructive integration as well as feasibility, only the mechanical domain was further examined and used in the wind energy harvester case

study in the next section. A detailed list and explanation of the mechanical attachment principles, enabling characteristics and examples can be seen in Appendix F.

6.3 ADAPTATION OF METHODOLOGY

Using only the mechanical attachment principles, a case study was conducted in order to test the effectiveness of the methodology as a design tool. The design goal of this case study was to not only non-destructively attach the wind energy harvester to any portion of the bridge, but also to exhibit the variety of feasible design concepts that can be generated using the attachment methodology described in the previous section. A set of requirements, listed in Table 6.2 below, was given before the brainstorming phase occurred.

Table 6.2: System requirements.

- No permanent alterations to any metal parts of the bridge
- No part of the wind harvester can hang below the lowest part of bridge (unless it is over water)
- No part of the wind harvester can be on the driving surface of the road and it cannot interfere with bridge traffic
- Time to install should be less than 1 hour
- Service life of attachment should be at least 10 – 15 years
- Device should be portable and easy to install with minimal tools

Each design was conceptualized using different combinations of the attachment principles, as well as from a set of Theory of Inventive Problem Solving, or TRIZ, principles. The intended purpose of using the TRIZ principles was to aid in generating solutions to some of the design conflicts stemming from the system requirements. This was accomplished by translating conflicting pairs of design requirements into TRIZ generalized engineering parameters. These parameters were derived from Altshuller's 39 generalized engineering principles (Altshuller, 1984). The TRIZ principles were then

selected from Altshuller's matrix of contradictions and used in conjunction with the attachment principles. A total of four attachment systems that best represent the attachment and TRIZ principles are described below.

Attachment System #1

This attachment system in Figure 6.3 uses a U-shaped metal hook to attach to the outer concrete portion of the bridge, based on the *hook* attachment principle. The system embodies the *axial compressive* attachment principle through screw clamps on both sides of the concrete. A weight is mounted on one side of the system to balance the moments caused by the wind harvester, using the TRIZ *principle of counterweight*. Finally, the TRIZ *principle of universality* was applied based on the fact that the location and attachment type of this system can be integrated with a wind or solar harvester.

- *Attachment Principles*: Axial compressive, Hook
- *TRIZ Principles*: Principle of counterweight, Principle of universality

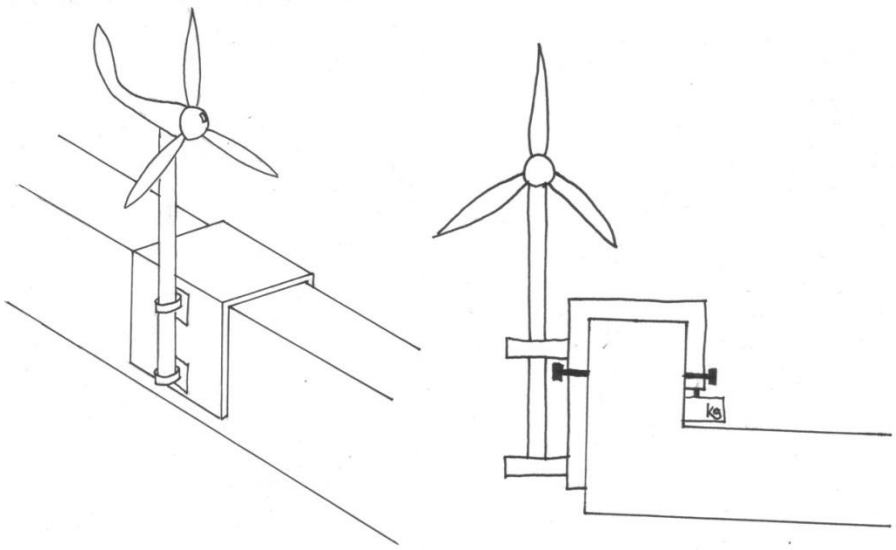

Figure 6.3: First attachment system with an isometric view (left) and side view (right)

Attachment System #2

The second attachment system in Figure 6.4 is mounted and secured between the two flanges of the I-beam underneath the bridge using the *axial expansive* attachment principle. There is no physical space for the wind harvester to rotate next to the I-beam, so the TRIZ *principle of moving into a new dimension* was applied to shift the wind harvester further away. The mechanical beams that perform this action were conceptualized using both the *radial compressive* attachment principle and the TRIZ *nesting principle*. Each beam has a smaller beam nested inside to change the extension length, and both beams are attached to the rod using clamps. Finally, the TRIZ *principle of segmentation* was applied to this system by separating the rod attached to the wind harvester into two parts: one for the harvester and one for the attachment system.

- *Attachment Principles*: Axial expansive, Radial compressive
- *TRIZ Principles*: Principle of moving into a new dimension, Nesting principle, Principle of segmentation

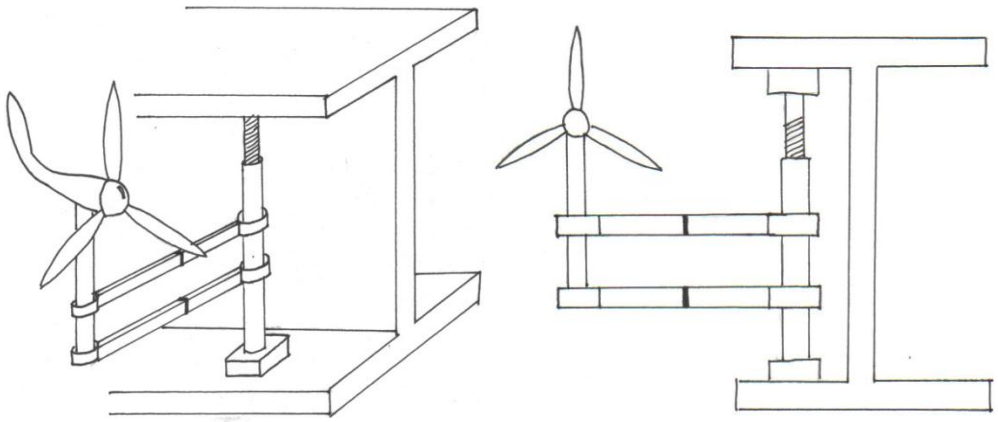

Figure 6.4: Second attachment system with an isometric view (left) and side view (right)

Attachment System #3

The third system in Figure 6.5 uses the radial expansive attachment principle to mount the wind harvester onto bridge, but the enabling characteristic was interpreted as a cavity in the bridge architecture instead of a hole. This way, three rods can radially expand in order to secure the wind harvester to different points on the bridge. The TRIZ *copying principle* was used by replicating the axially expansive rod from Attachment System #2 above.

- *Attachment Principles*: Radial expansive
- *TRIZ Principles*: Copying principle

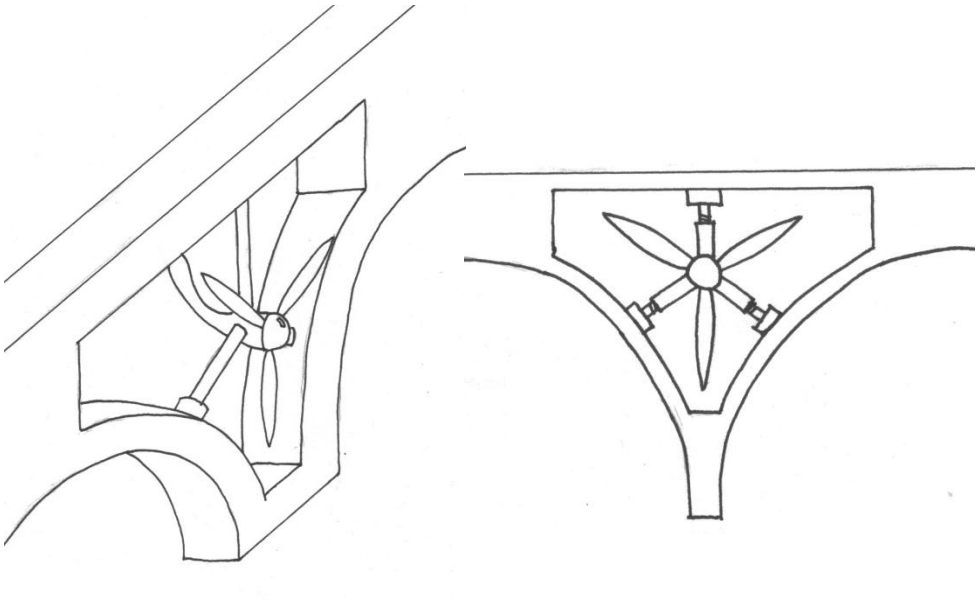

Figure 6.5: Third attachment system with an isometric view (left) and side view (right)

Attachment System #4

At this point all of the mechanical attachment principles were used in the previous examples, and exhibited a great deal of variety. However, the principles are not limited to

these solutions. They can be applied again in conjunction with other TRIZ principles in order to embody a larger design space. The following attachment system in Figure 6.6 uses the *axial compressive* and *hook* principles again, but this time with the TRIZ *principle of opposite solution*. The wind harvester is turned upside down and mounted to the L-shaped cross beam that spans between two I-beams. The wind harvester pole is welded to the metal hook, while the metal hook itself is secured to the bridge using screw clamps.

- *Attachment Principles*: Axial compressive, Hook
- *TRIZ Principles*: Principle of opposite solution

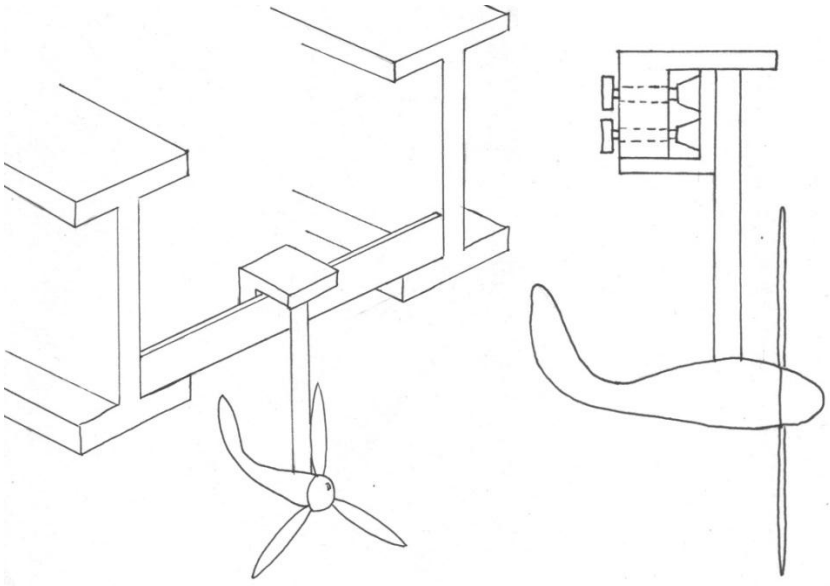

Figure 6.6: Fourth attachment system with an isometric view (left) and side view (right)

Attachment System #5

Although by definition it is destructive to drill into the concrete parts of the bridge, it was considered acceptable for the purposes of this project. For the fifth concept in Figure 6.7, the outer concrete portion of the bridge is used as the attachment location again, but this time the *radial expansive* attachment principle was applied by using anchor bolts to secure the L-shaped piece of metal. The TRIZ *nesting principle* was used again in this system as a way to adjust the height of the wind harvester.

- *Attachment Principles*: Radial expansive
- *TRIZ Principles*: Nesting principle, Principle of universality

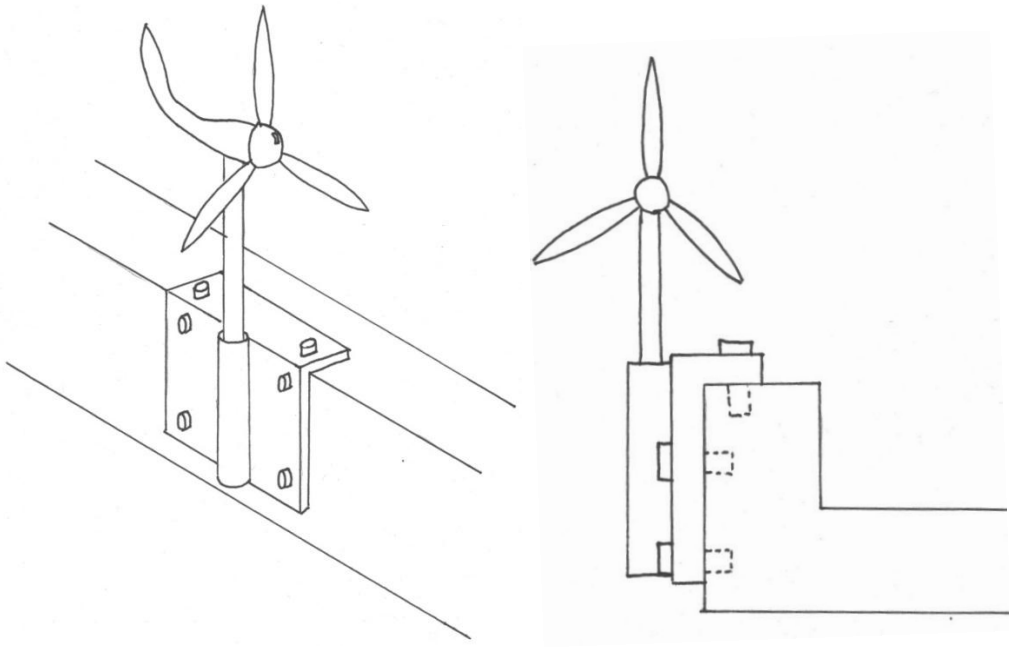

Figure 6.7: Fifth attachment system with an isometric view (left) and side view (right)

6.4 ATTACHMENT DESIGN EXPERIMENT AND RESULTS

In order to further justify the effectiveness of the proposed attachment methodology, a design experiment was conducted among a group of students. The

design problem reflected the exact same requirements and goal of the case study. The students were divided into two groups: a control group and an experimental group. Both groups drew concepts for 15 minutes, and then were separated. The control group read a paper as a distraction while the experimental group became familiar with the attachment methodology. Finally, both groups drew concepts again for 15 minutes. The designs were graded by four evaluators using four key design metrics: quantity, quality, novelty, and variety. The percentage increases and decreases of designs that exhibited each individual design metric within both the control and experimental group are displayed in the table below.

Table 6.3: The percentage increases between the first and second phases within each group.

Design Metric	**Percent Increase**	
	Control Group	Experimental Group
Quantity	12.5%	26.3%
Quality	-30.0%	2.3%
Novelty	-14.9%	-15.0%
Variety	13.7%	-10.7%

The results from Table 6.3 indicate that the experimental group formulated more designs than the control group after they were introduced to the methodology according to the *quantity* metric. The *novelty* metric exhibited a decrease across both groups, indicating that the methodology has no significant effect on the novelty of generated ideas. Both groups produced their most novel designs in the first design phase; the control group seemed to repeat the same ideas in the second phase, while the experimental group followed a methodology with suggested attachment principles,

inherently decreasing their novelty. The table also shows that the control group produced more designs that exhibited the *variety* metric. This suggests that the experimental group did indeed follow the suggested attachment principles and produced more designs that belonged in categories directly related to those principles, while the control group had no restrictions and produced designs across more diverse categories.

Although a greater variety may appear to be more beneficial for the control group, not all of these designs were deemed feasible. Probably the most interesting and significant design metric to observe is the *quality* metric. For the control group, there was a 30% decrease in quantity of designs that were by definition feasible, as opposed to a slight 2% increase in the experimental group. This indicates that the methodology discussed in this paper introduced key design attachment principles that the experimental group successfully applied. On the other hand, the control group hit a metaphoric wall in terms of coming up with additional feasible designs and had to resort to more unusual and obscure concepts of lower *quality*.

6.5 FINAL ATTACHMENT DESIGN

The final attachment design concept was derived from one of the case studies seen above, embellished with details, and used in conjunction with additional TRIZ and attachment principles. The goal of this attachment system was adjustability for any angle on a bridge, given that a flat concrete corner was available for mounting. The idea is to have the wind turbine oriented vertically independent of the slope angle of the bridge so that the wind turbine has a direct planar interaction with the oncoming wind. The final design and principles used are seen below in Figures 6.8 and 6.9:

- *Attachment Principles*: Axial compressive, Radial expansive, Hook
- *TRIZ Principles*: Principle of counterweight, Principle of universality, Nesting principle, Principle of moving into a new dimension

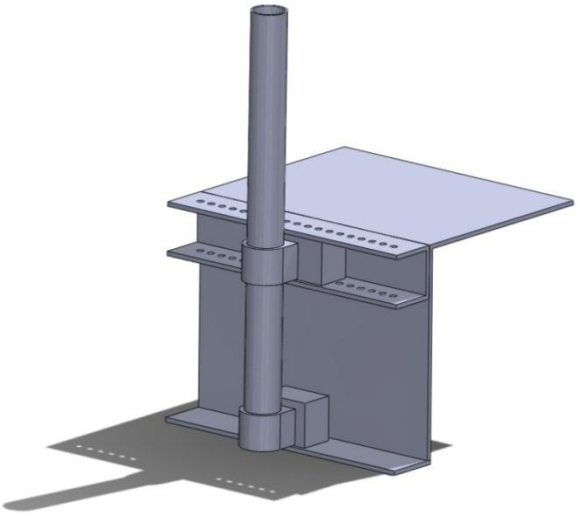

Figure 6.8: Final attachment design.

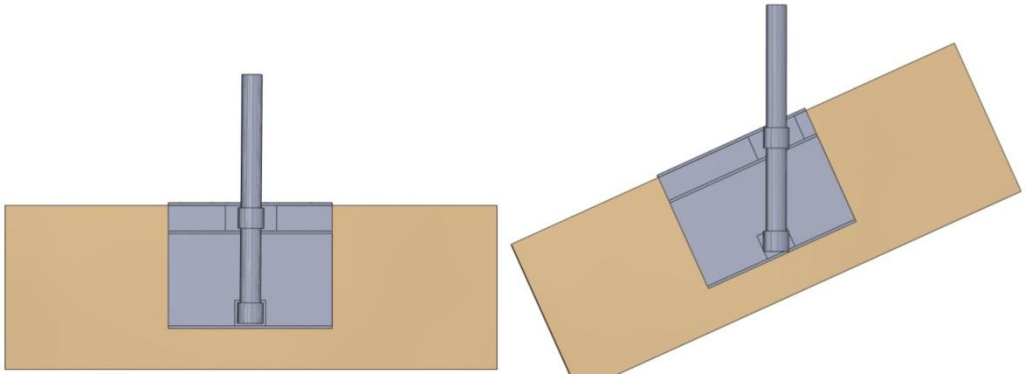

Figure 6.9: Attachment system with the ability to adjust for different bridge angles in order to maintain a vertically erect mount.

The wind turbine realized in the previous chapter can be integrated into the attachment system to fully complete the design of the next generation wind energy harvester. The system can be seen in Appendix G.

6.6 DISCUSSION

The results from the design experiment revealed that the methodology proved to be fruitful in generating concepts that were higher in quantity, quality, and more completely met the design requirements. The case studies demonstrated the usefulness of the methodology in the design of nondestructive attachment systems. The attachment principles in conjunction with the TRIZ principles produced a variety of feasible and innovative attachments concepts. Because the focus of this research was on non-destructive methods, only mechanical attachment principles were fully analyzed. Principles in other domains should be explored by performing additional design experiments. The goal for this methodology is to ultimately become a useful tool for designers based on their specific project requirements. Future improvements of this methodology should include a decision tree or survey to identify the most pertinent attachment principles based on the initial conditions of the design problem.

Chapter 7: Conclusions and Future Work

7.1 RESEARCH FINDINGS

The object of the thesis was to design a wind energy harvesting system to power a router for a remote wireless bridge health monitoring system. The research findings associated with the thesis can be broken down and summarized by chapter.

The problem was clearly described in the first chapter. Our nation's highway bridge infrastructure is in desperate need of more efficient methods to monitor their wellbeing. The current approach is time and labor intensive and does not provide access critical data on demand. There have recently been many developments in remote sensing equipment that enable continuous monitoring of crucial bridge features that could indicate failure, such as strain and corrosion. However, the proposed equipment requires power, and batteries must be replaced every couple of years, reverting back to the need of human labor. There is a clear need for energy harvesting to be installed in conjunction with these remote health monitoring system in order to continuously provide power or recharge energy storage devices.

The insights gained from the literature review successfully answered the questions posed at the beginning of the next chapter. The design space of wind turbines, including both horizontal and vertical axis domains, was fully explored in order to understand the aerodynamic performance and advantages of each type. The current state-of-the-art technology for small scale wind turbines was investigated to identify the different solutions applied to residential and commercial sectors and to understand the feasibility and financial issues that arise as turbines are scaled down for residential applications. It

was also found that it is more optimal, based on the ration of electricity generated to cost, to install one larger turbine as opposed to many smaller ones. The reason behind this finding is the technology to maximize energy harvesting capability such as blade pitch control and motor stall control is more beneficial at a large scale. It was also observed that there have been continuous efforts to optimize blade design for vertical axis wind turbines in order to improve their efficiency, but efficiencies of VAWTs are still inferior to HAWTs. Finally, the benefits and detriments of various types of generators were explored for different sizes of wind turbines.

A detailed analytical model was developed in order to assess the dynamic behavior of wind turbines and properly select the blade size and generator specifications necessary to achieve a high enough voltage. The model was used solve this coupled design problem. Using the previous proof of concept as a benchmark, the motor and turbine blades were appropriately sized and the results were compared to gage the feasibility of each approach. It was found that the resizing the generator would be infeasible and that the turbine needed to be redesigned first because it ultimately defines how much power and torque can be generated from a given wind profile. However, the differences in behavior between vertical Savonius-style turbine and horizontal axis turbines were also explored. It was found that HAWTs are more beneficial than Savonius VAWTs from an electricity generation standpoint, as supported by literature review completed in the previous chapter.

In the following chapter, an alpha level Savonius-style VAWT prototype was designed, and constructed and tested and compared to the results of the analytical model.

In case the model proved to be wrong and the prototype met the project specifications, it was designed to attach to an angle of a specific type of bridge (I-girder). After the prototype was modeled and carefully constructed, it was found that the prototype behaved similarly to what the model predicted, but an additional experimental plan was outlined to address an array of hypotheses. It was found that a 3-bladed Savonius system performs better than a 2-bladed system, and that the prototype could not reach voltages high enough to charge a 6V battery for reasonable wind speeds less than 20 mph. This was ultimately because the gear ratio in the generator significantly hindered performance by creating a high start-up torque. Furthermore, the inefficiency of the Savonius blade was observed through the measurement of the performance coefficient of the prototype, which was comparable to values found in literature. At this point in the research, it was decided that a HAWT was more beneficial for this project.

A small scale commercially available HAWT was purchased and benchmarked for performance. The experimental plan included monitoring the system over a short period of time (1 hour) in order estimate the generator speed constant, average cut-in speed, and TSR, as well as monitoring the system over a long period of time (2 weeks) in order to determine the power coefficient and wind speeds to start charging the battery. After the construction of an analytical model that assessed minimum blade size to achieve required power, these benchmarked values were appropriately scaled and used in the design of the next generation turbine. A design procedure was developed to organize decisions required to design the HAWT. The main features addressed were available wind power, blade geometry, generator specifications, and energy storage. The final

design was modeled and the defining features were found to be akin to those of the commercially available turbine.

Finally, the last step in the research was to integrate the next generation design into the infrastructure of a bridge. An attachment methodology was developed to structure and justify the design of the new attachment system. A series of case studies was performed and design experiments were executed to test the quality, quantity, variety and novelty of the ideas generated using the attachment methodology. The results from the design experiment revealed that the methodology proved to be fruitful in generating concepts that were higher in quantity, quality, and more completely met the design requirements. The case studies demonstrated the usefulness of the methodology in the design of nondestructive attachment systems. However, the full spectrum of attachment principles should be explored more fully and a design decision tree should be implemented to the methodology to aid designers in choosing the appropriate attachment principles for their specific design problem.

7.2 NEXT STEPS IN THE RESEARCH

The next step in this research will be to construct and test the prototype to determine whether the wind turbine can harness enough energy to achieve a high enough voltage and provide charge to a battery as predicted in the design process. The essential components of the wind turbine have been outlined along with the itemized bill of materials necessary for construction.

Once the system is verified to perform as expected, a crucial design issue needs to be addressed: an electro-mechanical brake is required to stall the turbine at high wind

speeds to serve as generator, blade and battery damage protection. There are two thresholds that need to be considered. The commercially available turbine begins to stall the system for speeds above 30 mph, but the system is still producing power. However, for wind speeds above 50 mph, the system completely shuts off. The first generation of this "brake" can be achieved by integrating an electrical sensor that mechanically decouples the generator from the turbine axis once it detects the angular speed threshold that would result in dangerously high voltages. This design should also include a clamp that can be activated using solenoids at the same time the sensor detects this threshold. Another generation of this "brake" could be designed using a variable resistive load in the generator that stalls the entire turbine when high angular speeds are reached. A higher resistive load means that the turbine must overcome a higher load torque, which would be beneficial in dangerously high winds. Both versions need to completely shut off at the second threshold of wind speeds.

Such brakes are usually implemented for small scale turbines, but pitch control could also be explored as another form of over-speed protection. However, cost may be a major issue at this scale. This function is more often used with induction generators that operate better at invariable speeds; blade pitch control moderates the rotational speed to match the design excitation capacitance of the generator.

Further down the road, a derivative should be designed that exhibits a better, sleeker encasing to maximize aerodynamic performance. Additionally, opportunities for mass production should be explored, such as injection molding for the blades to reduce long-term costs but to maintain their intricate geometry.

7.3 FUTURE WORK

The previous section describes research that will directly follow the work completed for this thesis. Additional ideas for the future of energy harvesting—especially for this project— are outlined here.

One possible idea for a harvester for small scale power generation is to combine two forms of energy: wind and vibration. A small scale Savonius style turbine can be constructed and allowed to spin freely on a simple bearing. The associated axis will have multiple extrusions that will strike a piezoelectric material multiple times as the extrusions pass by. The idea here is to completely abandon the use of a generator and harvest vibration energy. Savonius style turbines are limited in terms of speed, but they are extremely reliable in low and variable winds. For example, all anemometers come in the form of Savonius style turbines in order to detect all spectra of wind speeds. Since there would no longer be a generator, the turbine could rotate at a much slower pace, but every rotation would still result in one or more excitations of the piezoelectric material. This vibrational energy can then be collected using modules such as the "Energy Harvesting Modules" from Advanced Linear Devices that are designed to harvest intermittent and variable voltage and power spikes that are conditioned to a DC voltage (Advanced Linear Devices, 2012).

The idea of combining wind and vibration is not new. The Humdinger Windbelt seen in Figure 7.1 harvests vibrational energy due to wind excitation of a material in tension, creating an AC power in a generator (Humdinger, 2012). This can be converted into DC power if desired.

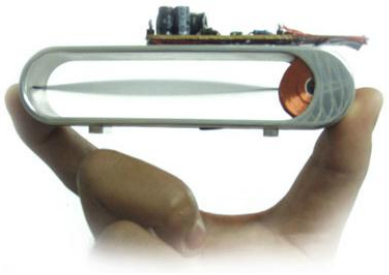

Figure 7.1: Wind vibration energy harvester (Humdinger, 2012).

Based on the research associated with this project, it seems more feasible to abandon the use of permanent magnet generators for milli-Watt and micro-Watt power generation. If the geographical location under question has a respectable amount of sunlight, it becomes much more beneficial to generate a small amount of power using solar energy rather than wind energy. A 6V 1W commercially available solar panel can be purchased for only $10. Spanning less than 10 in^2, such a system is static, so it has no moving parts and will last much longer because of the lack of variable stresses associated with the dynamics of a conventional turbine. However, if wind energy is in abundance, then the idea of wind vibration energy should most definitely be pursued to potentially power the sensors of the health monitoring system.

APPENDIX A – Dynamic Wind Turbine Behavior Code

VAWT STATE EQUATION

```
function w_dot = turbine(t,w)
global rho Cp H v R m b Ohm V_w_ratio
w_dot = .5*rho*Cp*H*v^2/m - (b*w/(m*R^2)) - (V_w_ratio^2*w/(Ohm*m*R^2));
```

HAWT STATE EQUATION

```
function w_dot = turbine_HAWT(t,w)
global rho Cp_HAWT v R m b Ohm V_w_ratio
w_dot = .5*rho*Cp_HAWT*pi*R*v^2/m - (b*w/(m*R^2)) -
(V_w_ratio^2*w/(Ohm*m*R^2));
```

EXECUTING THE SIMULATION

Determining voltage produced

```
clc
clear all

global rho Cp Cp_HAWT H v R m b Tm rho_m rho_m_HAWT V_w_ratio Ohm
Cp = .2;
rho = 1.21;
b = .05;
rho_m = 1010;
width = 1/1000; %meter
```

Motor specifications

```
Voltage = 24;
Speed_m = 5190;
Gear = 20;
Ohm = 7.31;
Eff = .87;
Battery = 6;
```

Determining minimum V_rpm ratio

```
V_rpm_ratio = Voltage*Gear/Speed_m;
V_w_ratio = V_rpm_ratio/(pi*30);
```

Average wind speed

```
v_mph = 8;
v_avg = (1610/3600)*v_mph;
```

Measuring minimum start-up torque

```
Tm = (1/1000)*45;
```

SAVONIUS

Determining minimum swept area

```
HR_m = (2*Tm)/(rho*Cp*v_avg^2);
HR_in = HR_m*100^3/2.54^3;
Diameter = ceil(HR_in^(1/3));
Height = Diameter;
Radius = Diameter;
```

Varying the radius

```
p = 1;
for v = .5*v_avg:v_avg/2:1.5*v_avg
   for R = Radius:Radius/2:2*Radius
      R = .0254*R;
      H = .0254*Height;
      m = rho_m*pi/2*((R+width)^2-R^2)*H;
      t = [0:.01:30];
      w0 = 0;
      [t,w] = ode45('turbine',t,w0);
      lambda_R(:,p) = w*R/v;
      voltage_produced(:,p) = Eff*V_rpm_ratio*(w*30/pi);
      p = p+1;
   end
end
```

Converting variables to strings

```
R1 = int2str(Radius);
R2 = int2str(1.5*Radius);
R3 = int2str(2*Radius);
H1 = int2str(Height);
H2 = int2str(1.5*Height);
H3 = int2str(2*Height);
v1 = int2str(.5*v_mph);
v2 = int2str(v_mph);
v3 = int2str(2*v_mph);
```

Plotting the varying radius at 50% average wind speed

```
t_bat = [0:1:30];
figure
```

```
plot(t,voltage_produced(:,1),t,voltage_produced(:,2),t,voltage_produced(:,3),t_bat,Battery
,'k*-')
xlabel('Time (s)')
ylabel('Voltage (V)')
legend(['R=',R1,' in'],['R=',R2,' in'],['R=',R3,' in'])
title(['Voltage Produced at Wind Speed of ',v1,' mph'])
```

Plotting the varying radius at average wind speed

```
figure
plot(t,voltage_produced(:,4),t,voltage_produced(:,5),t,voltage_produced(:,6),t_bat,Battery
,'k*-')
xlabel('Time (s)')
ylabel('Voltage (V)')
legend(['R=',R1,' in'],['R=',R2,' in'],['R=',R3,' in'])
title(['Voltage Produced at Wind Speed of ',v2,' mph'])
```

Plotting the varying radius at 150% average wind speed

```
figure
plot(t,voltage_produced(:,7),t,voltage_produced(:,8),t,voltage_produced(:,9),t_bat,Battery
,'k*-')
xlabel('Time (s)')
ylabel('Voltage (V)')
legend(['R=',R1,' in'],['R=',R2,' in'],['R=',R3,' in'])
title(['Voltage Produced at Wind Speed of ',v3,' mph'])
```

Plotting the tip to speed ratio at 50% average wind speed

```
figure
plot(t,lambda_R(:,1),t,lambda_R(:,2),t,lambda_R(:,3))
xlabel('Time (s)')
ylabel('Tip to Speed Ratio')
legend(['R=',R1,' in'],['R=',R2,' in'],['R=',R3,' in'])
title(['Tip to Speed Ratio at Wind Speed of ',v1,' mph'])
```

Plotting the tip to speed ratio at average wind speed

```
figure
plot(t,lambda_R(:,4),t,lambda_R(:,5),t,lambda_R(:,6))
xlabel('Time (s)')
ylabel('Tip to Speed Ratio')
legend(['R=',R1,' in'],['R=',R2,' in'],['R=',R3,' in'])
title(['Tip to Speed Ratio at Wind Speed of ',v2,' mph'])
```

Plotting the tip to speed ratio at 150% average wind speed

```
figure
```

```
plot(t,lambda_R(:,7),t,lambda_R(:,8),t,lambda_R(:,9))
xlabel('Time (s)')
ylabel('Tip to Speed Ratio')
legend(['R=',R1,' in'],['R=',R2,' in'],['R=',R3,' in'])
title(['Tip to Speed Ratio at Wind Speed of ',v3,' mph'])
```

Varying the height

```
clear voltage_produced
pp = 1;
for v = .5*v_avg:v_avg/2:1.5*v_avg
   for H = Height:Height/2:2*Height
      H = .0254*H;
      R = .0254*Radius;
      m = rho_m*pi/2*((R+width)^2-R^2)*H;
      t = [0:.01:30];
      w0 = 0;
      [t,w] = ode45('turbine',t,w0);
      lambda_H(:,pp) = w*R/v;
      voltage_produced(:,pp) = Eff*V_rpm_ratio*(w*30/pi);
      pp = pp+1;
   end
end
```

Plotting the varying height at 50% average wind speed

```
figure
plot(t,voltage_produced(:,1),t,voltage_produced(:,2),t,voltage_produced(:,3),t_bat,Battery
,'k*-')
xlabel('Time (s)')
ylabel('Voltage (V)')
legend(['H=',H1,' in'],['H=',H2,' in'],['H=',H3,' in'])
title(['Voltage Produced at Wind Speed of ',v1,' mph'])
```

Plotting the varying height at average wind speed

```
figure
plot(t,voltage_produced(:,4),t,voltage_produced(:,5),t,voltage_produced(:,6),t_bat,Battery
,'k*-')
xlabel('Time (s)')
ylabel('Voltage (V)')
legend(['H=',H1,' in'],['H=',H2,' in'],['H=',H3,' in'])
title(['Voltage Produced at Wind Speed of ',v2,' mph'])
```

Plotting the varying height at 150% average wind speed

```
figure
```

```
plot(t,voltage_produced(:,7),t,voltage_produced(:,8),t,voltage_produced(:,9),t_bat,Battery
,'k*-')
xlabel('Time (s)')
ylabel('Voltage (V)')
legend(['H=',H1,' in'],['H=',H2,' in'],['H=',H3,' in'])
title(['Voltage Produced at Wind Speed of ',v3,' mph'])
```

Plotting the tip to speed ratio at 50% average wind speed

```
figure
plot(t,lambda_H(:,1),t,lambda_H(:,2),t,lambda_H(:,3))
xlabel('Time (s)')
ylabel('Tip to Speed Ratio')
legend(['H=',H1,' in'],['H=',H2,' in'],['H=',H3,' in'])
title(['Tip to Speed Ratio at Wind Speed of ',v1,' mph'])
```

Plotting the tip to speed ratio at average wind speed

```
figure
plot(t,lambda_H(:,4),t,lambda_H(:,5),t,lambda_H(:,6))
xlabel('Time (s)')
ylabel('Tip to Speed Ratio')
legend(['H=',H1,' in'],['H=',H2,' in'],['H=',H3,' in'])
title(['Tip to Speed Ratio at Wind Speed of ',v2,' mph'])
```

Plotting the tip to speed ratio at 150% average wind speed

```
figure
plot(t,lambda_H(:,7),t,lambda_H(:,8),t,lambda_H(:,9))
xlabel('Time (s)')
ylabel('Tip to Speed Ratio')
legend(['H=',H1,' in'],['H=',H2,' in'],['H=',H3,' in'])
title(['Tip to Speed Ratio at Wind Speed of ',v3,' mph'])
```

HORIZONTAL AXIS

Determining the minimum swept area

```
R_HAWT = ceil((HR_in/pi)^(1/3));

Cp_HAWT = .2;
N = 3; %Number of blades
thick = (1/8)/1000; %Thickness (in)
wd = .0254*2; %width of blade (in)
rho_m_HAWT = 7800; %steel
```

Varying the Radius

```
clear voltage_produced
p = 1;
for v = .5*v_avg:v_avg/2:1.5*v_avg
   for R = R_HAWT:R_HAWT/2:2*R_HAWT
      R = .0254*R;
      m = N*rho_m_HAWT*R*wd*thick;
      t = [0:.01:5];
      w0 = 0;
      [t,w] = ode45('turbine_HAWT',t,w0);
      lambda_HAWT(:,p) = w*R/v;
      voltage_produced(:,p) = Eff*V_rpm_ratio*(w*30/pi);
      p = p+1;
   end
end
```

Converting variables to strings

```
R1 = int2str(R_HAWT);
R2 = int2str(1.5*R_HAWT);
R3 = int2str(2*R_HAWT);
```

Plotting the varying radius at 50% average wind speed

```
t_bat = [0:.1:5];
figure
plot(t,voltage_produced(:,1),t,voltage_produced(:,2),t,voltage_produced(:,3),t_bat,Battery
,'k*-')
xlabel('Time (s)')
ylabel('Voltage (V)')
legend(['R=',R1,' in'],['R=',R2,' in'],['R=',R3,' in'])
title(['Voltage Produced at Wind Speed of ',v1,' mph'])
```

Plotting the varying radius at average wind speed

```
figure
plot(t,voltage_produced(:,4),t,voltage_produced(:,5),t,voltage_produced(:,6),t_bat,Battery
,'k*-')
xlabel('Time (s)')
ylabel('Voltage (V)')
legend(['R=',R1,' in'],['R=',R2,' in'],['R=',R3,' in'])
title(['Voltage Produced at Wind Speed of ',v2,' mph'])
```

Plotting the varying radius at 150% average wind speed

```
figure
plot(t,voltage_produced(:,7),t,voltage_produced(:,8),t,voltage_produced(:,9),t_bat,Battery
,'k*-')
```

```
xlabel('Time (s)')
ylabel('Voltage (V)')
legend(['R=',R1,' in'],['R=',R2,' in'],['R=',R3,' in'])
title(['Voltage Produced at Wind Speed of ',v3,' mph'])

%Plotting the tip to speed ratio at 50% average wind speed
figure
plot(t,lambda_HAWT(:,1),t,lambda_HAWT(:,2),t,lambda_HAWT(:,3))
xlabel('Time (s)')
ylabel('Tip to Speed Ratio')
legend(['R=',R1,' in'],['R=',R2,' in'],['R=',R3,' in'])
title(['Tip to Speed Ratio at Wind Speed of ',v1,' mph'])
```

Plotting the tip to speed ratio at average wind speed

```
figure
plot(t,lambda_HAWT(:,4),t,lambda_HAWT(:,5),t,lambda_HAWT(:,6))
xlabel('Time (s)')
ylabel('Tip to Speed Ratio')
legend(['R=',R1,' in'],['R=',R2,' in'],['R=',R3,' in'])
title(['Tip to Speed Ratio at Wind Speed of ',v2,' mph'])
```

Plotting the tip to speed ratio at 150% average wind speed

```
figure
plot(t,lambda_HAWT(:,7),t,lambda_HAWT(:,8),t,lambda_HAWT(:,9))
xlabel('Time (s)')
ylabel('Tip to Speed Ratio')
legend(['R=',R1,' in'],['R=',R2,' in'],['R=',R3,' in'])
title(['Tip to Speed Ratio at Wind Speed of ',v3,' mph'])
%}
```

APPENDIX B – Dimension Drawings

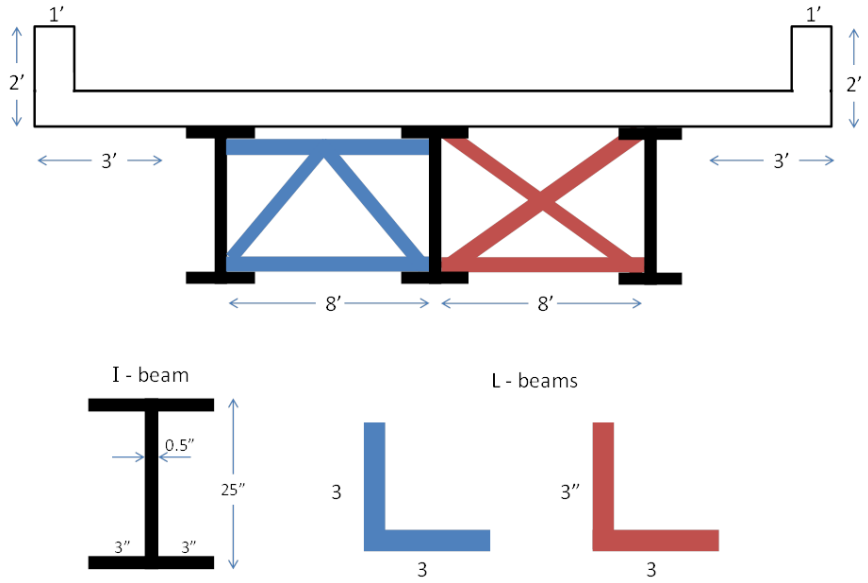

Figure B-1: Dimensions associated with the 183-71 bridge located in Austin.

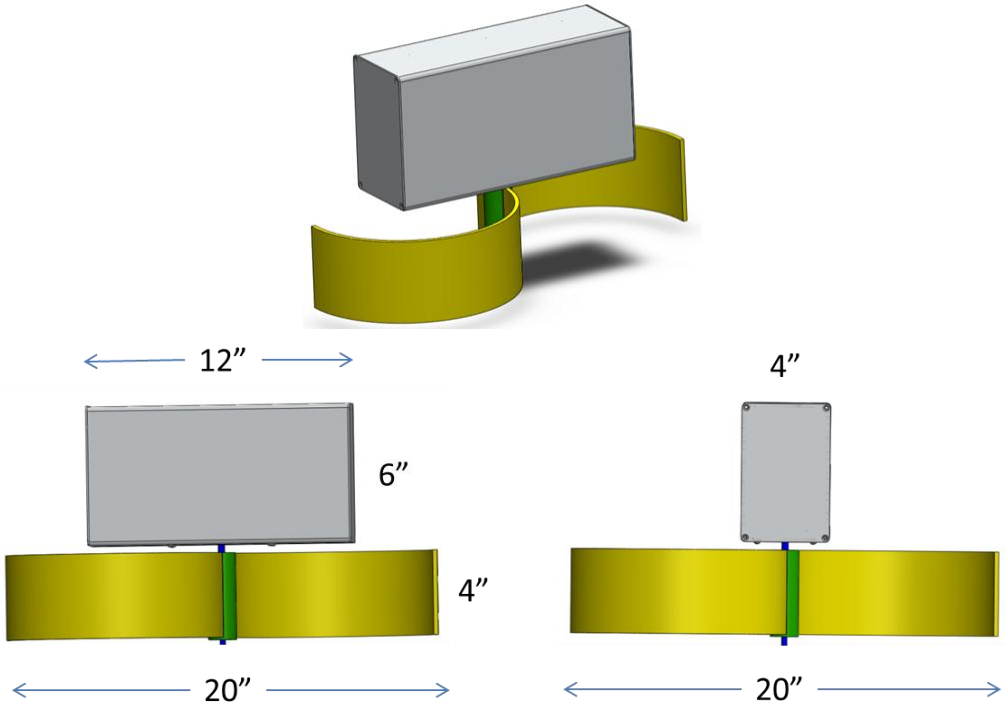

Figure B-2: Dimensions of the wind harvester prototype without the attachment mechanism.

APPENDIX C – First Generation Prototype Bill of Materials

Table C-1: First generation wind prototype bill of materials.

FIRST GENERATION WIND PROTOTYPE BILL OF MATERIALS					
Part #	Name	Quantity	Material	Stock Size	Price
Framework					
1	Casing	1	aluminum	weatherproof casings in stock from McMaster	$70
2	End seals	2	aluminum		$60
3	Hook	1	aluminum	4" x 4" x 1/8" (8 ft)	$64
4	Flush Mount	1	teflon	6" x 6" x 1/8"	$11.00
5	Plastic ring	1	teflon		
6	Shaft	1	aluminum	1/2" OD x 36"	$13.25
7	Motor mount	1	aluminum	6" x 3" x 1.5"	$49.00
8	6- 32 Screws	5	steel	6-32, 1" length	$5.00
9	1/2 - 20 screws w/ locknuts	4	steel		$5.00
10	Knobs	4		1/4 - 20, 1" head size, 3/8" thickness, round knob	$5.00
11	Spiral Insert	1	steel	1/4 - 20, 15/32" length	$15.00
12	Nylon insert hex locknut	1	steel	1/4 - 20 thread	$3.00
				Subtotal	$299.91
Turbine					
13	Turbine Blade	3	SLS		$900
14	Turbine Axis	2	SLS		$150
	Total Part Count	28		**Subtotal**	$1,050

Table C-1: First generation wind prototype bill of materials (cont'd).

Electronics					
15	WSN	1			Purchased
16	WSN Outdoor Casing	1			Purchased
17	6V Charge Controller	1			$20
18	6V Lead Acid Battery	1			$20
19	Brushless Motor EC45 Flat #251601 + GS45A / 18:1 #301175	1			$224
				Subtotal	$264
				TOTAL	**$1,614**

It should be noted that an exception was made with the requirement of the prototyping cost. The cost of the prototype without the SLS turbine is only $564 and therefore under the prototype cost of $600 stated in Chapter 4. The turbine was chosen to be made using Selective Laser Sintering as a quick prototyping method in order to minimize the time spent machining the complicated and cumbersome turbine blade shapes as well as to maximize the accuracy and therefore aerodynamic capability of the VAWT during testing.

APPENDIX D – First Generation Prototype Pictures

Pictures of the different parts and assemblies of the alpha prototype used for testing in Chapter 4.

SAVONIUS TURBINE ASSSEMBLY

Figure D-1: Shaft with screw end and turbine with threaded insert connecting into an assembly.

Figure D-2: Three-bladed SLS Savonius turbine with axis and blade assembly.

MACHINED PARTS

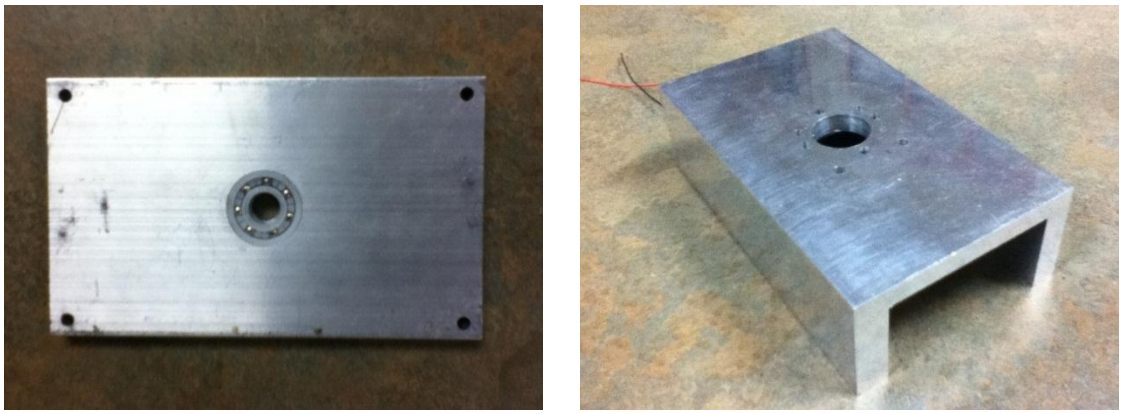

Figure D-3: Aluminum base with bearing (left) and generator mount (right).

Figure D-4: Shaft with threaded screw at the end and set screw used for piezoelectric hits.

MOTORS

Figure D-5: Stronger, newer motor (left) and the weaker, proof of concept (right).

CASING ASSEMBLY

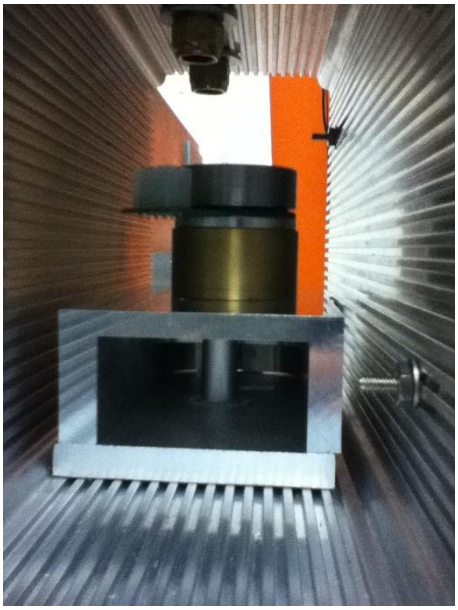

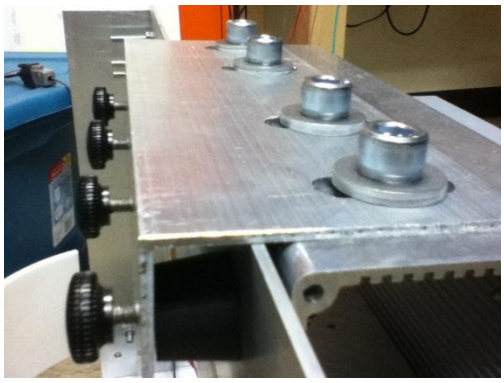

Figure D-6: Full assembly inside the casing (left) and the hook attachment method (right).

APPENDIX E – Power Modeling Code

CALCULATING POWER AND ENERGY BASED ON GIVEN WIND PROFILE

Constants

```
rho = 1.225; %kg/m^2
Cp = .35;
cut_in_mph = 8; %mph
cut_in_ms = cut_in_mph*(1610/3600); %m/s
```

Input Variables

```
data = xlsread('wind_battery.xlsx');
[p,q] = size(data);
wind = data(:,1);
vel = wind*(1610/3600);
battery = data(:,2);
```

Turbine Design Variables

```
TSR = 4;
R = 23; %in
```

Generator Design Variables

```
k_m = 25; %rpm/V
eff = .8;
G = 1;
```

Available Wind Power

```
P = (vel.^3).*(.5*Cp*rho*pi*(R*.0254)^2);
```

Usable Wind Power

```
i = 1;
wasted_e = 0;
while i <= p
   if vel(i)<cut_in_ms
      vel_use(i,1) = 0;
      wasted_e = 1+wasted_e;
   else
      vel_use(i,1) = vel(i);
   end
   cut_in_P(i,1) = (cut_in_ms^3)*(.5*Cp*rho*pi*(R*.0254)^2);
   cut_in_speed(i,1) = cut_in_mph;
   i=i+1;
end
```

```
P_use = (vel_use.^3).*(.5*Cp*rho*pi*(R*.0254)^2);
```

Energy

```
tt = 60*5*[1:p];
E = sum(trapz(tt,P))/3600/1000; %kWh
E_use = sum(trapz(tt,P_use))/3600/1000; %kWh
percent_usable_energy = E_use*100/E;
percent_time = 100*(1 - (wasted_e/p));
```

Generator Parameters

```
blade_speed = vel.*(TSR*30/(pi*R*.0254)); %rpm
gen_speed = blade_speed.*G; %rpm
volt = gen_speed.*(eff/k_m); %volts
amp = P./volt; %amps
```

GENERATING POWER CURVES

Power output from performance specifications

```
power_specs_steady = 0.0214*wind.^2.977;
power_specs_turb = 0.0001*wind.^4.4757;
```

Generating power curves

```
wind_space = linspace(0,30);
vel_space = wind_space*(1610/3600);
P_curve = (vel_space.^3).*(.5*Cp*rho*pi*(R*.0254)^2);
steady_curve = 0.0214*wind_space.^2.977;
turb_curve = 0.0001*wind_space.^4.4757;
```

PLOTTING RESULTS

Plotting

```
t = linspace(1,p/(12*24),p);

figure
plot(t,power_specs_steady,t,power_specs_turb,t,P,':')
title('Power for Measured Wind Profile')
xlabel('Day')
ylabel('Power (W)')
legend('Performance Spec. for Power under Steady Wind Conditions','Performance Spec.
for Power under Turbulent Wind Conditions','Predicted Power')

figure
plot(wind_space,steady_curve,wind_space,turb_curve,wind_space,P_curve)
```

```
title('Power Distribution Curves')
xlabel('Wind Speed (mph)')
ylabel('Power (W)')
legend('Performance Spec. for Power under Steady Wind Conditions','Performance Spec.
for Power under Turbulent Wind Conditions','Predicted Power')

figure
[AX,H1,H2] = plotyy(t,P,t,wind);
xlabel('Day')
set(get(AX(1),'Ylabel'),'String','Power (W)')
set(get(AX(2),'Ylabel'),'String','Wind Speed (mph)')
title('Wind Speed vs. Power')

figure
plot(t,P,t,cut_in_P,'r--');
xlabel('Day')
ylabel('Power (W)')
title('Available vs. Usable Power')
str = ['Usable power at ',num2str(round(cut_in_P(1))),' W at cut-in speed of
',num2str(cut_in_ms*(3600/1610)),' mph'];
legend('Available Power',str)
mTextBox = uicontrol('style','text');
set(mTextBox,'Units','characters');
set(mTextBox,'String',[num2str(round(percent_usable_energy)),'% of the energy is
usable ',num2str(round(percent_time)),'% of the time']);
set(mTextBox,'Position',[70 20 24 3])

figure
[AX2,H3,H4] = plotyy(t,volt,t,amp);
xlabel('Day')
set(get(AX2(1),'Ylabel'),'String','Voltage (V)')
set(get(AX2(2),'Ylabel'),'String','Amperes (A)')
title('Voltage vs. Amps')

figure
[AX3,H5,H6] = plotyy(t,wind,t,battery);
xlabel('Day')
set(get(AX3(1),'Ylabel'),'String','Wind Speed (mph)')
set(get(AX3(2),'Ylabel'),'String','Battery Voltage (V)')
title('Wind Speed and Battery Voltage')

hold on
plot(t,cut_in_speed,'r--')
```

```
legend('Wind Speed',['Cut-in speed of ',num2str(cut_in_mph),' mph'],'Battery Voltage')
```

PARAMETRIC STUDIES

```
mph = linspace(0,10);
v = (1610/3600)*mph;
```

Varying the Radius

```
x = 5;
y = 1;
z = 9;
Cp = .05;

k = 1;
for R = x:y:z
   P_par = (v.^3).*(.5*Cp*rho*pi*(R*.0254)^2);
   P_matrix(:,k) = P_par';
   k = k+1;
end

figure
plot(mph,P_matrix(:,1),mph,P_matrix(:,2),mph,P_matrix(:,3),mph,P_matrix(:,4),mph,P_
matrix(:,5),'k')
xlabel('Wind Speed (mph)')
ylabel('Power (W)')
title(['Predicted Power for Varying Radii at Cp = ',num2str(Cp)])
legend(['R = ',num2str(x),' in'],['R = ',num2str(x+y),' in'],['R = ',num2str(x+2*y),' in'],['R
= ',num2str(x+3*y),' in'],['R = ',num2str(z),' in'],'Location','NorthWest')
```

Varying Radius and one Cp

```
xx = .1;
yy = .1;
zz = .2;
R = z;
k = 1;
for Cp = xx:yy:zz
   P_par = (v.^3).*(.5*Cp*rho*pi*(R*.0254)^2);
   P_matrix2(:,k) = P_par';
   k = k+1;
end

hold on
plot(mph,P_matrix2(:,2),'k--',mph,P_matrix2(:,1),'k:')
```

```
legend(['R = ',num2str(x),' in'],['R = ',num2str(x+y),' in'],['R = ',num2str(x+2*y),' in'],['R
= ',num2str(x+3*y),' in'],['R = ',num2str(z),' in at Cp = ',num2str(.3)],['R = ',num2str(z),'
in at Cp = ',num2str(zz)],['R = ',num2str(z),' in at Cp =
',num2str(xx)],'Location','NorthWest')
title('Predicted Power for Varying Radii and Power Coefficients')
```

Power Coefficient Specs

```
xx = .1;
yy = .05;
zz = .3;
```

Varying the Power Coefficient

```
R = 23;
k = 1;
for Cp = xx:yy:zz
   P_par = (v.^3).*(.5*Cp*rho*pi*(R*.0254)^2);
   P_matrix3(:,k) = P_par';
   k = k+1;
end

figure
plot(mph,P_matrix3(:,1),mph,P_matrix3(:,2),mph,P_matrix3(:,3),mph,P_matrix3(:,4),mp
h,P_matrix3(:,5))
xlabel('Wind Speed (mph)')
ylabel('Power (W)')
title(['Predicted Power for Varying Power Coefficients at R = ',num2str(R)])
legend(['Cp = ',num2str(xx)],['Cp = ',num2str(xx+yy)],['Cp = ',num2str(xx+2*yy)],['Cp =
',num2str(xx+3*yy)],['Cp = ',num2str(zz)],'Location','NorthWest')
```

APPENDIX F – Mechanical Attachment Principles

Listed below are the definitions and examples of the mechanical attachment principles which were used in the case study. Also listed are the "enabling parent characteristics" which are features of the parent that serve as indicators to whether or not a particular principle is a viable option.

Radial Expansive

Attachment principle which applies a radially outward force within a hole.

Examples: Anchor bolts, Press fit threaded inserts, Dowel pin

Enabling characteristics: Hole

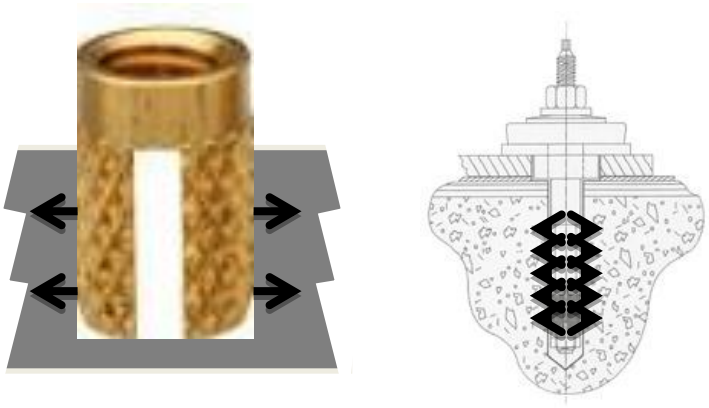

Figure F-1: Press fit threaded insert (left) and anchor bolt (right).

Radial Compressive

Attachment principle which applies a radially inward force on an extrusion.

Examples: Zip ties, Hose clamps, Car cup holders

Enabling characteristics: Extrusion

Figure F-2: Hose clamp (left) and zip tie (right).

Axial Expansive

Attachment principle which applies axially outward opposing forces perpendicular to two surfaces.

Examples: Shower rod, Car jack

Enabling characteristics: Two parallel flat surfaces, two angled flat surfaces

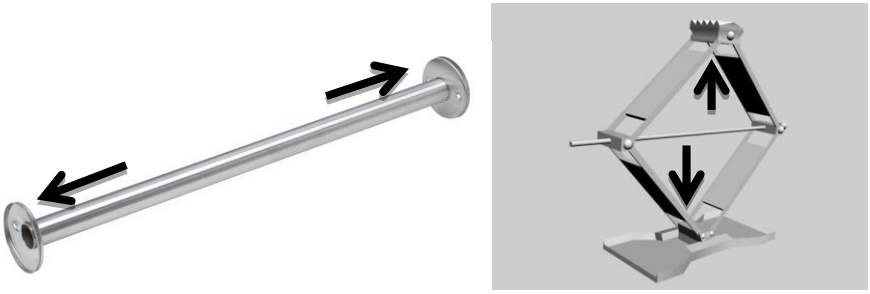

Figure F-3: Shower rod (left) and car jack (right).

Axial Compressive

Attachment principle which applies axially inward forces perpendicular to two surfaces.

Examples: Rivet, Clamp lamp, Pull up bar

Enabling characteristics: Perpendicular edges, two parallel flat surfaces

Figure F-4: Doorway pull up bar (left) and clamp lamp (right).

Hook

Attachment principle where the object is suspended through the contact interface between the upward facing surfaces of an extrusion and the downward facing surfaces of the object.

Examples: Hanger, Backpack, Velcro

Enabling characteristics: Extrusion

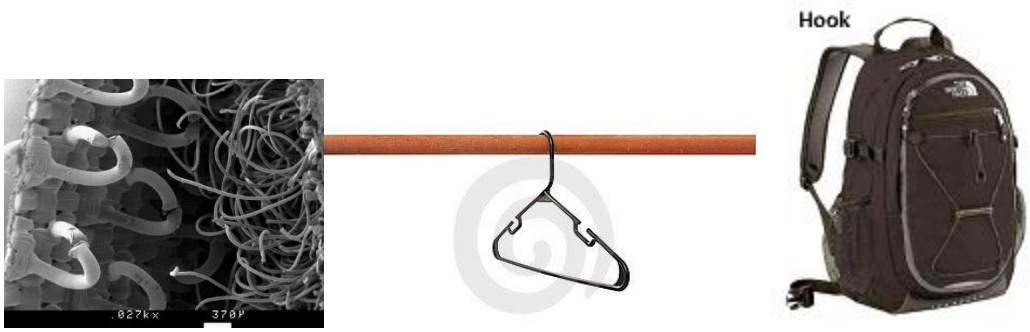

Figure F-5: Magnified view of Velcro (left), hanger (middle) and backpack (right).

APPENDIX G – Next Generation Wind Energy Harvester

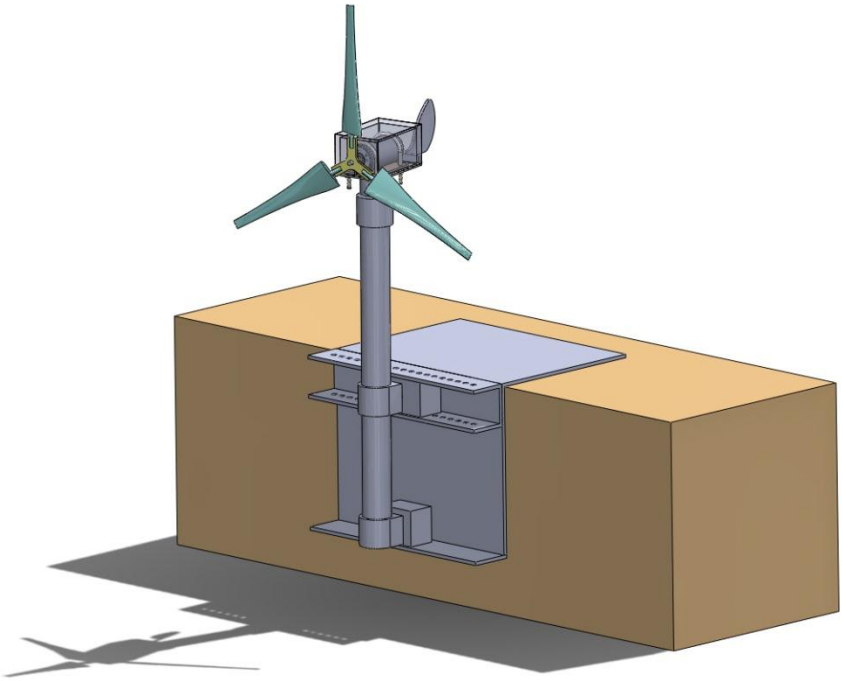

Figure G-1: Isometric view of the next generation wind energy harvester.

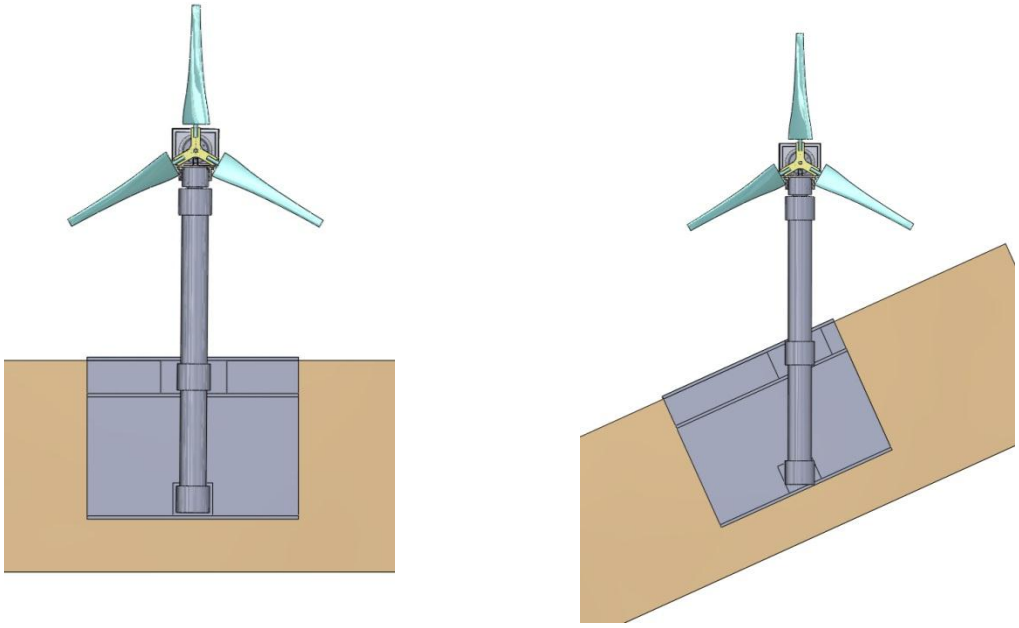

Figure G-2: Adaptability of next generation system onto different bridge angles.

References

Advanced Linear Devices. (2012). *EH300/301 EPAD® ENERGY HARVESTING TM MODULES.* Retrieved on Apr. 16, 2012 from http://www.aldinc.com/pdf/EH300.pdf

Air X Owner's Manual. (2012). Retrieved on Mar. 22, 2012 from www.windenergy.com/sites/all/files/3-CMLT-1004_REV_E_AIR_X_OWNERS_MANUAL.pdf.

Alam, Jahangir & Iqbal, M.T. (2010). *A Low Cut-in Speed Marine Current Turbine*. The Journal of Ocean Technology. Safety@Sea, Vol. 5, No. 4. (p 53).

Altshuller, G. (1984). *Creativity as an Exact Science*. Luxembourg: Gordon and Breach.

Beaman, J. J., & Paynter, H. M. (1993). *Modeling of Physical Systems*.

Berengueres, J., Tadakuma, K., Kamoi, T., & R. A. K. R. Kratz. (2007). *Compliant distributed magnetic adhesion device for wall climbing*. Robotics and Automation, 2007 IEEE International Conference. (pp 1256-1261).

Brandon, D., Kaplan, D. (1997). *Joining processes: an introduction*. John Wiley & Sons: Chichester. ISBN 0-471-96488-3.

Coyle, Franklin. (2011). *Introduction to Wind Power*. Delhi: The English Press. ISBN 978-93-81157-74-9.

CNN Wire Staff. (2010). *Settlement reached in Minnesota bridge collapse case*. Retrieved on Apr. 16, 2012 from http://www.cnn.com/2010/US/08/23/minnesota.bridge.settlement/index.html,

Design Styles. (2012). *Wind Energy-The Facts*. Retrieved on Feb. 15, 2012 from http://www.wind-energy-the-facts.org/en/part-i-technology/chapter-3-wind-turbine-technology/evolution-of-commercial-wind-turbine-technology/design-styles.html.

Dierks, Eric. (2011). *Design of an Electromagnetic Vibration Energy Harvester for Structural Health Monitoring of Bridges Employing Wireless Sensor Networks*. The University of Texas at Austin. (pp 1-14).

Electric Power Monthly. (2012). *Independent Statistics and Analysis*. US Energy Information Administration. Retrieved on Jan. 10, 2012, from http://www.eia.gov/electricity/monthly.

Elliot, M., Morris, W., Xiao, J. (2006). *City-Climber, a new generation of wall-climbing robots*. Video Proceedings of 2006 IEEE International Conference on attitude; The Robotics and Automation.

Energy Saver. (2012). *Energy Efficiency and Renewable Energy*. Us Dept. of Energy. Retrieved on Jan. 10, 2012, from http://www1.eere.energy.gov/consumer/tips/m/home_energy.html.

Eriksson, S., Bernhoff, H., & Leijon, M. (2008). Evaluation of different turbine concepts for wind power. *Renewable and Sustainable Energy Reviews*, *12*(5), 1419-1434. doi: 10.1016/j.rser.2006.05.017.

Fernando, Vincent. (2010). *America Has Enough Offshore Wind to Power Itself Four Times*. Retrieved on Feb. 10, 2012, from http://articles.businessinsider.com/2010-10-12/markets/29998566_1_offshore-wind-land-based-wind-wind-power.

Four Seasons Windpower. (2012). Retrieved on Jan. 10, 2012 from http://www.fswindpower.com/Faqs.html.

GotWind.org. (2010). *DC Motor Advice*. Retrieved on Nov. 22, 2011, from http://gotwind.org/forum/viewtopic.php?f=31&t=3451.

Green, Jim. (1999). *Small Wind Turbine Applications: Current Practice in Colorado.* Colorado Renewable Energy Conference. NREL/CP-500-27080. (pp 9-10).

Green Energy (2012). *The Green Energy Website*. Retrieved on Feb. 15, 2012 from http://www.thegreenenergywebsite.com/savonious.htm.

Grimshaw. (2012). *Infrastructure Projects: Aerogenerator X*. Retreived on Feb. 22, 2012 from http://grimshaw-architects.com/project/the-aerogenerator

Gupta, R., Das, R., & Sharma, K.K. (2006). *Experimental Study of a Savonius-Darrieus Wind Machine*. International Conference on Renewable Energy for Developing Countries (pp 1-11).

Hau, Erich (2011). *Wind Turbines: Fundamentals, Technologies, Application, Economics*. Berlin: Springer-Verlag. (pp 90-102 & 210-214).

HelixWind. (2012). *Products: S594 Wind Turbine*. Retrieved on Jan. 20, 2012, from http://www.helixwind.com/en/S594.php.

HiVAWT (2012). *DS-3000W Vertical Axis Wind Turbine*. Retrieved on Feb. 15, 2012 from http://www.hi-vawt.com.tw/en/ds3000w.html.

Horizon Wind (2012). *How Does a Wind Turbine Work?* Retrieved on May 1, 2012 from http://www.horizonwind.com/about/ftkc/howdoeswindturbinework.aspx.

Hughes, Austin. (2005). *Electric Motors and Drives: Fundamentals, Types, and Applications*. Boston: Newnes. (p 374).

Humdinger. (2012). *Windbelt Innovation: Microwatt (mW)*. Retrieved on Apr. 16, 2012 from http://www.humdingerwind.com/#/wi_micro/

Inamdar, S. (2009). *Optimal Rotor Designs to Application Conditions, using Blade Element Momentum Theory and Experimental Wind Tunnel Testing.* (pp 1-6).

Jamieson, Peter. (2011). *Innovation in Wind Turbine Design*. John Wiley & Sons: Chichester. (pp 236-238).

Kamoji, M.A., Kedare, S.B., Prabhu, S.V. (2008). *Experimental investigations on single stage, two stage and three stage conventional Savonius rotor*. International Journal of Energy Research. Ed. 32. (pp 877-895).

Kamoji, M.A., Kedare, S.B., Prabhu, S.V. (2008). *Performance tests on helical Savonius rotors*. Elsevier: Journal of Renewable Energy. Ed. 34. (pp 521-529).

Khaligh, A., & Onar, O. C. (2010). *Energy Harvesting: Solar, Wind, and Ocean Energy Conversion Systems*. Boca Raton: CRC Press. (pp 101-165).

Kikuchi, T., & Kenjo, T. (1998). *In-depth Learning of Cogging/Detenting Torque through Experiments and Simulations*. IEEE. Retrieved on Feb. 1, 2012 from http://ewh.ieee.org/soc/es/Nov1998/12/BEGIN.HTM.

Kim, T.H., Setoguchi, T., & Kaneko, K. (2001). *The Optimization of Blade Pitch Settings of an Air Turbine Using Self-Pitch-Controlled Blades For Wave Power Conversion*. Journal of Solar Energy Engineering. ASME Vol. 123 (pp 382-386).

Kindwind Science Snack: Betz Limit. (2012). *Understanding Coefficient of Power (Cp) and Betz Limit*. Retrieved on Jan. 24, 2012, from http://learn.kidwind.org/sites/default/files/betz_limit_0.pdf.

Koller, R. (1984). *Entwicklung einer Systematik für Verbindungen – ein Beitrag zur Konstruktionsmethodik*. Konstruktion 36 (1984) H. 5, Springer-Verlag. (pp 173-180).

LG Barcus & Sons. (2012). *Snooper Truck Services*. Retrieved on Apr. 16, 2012 from http://www.barcus.com/heavy-construction-a-bridges/heavy-construction-a-bridges/snooper-truck-services-gallery.

Madescu, G., Biriescu, M., Prostean, O., Greconici, M., Mihut, T., & Mot, M. (2011). *Low Speed PM Generator for Wind Turbines Applications*. IEEE: International Conference on Computer as a Tool. (pp 1-5).

Maxon Motors. (2011). *Maxon DC Motor: Generation Operation*. Retrieved on June 9, 2011, from Mark Dwyer, a Maxon Motor representative.

Maxon Technology. (2012). *Maxon DC motor: Technology – short and to the point*. Retrieved on March 15, 2012 from Mark Dwyer, a Maxon Motor representative.

McCroskey, W.J. (1987). *A Critical Assessment of Wind Tunnel Results for the NACA 0012 Airfoil*. NASA. (pp 1-24).

McEvoy, Travis. (2011). *Wind Energy Harvesting for Bridge Health Monitoring*. The University of Texas at Austin. (pp 91-93).

Mohamed, M.H., Janiga, G., Pap. E., & Thevenin, D. (2010). *Optimal blade shape of a modified Savonius turbine using an obstacle shielding the returning blade*. Elsevier: Journal of Energy Conversion and Management. Ed. 52. (pp 236-242).

Mok, Ken. (2005). *Identification of the Power Coefficient of Wind Turbines*. IEEE. University of California. (pp 1-5).

Munson, B. R., Young, D. F., & Okiishi, T. H. (1998). *Fundamentals of Fluid Mechanics*. 3rd edition. New York: John Wiley & Sons, Inc.

NCDC. (2008). *Wind – Average Wind Speed – (MPH)*. Retrieved on Jan. 20, 2012, from http://lwf.ncdc.noaa.gov/oa/climate/online/ccd/avgwind.html.

Neammanee, B., Sirisumrannukul, S., & Chatratana, S. (2007). *Development of a Wind Turbine Simulator for Wind Generator Testing*. International Energy Journal. Ed 8. (pp 21-28).

NREL. (2011). *Wind Maps – Dynamics Maps, GIS Data, & Analysis Tools*. Retrieved on Feb. 17, 2012 from http://www.nrel.gov/gis/wind.html.

Ostman, Sarah. (2011). *Patents, Awards Come Out of Senior Engineering Design Class*. Retrieved on Feb. 7, 2012 from http://www.mccormick.northwestern.edu/news/articles/article_988.html.

Parallax (2012). *Solar Panel 6V@1W, 125x63mm*. Retrieved on Apr. 12, 2012 from http://www.parallax.com/Store/Components/Optoelectronics/tabid/152/CategoryID/39/List/0/SortField/0/Level/a/ProductID/619/Default.aspx

Patel, Mukun R. (2006). *Wind and Solar Power Systems: Design, Analysis, and Operation*. 2nd edition. Boca Raton: Taylor & Francis Group.

Pitch vs. Stall. (2012) *Wind Energy – The Facts*. Retrieved on Feb. 17, 2012 from http://www.wind-energy-the-facts.org/en/part-i-technology/chapter-3-wind-turbine-technology/technology-trends/pitch-versus-stall.html.

Polinder, H., van der Pijl, F. F. A., de Vilder, G., & Tavner, P. J. (2006). *Comparison of Direct-Drive and Geared Generator Concepts for Wind Turbines*. IEEE Transactions on energy conversion, Vol. 21, No. 3. (pp 725-733).

Ragheb. M. (2011). *Optimal Rotor Tip Speed Ratio*. Retrieved on Mar. 30, 2012 from https://netfiles.uiuc.edu/mragheb/www/NPRE%20475%20Wind%20Power%20Systems/Optimal%20Rotor%20Tip%20Speed%20Ratio.pdf.

Ragheb, M. (2011). *Vertical Axis Wind Turbines*. Retreived on Feb. 22, 2012 from https://netfiles.uiuc.edu/mragheb/www/NPRE%20475%20Wind%20Power%20Systems/Vertical%20Axis%20Wind%20Turbines.pdf.

Renewable Energy Consumption: Residential and Commercial Sectors. (2012). *Energy Information Administration*. Retrieved on Jan. 10, 2012, from http://www.eia.gov/totalenergy/data/monthly/pdf/sec10_4.pdf.

Roth, K. (2000). *Konstruieren mit Konstruktionskatalogen.* 3. Auflage, Band I:Konstruktionslehre. Springer-Verlag: Berlin.

Saha, U.K., Thotla, S., & Maity, D. (2008) *Optimum deisgn configuration of Savonius rotor through wind tunnel experiments*. Elsevier: Journal of Wind Engineering and Industrial Aerodynamics. (pp 1359-1375).

Singh, Mohit. (2011). *Dynamic Model for Wind Power Plants*. The University of Texas at Austin.

Southwest WindPower (2012). Retreived on Jan. 10, 2012 from http://store.windenergy.com/Air-Breeze-Marine-Wind-Generator/dp/B005IYMPF6.

Thumthae, C. & Chitsomboon, T. (2008). *Optimal angle of attack for untwisted blade turbine*. Journal of Renewable Energy. Vol 34, Issue 5. (pp 1279-1284).

Tudorache, T., Melcescu, L., & Popescu, M. (2010). *Methods for Cogging Torque Reduction of Directly Driven PM Wind Generators*. IEEE: International Conference on Optimization of Electrical and Electrical Equipment. (pp. 1161-1166).

UGE First Step. (2012). *Urban Green Energy*. Retrieved on Feb. 10, 2012, from http://www.urbangreenenergy.com/products/uge-first-step.

US. Department of Transportation. (2006). *2006 Traffic Volumes in St. Paul-Minneapolis Seven Country Area*. Retrieved on Apr. 16, 2012 from http://www.dot.state.mn.us/traffic/data/maps/indexmaps/2006/mplsin.pdf.

Venturi Wind. (2012). *Venturi Wind Turbines*. Retrieved on Feb. 22, 2012, from http://www.venturiwind.com.

Vestas (2012). *Vestas V80 – 2.0 MW Turbine Overview*. Retrieved on Feb. 1, 2012, from http://www.vestas.com/en/wind-power-plants/procurement/turbine-overview/v80-2.0-mw.aspx#/vestas-univers

Weaver, J., Wood, K., Crawford, R. *Design of Energy Harvesting Technology: Feasibility for Low-Power Wireless Sensor Networks*. Proceedings of the ASME IDETC & CIEC Conference in Montreal, Canada. (pp 1-11).

WE Handbook (2012). *Wind Turbine Blade Aerodynamics*. Retrieved on Mar. 30, 2012 from http://www.gurit.com/files/documents/2_aerodynamics.pdf.

WindDose (2012). *Windaholics' on-line relief*. Retrieved on Feb 15. 2012, from http://winddose.com/wind-turbine-techologies.html.

Wind Energy – The Facts: A guide to the technology economics and future of wind power. (2009). *European Wind Energy Association*. London: Earthscan. (pp 120-130).

Windspire. (2012). *The Windspire: Photos and Videos*. Retrieved on Jan. 20, 2012, from http://www.windspireenergy.com/windspire/photos-and-videos.

WindTronics. (2012). *The Honeywell Wind Turbine – Model WT6500.* Retrieved on Feb. 17, 2012 from http://www.windtronics.com/honeywell-wind-turbine.

WindyNation. (2010). *Making Wind Power: How to Choose the Right Motor*. Retrieved on Dec. 9, 2011, from http://www.windynation.com/articles/wind/making-wind-power-how-choose-right-motor.

Wood, David (2011). *Small Wind Turbines: Analysis, Design, and Application*. London: Springer.

Yamamoto, A., Nakashima, T., Higuchi, T. (2007). *Wall Climbing Mechanisms Using Electrostatic Attraction Generated by Flexible Electrodes*. International Symposium on Micro-NanoMechatronics and Human Science: Nagoya, Japan. (pp 389-394).

Vita

Krystian Amadeusz Zimowski graduated Cum Laude from Northwestern University in June of 2010, receiving his Bachelor of Science in Mechanical Engineering. His senior design project at Northwestern consisted of designing and building an Automatic Meat Casing Remover (AMCaR) that is currently patent pending. He has had several internships at Sandia National Laboratories where he worked on designing fail-safe systems for containing plutonium in the Z-Machine, a large X-ray generator. Krystian also participated in entrepreneurial organizations, such as the Austin Technology Incubator and 1 Semester Startup, to gain crucial skills in technology commercialization. Upon completion of this thesis, he is planning on moving to Washington, D.C. to work for a product development consulting firm.

Email: krystian.zimowski@gmail.com

This thesis was typed by the author.